University of Alberta

Zinc in Precambrian iron formations:
The record, partitioning, diagenetic effects and implications for eukaryotic metallome evolution

by

Leslie James Robbins

A thesis submitted to the Faculty of Graduate Studies and Research
in partial fulfillment of the requirements for the degree of

Master of Science

Department of Earth and Atmospheric Sciences

Fall 2013
Edmonton, Alberta

Abstract

Zinc is amongst the most important trace elements for eukaryotes. Previous work has suggested it to have been at biolimiting concentrations for much of the Precambrian, thereby limiting eukaryotic evolution. Yet, the iron formation (IF) record, a critical proxy for paleomarine conditions, has remained unexplored. Here, we examine aspects of the IF record and its geochemistry, including: thermodynamic models for Zn in paleomarine conditions, the abundance of Zn through geological time, and hypothesized partitioning models. Further, experimental constraints such as, derived partitioning isotherms and an assessment of the mobility of Zn (and for comparison Ni) during IF diagenesis are presented. Taken together, these examinations inform our interpretation of the IF record, indicating a static Zn reservoir throughout geological time that was unlikely to have been biolimiting to early eukaryotes. Instead, the most parsimonious explanation for a delay in eukaryotic evolution is tied to biological development, rather than marine geochemistry.

Acknowledgements

This thesis would not have been possible without the input and advice of many of my colleagues. I would especially like to recognize Dr. Stefan Lalonde for his guidance and support. During my MSc I have had the opportunity to collaborate with a number of colleagues that I would like to acknowledge, including: Dr. Noah Planavsky, Dr. Elizabeth Swanner, Merle Eickhoff, Dr. Murray Gingras, Dr. Andreas Kappler, Dr. Chris Reinhard, Dr. Mak Saito, Dr. Chris Dupont and Dr. Clint Scott. Working with each of them has been a sincere pleasure. Thanks also to Guangcheng Chen at the University of Alberta and Ellen Struve and Sabine Flaiz at the University of Tübingen for their assistance with analyses. I would also like to recognize the other members of my lab group for their support, including: Dr. Ernesto Pecoits, Natalie Aubet, Daniel Petrash, Rasmus Haugaard, Aleksandra Mloszewska, Megan Paranich and Set Castro.

My most sincere thanks go to Dr. Kurt Konhauser who opened up his lab to me as an undergraduate student and allowed me to continue working under his guidance as a graduate student. I feel fortunate to have had such an excellent supervisor and privileged to have been considered a colleague and friend rather than solely as a student. Dr. Konhauser has provided me with a number of tremendous opportunities to travel and research while completing my MSc, for which I am eternally grateful.

Finally, I would like to extend my thanks to my family and friends, for their belief in me. Foremost, I would like to thank my parents, sisters, Meghan Black, Amie St. Arnaud and Peter Sukhdeo. I would also like to thank Chris Atkins, Laura Brin, Devin Cathro, Saulo Castro, Alexandra Der, Bryant Eriks, Ellen Sykes and Josh Thomas for their ongoing friendship and support.

Table of Contents

List of Tables

List of Figures

List of Abbreviations and Nomenclature

BF – biogenic ferrihydrite cell-mineral aggregates

BIF – banded iron formations

EXAFS – X-ray absorption extended fine structure spectroscopy

Fh – synthetic 2-line ferrihydrite

GIF – granular iron formations

GOE – Great Oxidation Event

ICP-MS – Inductively Couple Plasma Mass Spectrometer

ICP OES – Inductively Coupled Plasma Optical Emission Spectroscopy

IF – iron formations

K_D – distribution coefficient

PAL – present atmospheric level

Q-ICP MS – Quadrupole – Inductively Coupled Plasma Mass Spectrometer

REE – rare earth element

REE+Y – rare earth element and yttrium

TE – trace element

TM-HNO_3 – trace metal grade nitric acid

U of A – University of Alberta

WHOI – Woods Hole Oceanographic Institute

XAS – X-ray absorption spectroscopy

CHAPTER 1

An introduction to Precambrian iron formations as paleomarine proxies for key trace elements of biological importance

1.1 Iron formations

Iron formations (IF) is as a general term that includes several important types of iron-rich (≥15% Fe) sedimentary deposits, including: Precambrian banded iron formations (BIF) and granular iron formations (GIF), Phanerozoic oolitic ironstones and modern hydrothermal exhalites. IF were chemically precipitated in the Precambrian ocean, from the Archean to the Paleoproterozoic (>3.8 to ~1.8 Ga), but are conspicuously absent between the Mesoproterozoic and middle Neoproterozoic (1.8 and 0.8 Ga). Their resurgence in the Neoproterozoic, after a billion year hiatus, has been linked to a pair of major climatic perturbations ("Snowball Earth" events).

BIF are characterized by alternating bands of iron- and silica-rich layers, which are laterally extensive and typically range in thickness from few mm to several cm (Klein, 2005). They formed in water below depths of 200 meters, likely on the continental shelf or slopes of ancient cratons (see Bekker et al., 2010 for review). Accordingly, they lack any features of current or wave action. By contrast, GIF are lithologically distinctive and lack the banding typically observed in BIF, but instead contain granules or other sedimentary structures indicative of a near shore depositional environment (Trendall, 2002). Nonetheless, it has been demonstrated that GIF may still contain valuable paleoenvironmental information within their trace element contents (Konhauser et al., 2011).

In general BIF can be classified as one of two types, Algoma or Superior type. Algoma type-BIF are generally associated with submarine volcaniclastic settings, whereas Superior type-BIF are considered to be indicative of continental shelf environments (Gross, 1980, Bekker et al., 2010). Although, the use of these general designations is somewhat controversial, as Trendall has questioned the

application of these generalized terms to IF deposited throughout the Proterozoic in different settings, such as the Hamersley Basin IF in Australia versus the Lake Superior IF in Canada (cf. Trendall, 2012 and Bekker et al., 2012). For the remainder of this discussion, and within subsequent chapters, we will examine the entire record of iron chemical deposits and employ the more general term of IF.

1.2 Iron formations as seawater proxies

IF are considered to be useful geochemical proxies as they record trace-element signatures characteristic of marine conditions at the time of deposition. This is largely supported by the preservation of rare earth element and yttrium (REE+Y) patterns in ancient IF, similar to those observed in modern ironstones and exhalative sediments (e.g., Kimberley, 1989; Bau and Dulski, 1996; Alexander et al., 2008). Previous work using IF as paleomarine proxies has mainly focused on evaluating the relative contributions of continentally- versus hydrothermally-sourced REE+Y inputs into paleomarine basins (e.g., Bau and Möller, 1993; Bau and Dulski, 1996; Alexander et al., 2008), as well as the reconstruction of paleoredox conditions in the ocean (e.g., Bau and Möller, 1993; Planavsky et al., 2009). Most recently, trace element contents in IF have been used to evaluate the bioavailability of trace metals (e.g., Bjerrum and Canfield, 2002; Konhauser et al., 2007; 2009), as well as the effect that microorganisms had on trace metal mobility and supply to the ocean realm (e.g., Konhauser et al., 2009; 2011).

The demise of IF in the Paleoproterozoic has been linked to oxidation of the oceans (Holland, 1984) or widespread development of euxinic (sulfidic) conditions (Canfield, 1998). More recently, Planavsky et al (2011) challenged this idea and suggested that ferruginous conditions (anoxic and non-sulfidic) were rather extensive during the Mesoproterozoic and that euxinic conditions occurred along continental margins, where organic productivity and sulfate reduction were high. Hence, the deeper waters remained ferruginous, much like oceans before 1.8 Ga (Poulton et al., 2010). As such, IF are an ideal proxy for recording authigenic marine seawater signatures from the Precambrian, which can then be used to infer the bioavailability of trace elements such as Zn, the main focus of this work.

1.3 Zinc and nickel: biological significance and previous paleomarine estimates

Zinc is an important trace metal for eukaryotic life, and becomes biolimiting as concentrations approach 10^{-13} M (e.g., Brand et al, 1983). It has been proposed that concentrations of Zn were low in the Archean through the Proterozoic when the oceans were highly ferruginous and possibly sulfidic; they then rose drastically following Neoproterozoic ocean oxygenation (Saito et al., 2003).

Modern hydrothermal systems are a significant source of Zn (Elderfield and Schultz, 1996; Douville et al., 2002), although, in modern settings much of the Zn is removed adjacent to the vent (John et al., 2008). Conversely, in the anoxic to suboxic Precambrian oceans the Zn sourced from hydrothermal vents most likely became well mixed into the oceans, similar to Fe. Hence, IF are an attractive sedimentary proxy for investigating paleomarine Zn conditions.

The proteomic record, based on the phylogenetic structure, abundance and incorporation of trace metals into metalloenzymes, has the potential to record changes in paleomarine concentrations of these elements (e.g., Dupont et al., 2006, 2010; Caetano-Anollés et al., 2009). Current estimates for paleomarine Zn concentrations are taken almost exclusively from geochemical modeling studies and inferences drawn from the proteomic record (Saito et al., 2003; Dupont et al., 2006, 2010). They suggest Zn was at concentrations that should have been biolimiting to early eukaryotes for much of the Precambrian. Recent examinations of the IF and shale records suggest that Zn was at concentrations were not as drawn down as previously thought, and likely consistently within an order of magnitude of modern oceans since the Archean (e.g., Mloszewska et al., 2012; Robbins et al., 2011; Scott et al., 2013). This discrepancy highlights the need for a combined approach considering both the proteomic and sedimentary records.

A case study where the proteomic and IF record do indeed parallel each other is observed when considering nickel (Ni), another transition metal. A decrease in marine Ni concentrations about 2.7 Ga, as recorded in the IF record, has been suggested to correspond to a decrease in the utilization of Ni in

metalloenzymes and the subsequent starvation of methanogens (Konhauser et al., 2009). In this scenario, the authors proposed that the decline of methanogens aided in the rise of atmospheric oxygen that ultimately lead to the Great Oxidation Event (GOE). However, a combined approach accounting for both the proteomic and IF record has yet to be put forth for Zn.

1.4 Significance of trace element partitioning to Fe-minerals

In recent studies it has been demonstrated that understanding the partitioning behavior for elements adsorbed to precipitating iron (III) oxyhydroxides allows for refinement of first order approximations for paleomarine trace element concentrations by combining them with the IF record. So far this approach has been only used to produce estimates for paleomarine phosphorous (P) and Ni concentrations (Bjerrum and Canfield, 2002; Konhauser et al., 2007; Konhauser et al., 2009).

The partitioning behavior of a trace element (TE) can be defined by the term K_D (a partitioning coefficient), which is a measure of the affinity for a TE to sorb (including both adsorption and absorption) to a solid phase. In this case it refers to a TE affinity to sorb to precipitating Fe oxyhydroxides. This represents a special case of the Freundlich isotherm where the exponent is equal to one (Langmuir, 1997). The K_D term can be thought of as the slope of the line governing the relationship between the ratio of TE/Fe in the particle and the equilibrium value of the TE dissolved in seawater (Eq. 1).

$$K_D = (\text{Molar TE/Fe})_{particle}/[TE]_{equilibrium} \qquad \text{Eq. 1}$$

Initially, the IF record was combined with K_D, values determined from modern marine environments to extrapolate paleomarine phosphate concentrations (Bjerrum and Canfield, 2002). However, in response to this, Konhauser et al. (2007) have demonstrated that for the extraction of paleomarine estimates during the Precambrian, a consideration of the paleomarine silica (SiO_2) concentrations must be taken into account because it effectively competes for

binding sites with other ions, such as phosphate or nickel. Therefore, not considering paleomarine silica concentrations can lead to significant differences in paleomarine reconstructions (Konhauser et al, 2007; 2009; Planavsky et al., 2010a); throughout much of the Precambrian dissolved silica levels were significantly higher than they are in modern oceans, possibly approaching saturation with respect to cristoballite, or even amorphous silica. Siever (1992) attributed the decrease in silica to the evolution of silica-secreting organisms, such as sponges and radiolarians in the Phanerozoic. It is likely that silica concentrations did not decrease to modern levels until the Cretaceous when diatoms then evolved, as evidenced by the deposition of chert beds in the Mesozoic (Grenne and Slack, 2003). Hence, it is important to have a strong understanding regarding the function that silica plays on changing the slope of the isotherm (K_D) and how trace metals adsorb to co-precipitating Fe-oxyhydroxides. To date this methodology has only been applied to P (Konhauser et al., 2007) and Ni (Konhauser et al., 2009); but other TEs (e.g., Zn) at the intersection of geochemical and biological evolution have yet to be investigated.

1.5 Potential for trace metal mobility during diagenesis

Although several studies have utilized trace metal contents in IF, it has been largely assumed - based on REE+Y patterns - that trace metals are relatively immobile. This is based primarily on the preservation of Eu anomalies and a consistent seawater-like signature (e.g., Derry and Jacobsen, 1990; Bau, 1993, Alexander et al., 2008, Planavsky et al., 2010b; Mloszewska et al., 2012). However, there are very few studies examining the specific mobility of trace elements in Fe-mineral phases, especially during diagenesis (e.g., McConchie, 1984; Frierdich et al., 2011; Frierdich and Catalano, 2012;). As such, experiments presented herein should provide a critical preliminary assessment of the effects that diagenesis has on the trace metal contents of IF. The mobility of Ni will also be examined, as like Zn, it is a biologically relevant trace element. Further, this should allow for speculation regarding the impacts of diagenetic processes on estimated paleomarine trace metal concentrations, allowing for a test of the

robustness of findings derived from the IF record, and ultimately, a refinement of paleomarine Zn estimates derived from the IF record.

1.6 Objectives of this work

This work will investigate Zn concentrations in IF through time in order to refine estimations of paleomarine Zn concentrations derived from geochemical modeling and phylogenetic analysis (Saito et al., 2003; Dupont et al., 2010). In Chapter 2, it will be accomplished in three stages, first by examining the IF record for temporal trends in Zn abundance as normalized by Zn/Fe ratios. This examination will be complemented by updated thermodynamic geochemical models aimed at resolving the discrepancy between the IF record and previous estimates for paleomarine Zn which have been dominantly influenced by Zn-sulfide speciation. Likewise, hypothetical-partitioning scenarios derived directly from the Zn-Fe relationship in the IF record will be used to provide an estimate for paleomarine Zn. The proposed study will allow for inferences regarding the bioavailability of Zn in the Precambrian ocean and its paleobiological implications.

In Chapter 3, experiments will be described that evaluated the experimental partitioning scenarios outlined in Chapter 2. This work involves a preliminary assessment of the mobility of Zn during diagenesis; the mobility of Zn will also be compared to Ni in order to test the robustness of the IF record to record authigenic signatures of biologically relevant trace elements despite potential diagenetic remobilization. These considerations will ultimately validate or challenge the inferences drawn directly from the IF record.

Chapter 4 summarizes the use the IF record and subsequent experimental considerations to draw inferences about the paleomarine bioavailability of Zn and its implications for the rapid diversification of eukaryotes following Neoproterozoic ocean oxygenation.

1.7 References

Alexander BW, Bau M, Andersson P, Dulski P (2008) Continentally-derived solutes in shallow Archean seawater: Rare earth element and Nd isotope evidence in iron formation from the 2.9 Ga Pongola Supergroup, South Africa. *Geochimica et Cosmochimica Acta*, **72**, 378-394.

Bau M (1993) Effects of syn- and post depositional processes on the rare-earth element distribution in Precambrian iron-formations. *European Journal of Mineralogy*, **5**, 257-267.

Bau M, Möller P (1993) Rare earth element systematics of the chemically precipitated component in Early Precambrian iron formations and the evolution of the terrestrial atmosphere-hydrosphere-lithosphere system. *Geochimica et Cosmochimica Acta*, **57**, 2239-2249.

Bau M, Dulski P (1996) Distribution of yttrium and rare-earth elements in the Penge and Kuruman iron-formations, Transvaal Supergroup, South Africa. *Precambrian Research,* **79**, 37-55.

Bekker A, Slack JF, Planavsky N, Krapež B, Hofmann A, Konhauser KO, Rouxel OJ (2010) Iron Formation: The Sedimentary Product of a Complex Interplay among Mantle, Tectonic, Oceanic and Biospheric Processes. *Economic Geology*, **105**, 467-508.

Bekker A, Krapež B, Slack JF, Planavsky N, Hofmann A, Konhauser KO, Rouxel OJ (2012) Iron Formation: The Sedimentary Product of a Complex Interplay among Mantle, Tectonic, Oceanic and Biospheric Processes – a Reply. *Economic Geology*, **107**, 379-380.

Bjerrum CJ, Canfield DE (2002) Ocean productivity before about 1.9 Gyr ago limited by phosphorus adsorption onto iron oxides. *Nature*, **417**, 159-162.

Caetano-Anollés G, Want M, Caetano-Anollés D, Mittenthal JE (2009) The origin, evolution and structure of the protein world. *Biochemical Journal*, **417**, 621-637.

Canfield DE (1998) A new model for Proterozoic ocean chemistry. *Nature*, **396**, 450-453.

Brand LE, Sunda WG, Guillard RRL (1983) Limitation of Marine Phytoplankton Reproductive Rates by Zinc, Manganese, and Iron. *Limnology and Oceanography*, **28**, 1182-1198.

Derry LA, Jacobsen SB (1990) The chemical evolution of Precambrian seawater: evidence from REEs in banded iron formations. *Geochimica et Cosmochimica Acta*, **54**, 2965-2977.

Douville E, Charlou JL, Oelkers EH, Bienvenu P, Jove Colon CF, Donval JP, Fouquet Y, Prieur D, Appriou P (2002) The rainbow vent fluids (36º14'N, MAR): the influence of ultramafic rocks and phase separation on trace metal content in Mid-Atlantic Ridge hydrothermal fluids. *Chemical Geology*, **184**, 37-48.

Dupont CL, Yang S, Palenik B, Bourne PE (2006) Modern proteomes contain putative imprints of ancient shifts in trace metal geochemistry. *Proceedings of the National Academy of Sciences*, **103**, 17822-17827.

Dupont CL, Butcher A, Valas RE, Bourne PE, Caetano-Anollés G (2010) History of biological metal utilization inferred through phylogenomic analysis of protein structures. *Proceedings of the National Academy of Sciences*, **107**, 10567-10572.

Elderfield H, Schultz A (1996) Mid-ocean ridge hydrothermal fluxes and the chemical composition of the ocean. *Annual Review of Earth and Planetary Sciences*, **24**, 191-224.

Frierdich AJ, Luo Y, Catalano JG (2011) Trace element cycling through iron oxide minerals during redox driven dynamic recrystallization. *Geology*, **39**, 1083-1086.

Frierdich AJ, Catalano JG (2012) Controls on Fe(II)-activated trace element release form Goethite and Hematite. *Environmental Science and Technology*, **46**, 1519-1526.

Grenne T, Slack JF (2003) Paleozoic and Mesozoic silica-rich seawater: Evidence from hematitic chert (jasper) deposits. *Geology*, **31**, 319-322.

Gross GA (1980) A classification of iron formations based on depositional environments. *Canadian Mineralogist*, **18**, 215-222.

Holland (1984) *The Chemical Evolution of the Atmosphere and Oceans*. Princeton University Press, New Jersey.

John SG, Rouxel OJ, Craddock PR, Engwall AM, Boyle EA (2008) Zinc stable isotopes in seafloor hydrothermal vent fluids and chimneys. *Earth and Planetary Science Letters*, **269**, 17-28.

Kimberely MM (1989) Exhalative origins of iron formations. *Ore Geology Reviews*, **5**, 13-145.

Klein C (2005) Some Precambrian banded iron-formations (BIFs) from around the world: Their age, geological setting, mineralogy, metamorphism, geochemistry and origin. *American Mineralogist*, **90**, 1473-1499.

Konhauser KO, Lalonde SV, Amskold L, Holland HD (2007) Was there really an Archean phosphate crisis? *Science*, **315**, 1234

Konhauser KO, Pecoits E, Lalonde SV, Papineau D, Nisbet EG, Barley ME, Arndt NT, Zahnle K, Kamber BS (2009) Oceanic nickel depletion and a methanogen famine before the Great Oxidation Event. *Nature*, **458**, 750-753.

Konhauser KO, Lalonde SV, Planavsky NJ, Pecoits E, Lyons TW, Mojzsis SJ, Rouxel OJ, Barley ME, Rosìere C, Fralick PW, Kump LR, Bekker A (2011) Aerobic bacterial pyrite oxidation and acid rock drainage during the Great Oxidation Event. *Nature*, **478**, 369-373.

Langmuir D (1997) Aqueous Environmental Geochemistry. Prentice Hall, Upper Saddle River, New Jersey pp. 1-600.

McConchie D (1984) The geology and geochemistry of the Joffre and Whaleback Shale members of the Brockman Iron Formations, Western Australia. PhD Thesis, University of Western Australia.

Mloszewska AM, Pecoits E, Cates NL, Mojzsis SJ, O'Neil JO, Robbins LJ, Konhauser KO (2012) The composition of Earth's oldest iron formations: The Nuvvuagittuq Supracrustal Belt (Québec, Canada). *Earth and Planetary Science Letters*, **317-318**, 331-342.

Planavsky N, Rouxel O, Bekker A, Shapiro R, Fralick P, Knudsen A (2009) Iron oxidizing microbial ecosystems thrived in late Paleoproterozoic redox-stratified oceans. *Earth and Planetary Science Letters*, **286**, 230-242.

Planavsky NJ, Rouxel OJ, Bekker A, Lalonde SV, Konhauser KO, Reinhard CT, Lyons TW (2010a) The evolution of the marine phosphate reservoir. *Nature*, **467**, 1088-1090.

Planavsky N, Bekker A, Rouxel OJ, Kamber B, Hofmann A, Knudsen A, Lyons TW (2010b) Rare earth element and yttrium compositions of Archean and Paleoproterozoic Fe formations revisited: New perspectives on the significance and mechanisms of deposition. *Geochimica et Cosmochimica Acta*, **74**, 6387-6405.

Planavsky NJ, McGoldrick P, Scott CT, Li C, Reinhard CT, Kelly AE, Chu X, Bekker A, Love GD, Lyons TW (2011) Widespread iron-rich conditions in the mid-Proterozoic ocean. *Nature*, **477**, 448-451.

Poulton SW, Fralick PW, Canfield DE (2010) Spatial variability in oceanic redox structure 1.8 billion years ago. *Nature Geoscience*, **3**, 486-490.

Robbins LJ, Lalonde SV, Mloszewska AM, Konhauser KO (2011) The evolution of the marine Zn reservoir: Comparing the proteomic and sedimentary records. *Goldschmidt 2011 Poster [Gold2011:abs:4813]*.

Saito MA, Sigman DM, Morel FMM (2003) The bioinorganic chemistry of the ancient ocean: the co-evolution of cyanobacterial metal requirements and biogeochemical cycles at the Archean-Proterozoic boundary? *Inorganica Chimica Acta*, **356**, 308-318.

Scott C, Planavsky NJ, Dupont CL, Kendall B, Gill B, Robbins LJ, Husband KF, Arnold GL, Wing B, Poulton SW, Bekker A, Anbar AD, Konhauser KO, Lyons TW (2013) Bioavailability of zinc in marine systems through time. *Nature Geoscience*, **6**, 125-128.

Siever R (1992) The silica cycle in the Precambrian. *Geochimica et Cosmochimica Acta*, **56**, 3265-3272.

Trendall AF (2002) The significance of iron-formation in the Precambrian stratigraphic record. *Special Publications of the International Association of Sedimentologists*, **33**, 33-66.

Trendall A (2012) Iron Formation: The Sedimentary Product of a Complex Interplay among Mantle, Tectonic, Oceanic and Biospheric Processes – a Reply. *Economic Geology*, **107**, 377-378.

CHAPTER 2

Authigenic iron oxide proxies for marine Zinc over geological time and implications for eukaryotic metallome evolution[1]

2.1 Introduction

Zinc is the most common inorganic co-factor in eukaryotic metalloenzymes (Berg and Shi, 1996; Maret, 2001; Dupont et al., 2010), and as a consequence, it has become the basis for a hypothesis that the biological use of Zn may have evolved in the late Precambrian when it became available in seawater (Williams and da Silva, 1996; Dupont et al., 2006; 2010; Saito et al., 2003). Modern marine phytoplankton differ significantly in their ability to grow at low Zn concentrations; modern surface seawater has concentrations that range from ~0.04-0.5 nM (e.g., Bruland, 1989; Lohan et al., 2002). Studies of marine cyanobacteria have found little to no measurable Zn requirement under the conditions tested thus far in the globally abundant *Prochlorococcus* and *Synechococcus* (Sunda and Huntsman 1995; Saito et al., 2002). In contrast, eukaryotic phytoplankton have been observed to be quite sensitive to low zinc conditions. Some, notably neritic diatoms (those that inhabit shallow marine waters from the littoral zone to the edge of the continental shelf), are more sensitive and experience growth rates that are significantly reduced at free Zn^{2+} concentrations below $10^{-11.5}$ M, while others show only minor reductions in growth rates at 10^{-13} M (Brand et al., 1983). The centric diatom *Thalassiosira* sp. displays dramatically reduced growth rates in coastal species at Zn concentrations of $10^{-12.5}$ M (Tortell and Price, 1996); however, species from offshore oligotrophic environments, such as *Thalassiosira oceanica*, are more tolerant of low Zn conditions (Sunda and Huntsman, 1995). The unicellular algae, *Emiliania huxleyi*

[1] A version of this chapter has been published. Robbins LJ, Lalonde SV, Saito MA, Planavksy NJ, Mloszewska AM, Pecoits E, Scott C, Dupont CL, Kappler A, Konhauser KO (2013) *Geobiology*, doi: 10.1111/gbi.12036.

(a coccolithopharad), shows decreased levels of alkaline phosphatase activity as Zn approaches picomolar concentrations (Shaked et al., 2006). Concentrations are low enough in modern environments that Zn stimulation or co-limitations of marine phytoplankton communities have been observed in some high nutrient, low chlorophyll environments (Franck et al., 2003; Jakuba et al., 2012), but not other environments (Crawford et al., 2003; Coale et al., 2005). While physiological studies of phytoplankton Zn requirements are limited and it is apparent that no single dissolved Zn concentration can be pinpointed as universally limiting, it is also apparent that severely suppressed marine Zn concentrations would have significant consequences for the activity and abundance of modern eukaryotic phytoplankton.

Such may have been the case in deep geological time. A survey of physiological experiments found that marine prokaryotic microbes, particularly the cyanobacteria, show metal nutritional requirements consistent with hypothesized Precambrian seawater compositions (Saito et al., 2003). From this it was suggested that during much of the Precambrian, the bioavailable marine Zn reservoir, as well as those of Cu and Cd, may have been much lower than in the modern oxygenated ocean due to the formation of strong aqueous complexes between Zn and sulfide that are likely not bioavailable (Luther et al., 1996; Edgcomb et al., 2004). Proteomic-based phylogenetic analyses also indicate a relatively late origin for most Zn-binding domains in eukaryotic metalloenzymes, leading to the suggestion that in addition to depressed oxygen availability, marine Zn biolimitation stemming from higher Precambrian sulfide concentrations and expanded euxinia during the mid-Proterozoic (1800 to 800 Ma) may have impeded eukaryotic diversification (Dupont et al., 2006; 2010). Accordingly, seemingly rapid eukaryotic diversification in the Neoproterozoic (1000 to 542 Ma) may, in part, be tied to an enhanced bioavailable marine Zn reservoir accompanying oxygenation of the oceans. This model provides a simple link between the enigmatic and protracted diversification of eukaryotes and the shifting availability of bio-essential metals in a manner akin to a ‘bio-inorganic bridge’ (Anbar and Knoll, 2002).

However, until recently this possibility has yet to be evaluated in light of sedimentary proxies for the evolution of the paleomarine Zn reservoir. A recent examination of the shale record (Scott et al., 2013) indicates that Zn may have been near modern abundances and was likely bioavailable to eukaryotes throughout the Precambrian, casting doubt on the coupled geochemical and eukaryotic evolutions with respect to Zn utilization. Here, guided by new chemical speciation models, we explore eukaryotic evolution as revealed by a ~3.8 billion year record of marine authigenic iron oxide deposition, in the form of Precambrian iron formations, Phanerozoic ironstones and Fe-rich exhalites, herein collectively referred to as iron formations (IF). We use the rock record to shed light on the poorly understood relationships between marine trace metal availability, metalloenzyme proliferation, and biological innovation.

Zn is predominantly bound by organic ligands in modern seawater (e.g., Crawford et al., 2003), but it also occurs in aqueous form, i.e., Zn^{2+}, $Zn(OH)^{+}$, $Zn(OH)_2$, $ZnCO_3$, $ZnSO_4$, and $ZnCl_2$, suspended solids (e.g., ZnS), or adsorbed onto particle (e.g., Zirino and Yamamoto, 1972). Furthermore, Zn may be strongly complexed by aqueous sulfide (Luther et al., 1996) such that in anoxic environments, where HS^- is present, inorganic bisulfide and potentially polysulfide Zn complexes may play key roles in dominating the speciation of dissolved Zn (e.g., Gardner, 1974). Luther et al. (1999) provide an example of when polysulfides may become dominant, which occurs when 10 μM Zn is titrated with sulfide in excess of 5 μM. In some conditions where a strong redoxcline exists, such as Jellyfish Lake, Palau (Landing et al., 1991), total dissolved Zn concentrations may actually increase at depth due to the formation of aqueous sulfide complexes. The proportion of Zn that is bioavailable is controlled by either sulfide complexation (Luther et al., 1996; Edgcomb et al., 2004) or by organic ligand complexation. However, complicating the issue of bioavailability is recent evidence that suggests organic complexation of Zn may in fact increase the potential for uptake (Aristilde et al., 2012).

In surface layers of the open ocean, horizontal and vertical mixing, atmospheric fallout, biological uptake, and particulate removal are the main

controls on Zn abundance (Bruland, 1980). Accordingly, total dissolved Zn follows a nutrient profile in the modern oceans, where Zn is between ~0.04-0.5 nM in the surface layers, increasing below the photic zone to ~8-10 nM, where it remains relatively constant down to the seafloor (Bruland et al., 1994; Lohan et al., 2002; Nolting and de Baar, 1994). Despite this variability, for the purposes of discussion we assume a concentration of 10 nM as a "modern" value effectively describing the majority of the water column. While uptake in the photic zone could have lead to surface-deplete nutrient-type Zn depth profiles in the deep past, especially if concentrations were limiting, the Zn concentration of deep waters obviously plays an important role in the upward diffusive resupply of Zn (John, 2007) and thus upper water column Zn concentrations.

In terms of the modern zinc budget, inputs from mid-ocean ridge hydrothermal systems (~4.4×10^9 mol/yr) dominate riverine fluxes (~3.4×10^8 mol/yr) by a factor of 13, while diffuse off-axis venting contributes little marine Zn (~1×10^6 mol/yr)(Wheat et al., 2002). However, the efficiency of scavenging of hydrothermal zinc is poorly constrained. Modern aeolian Zn deposition is significant (~$0.7 - 3.5 \times 10^9$ mol/yr), although roughly 75% is anthropogenic (Duce et al., 1991). Modern sinks are poorly constrained but likely include organic matter, metal hydroxides, and sulfide burial fluxes. Modern hydrothermal fluids, the primary natural Zn input, are enriched by 16,000 - 88,000 times the seawater Zn value at their source (Doe, 1994), but these values drop significantly with distance from the vent due to seawater dilution and Zn incorporation into sulfide and metal hydroxide phases (Trocine and Trefry, 1988; German et al., 1991). Given higher mantle recycling rates (e.g., Sleep and Windley, 1982), we consider a hydrothermal Zn component to be more relevant during the Precambrian. Under anoxic and ferruginous (Fe-rich) seawater conditions, with Fe(II)>S(-II) as required for iron(III) oxyhydroxide formation, it is likely that hydrothermal Zn would have dispersed over wider areas of the deep ocean for a lack of an effective sink, with a spatial distribution and areal extent similar to Fe in the case of Precambrian iron formations (e.g., 10^6 km^2 in the Hamersley basin; Morris, 1993).

Based on the low solubility of Zn sulfide minerals and the formation of strong aqueous Zn-S complexes, expanded euxinia during the late Paleoproterozoic and Mesoproterozoic has been proposed to have limited the bioavailability of Zn and other sulfide-reactive trace metals (e.g., Cu, Cd), and thereby influenced metallome evolution (Williams and Da Silva, 1996; Sunda and Huntsman, 1995; Saito et al., 2003). However, recent work suggests that Proterozoic oceans were almost certainly laterally heterogeneous in their geochemical characteristics (e.g., Planavsky et al., 2011), such that sulfidic conditions may have been limited to shallow or coastal areas (e.g., Poulton et al., 2010). Such considerations therefore warrant a re-examination of trace metal evolution in the context of a dominantly ferruginous Proterozoic ocean, especially with regards to elements vital for eukaryotic evolution such as Zn. Precambrian authigenic iron oxides, comprising laterally extensive IF that are highly Fe-rich and S-poor, necessitate Fe-rich and sulfide-poor conditions at the time of their deposition (Klein, 2005; Bekker et al., 2010). In this regard, the Precambrian IF record may be considered to represent large areas with conditions where Fe(II)>>S(-II). Such chemical deposits thus record ancient seawater where no strong euxinic metal sink was locally present; this makes the IF record an ideal target for exploring paleomarine concentrations of Zn.

2.2 Methods

Geochemical equilibrium calculations (Fig. 2-1) were performed using Visual MINTEQ 3.0 (Gustafsson, 2011) and the primary thermodynamic database provided (thermo.vdb) was modified to account for multiple aqueous Zn sulfide complexes as well as Zn complexation by organic ligands (Appendix Table A1-1). Modeling conditions included seawater-like salinity (0.56 M NaCl), standard temperature (25ºC), the exclusion of molecular O_2 and a pCO_2 of 10 times present atmospheric levels (PAL). Calcium, pH and Fe were determined by equilibrium reactions with excess calcite and siderite. Redox considerations were omitted such that all Fe and S species are +II and –II, respectively. Supersaturated minerals were permitted to precipitate and activity corrections were made using the Davies

equation. Figure 2-1 presents chemical equilibrium models of speciation in the Fe(II)-S(-II)-Zn-organic-ligand system in terms of molar concentrations and mineral saturation indices (IAP/K_{sp}) and as a function of increasing total system sulfide concentration (sulfide in both dissolved form and bound in minerals). In this model, Fe(II) is available at concentrations in equilibrium with siderite (as per Holland, 1984), pH is determined by equilibrium with siderite and calcite at pCO_2 = 10X PAL (present atmospheric level). We consider a pCO_2 of 10 times PAL as an intermediate value between high-end estimates for pre-1.8 Ga (>100 PAL, Ohmoto et al., 2004) and the modern. Total zinc is fixed at an approximately modern value of 10^{-8} M (consistent with Zn concentrations derived from the IF record presented below, as well as those used by Saito et al., 2003), and the system is effectively titrated with increasing quantities of sulfide (total S-II added).

Our dataset of Zn in authigenic iron oxides includes new analyses and a comprehensive literature compilation (refer to Appendix Table A1-2 and associated references). We assign iron formations to one of four broad categories – Algoma IF, Superior IF, ironstones, and Phanerozoic hydrothermal deposits. Algoma IF are characterized by limited areal extent and close association with submarine volcanic sources. Superior IF are laterally extensive and typically formed on continental shelves. Ironstones encompass Precambrian granular and oolitic iron formations, as well as more modern iron oolite-pisolite occurrences that formed in shallow, nearshore environments. Phanerozoic hydrothermal deposits represent modern, oxic seawater deposits where Fe(III) deposition occurred near hydrothermal sources (Bekker et al., 2010).

Zn was analyzed in drill core and fresh hand samples (i.e., samples collected in the field from outcrop), which were sub-sampled, then powdered and subjected to trace element analysis. Importantly, samples showing evidence of weathering, alteration or signs of severe metamorphic or diagenetic overprinting were excluded. Exclusion criteria include association with a lateritic profile, Fe concentrations greater than 60%, extensive veining, for all but Eoarchean samples recrystallization of chert to macrocrystalline quartz, intense folding, and above-

greenschist facies metamorphism. Analyses were performed on powder digests or by *in situ* laser ablation (New Wave Research UP-213) using a Perkin Elmer Elan6000 Quadrupole – Inductively Coupled Plasma Mass Spectrometer (Q-ICP-MS) at the University of Alberta (U of A). Precision was monitored by repeated analyses of well-constrained international standards (BE-N Basalt, CRPG Nancy for digests and NIST SRM 610 or 612 for laser ablation). Sample analyses at Woods Hole Oceanographic Institute (WHOI) were conducted on a ThermoElectron Inc. Element 2 high-resolution sector field ICP-MS and precision and accuracy assessed by analysis of USGS geostandard BHVO-1. Sample selection and analytical methods are identical to our previous work (Konhauser et al., 2009, 2011) and are described in detail therein. At the U of A repeated analyses (n = 3) of BE-N produced a value for Zn of 128±19 ppm at the two standard deviation level, comparable to a recommended value of 120±13 ppm. Repeat analyses of laser ablation standards NIST SRM 610 and 612 at the U of A yielded average values of 474±66 ppm (n = 46) and 38.7±5.0 ppm (n=31) at the single standard deviation level. These are comparable to mean literature values for laser ablation of NIST STM 610 and 612 of 469±34 ppm and 40±2 ppm, respectively (Jochum et al., 2011). At WHOI repeated analysis of BHVO-1 produced a value for Zn of 91±19 ppm at the two standard deviation level, compared to a recommended value of 105±5ppm.

From a database of over 3800 new and literature IF analyses, 1660 have available Zn data, and of those, 590 samples passed filters for detrital contamination (<1% Al_2O_3 and <0.1% TiO_2; Fig. 2-2) and compatible mineralogy; the unfiltered and filtered records are presented in Fig 2-3A and B, respectively. Compatible mineralogies were restricted to Fe and Si-rich chemical sediments, thereby excluding volcanics, sulfides, and carbonates. For authigenic iron oxide sediments with low detrital contamination, molar Zn and Fe data were compared to hypothetical partitioning scenarios to constrain potential paleomarine Zn concentrations.

The simple partitioning models presented herein (lines in Figure 2-4) constitute an effort towards developing trace element proxies in IF that are better

informed by the rock record itself and are independent of experimentally-determined partition coefficients. The slope in Zn-Fe space (a Zn/Fe ratio) is calculated by assuming quantitative precipitation of both Zn and Fe from a given volume of seawater, such that hypothetical seawater Zn and Fe concentration scenarios may be compared directly with rock record data. In reality, only a fraction of total dissolved Zn will be removed at any given time, but as this is also the case with Fe, and as Zn adsorption depends on available Fe(III) oxyhydroxide surface sites, partial co-removal of Zn and Fe approaches the scenario of quantitative removal proposed by the simple, hypothetical partitioning scenarios.

The hypothetical partitioning scenarios presented in Figure 2-4 are dependent on several important assumptions: (1) that adsorption occurred to Fe(III) oxyhydroxides, such that any particular trace element should scale with Fe (but not Si), (2) that maximum dissolved Fe concentrations may be constrained (as per Holland, 1984) by either mineral solubility (e.g., ~1-10 ppm for siderite) or sedimentation rate (e.g., 20 mg/cm^2 per year under a water column of at least 100 m, thus 2 ppm), and (3) that Zn and Fe precipitated quantitatively. Assumption (1) is supported by Fig. 2-4, and while assumption (3) is unlikely, it is conservative in that a maximum estimate of partitioning efficiency and thus a minimal potential seawater concentration is achieved.

2.3 Results

Results of the geochemical models are presented in Figure 2-1 and described in detail herein. Mineral saturation indices (upper dashed lines) indicate that saturation with respect to sphalerite is achieved at total sulfide concentrations over 10^{-9} M and limits total dissolved Zn (combination of Zn^{2+} and ZnS) thereafter. Total sulfide concentrations above 5×10^{-5} M (saturation with respect to mackinawite) are effectively excluded by the S-poor mineralogy of IF samples. Three models are considered: (1) in the absence of organic ligands (Fig. 2-1A), (2) with 1 nM of an uncharacterized organic ligand binding Zn^{2+} with a conditional log K of 11, as described for Central North Pacific seawater by

Bruland (1989)(Fig. 2-1B), and (3) with 100 nM of the same organic ligand, as a sensitivity test for historical differences in the availability of organic ligands (Fig. 2-1C). In all models, total Zn concentration is effectively limited by the sulfide-dependent solubility of sphalerite. In the absence of organic complexation (Fig. 2-1A), it can be seen that the hydrated metal aquo complexes of Zn^{2+} and Fe^{2+} dominate under all conditions, with the exception of the highest permitted sulfide concentrations, where Zn^{2+} and $ZnS_{(aq)}$ become approximately equimolar (see discussion). When organic complexation of zinc is considered, at modern concentrations of strong Zn binding ligands (~1-3 nM, Bruland, 1989; Jakuba et al., 2012), organic zinc complexes quickly become the dominant form of dissolved Zn. When total S(-II) is further increased, sphalerite precipitation draws down the total dissolved reservoir to parity with the strong Zn binding organic ligand (at ~10^{-7} M total S(-II) added). In the case of Zn-binding organic ligand concentrations 100X that of modern (Fig. 2-1C), regardless of the ambient sulfide concentration, the total dissolved Zn pool is effectively dominated by organic complexes, free Zn^{2+} is suppressed even under sulfide-poor regimes, and the total Zn inventory is buffered against sphalerite precipitation losses. While these geochemical models reaffirm a strong role for organic complexation in determining the bioavailable Zn pool, bioavailable Zn^{2+} does not descend significantly below concentrations considered limiting for all organisms investigated (10^{-12} M), unless upper water column depletion of Zn is also considered (see discussion).

Compositional data for modern and ancient authigenic iron oxides are presented in Figures 2-2 through 2-4. Zn concentrations in detritally-filtered samples average 130 ppm (nearly twice the upper crustal value of 67 ppm; Rudnick and Gao, 2003), with average molar Zn/Fe ratios of 0.00228 and a standard deviation of 0.0238. For samples with Al or Ti values above detrital filter cutoffs, Zn concentrations tend towards upper crustal values, suggesting an increased Zn contribution from siliciclastic sources (Fig. 2-2); samples below detrital filter cutoffs lack correlation of Zn with Al and Ti but show Zn concentrations that scale with Fe (Fig. 2-4). This indicates authigenic Zn

enrichment conforming to distribution coefficient behavior in these samples. It is likely that Zn was acquired during initial ferric oxyhydroxide precipitation by adsorption processes (e.g., Benjamin and Leckie, 1981), which during the Archean and early Proterozoic, most likely occurred in the marine photic zone (Konhauser et al., 2002; Kappler et al., 2005; Planavsky et al., 2010).

Figure 2-3A-B display all available data and those passing detrital filters, respectively, as a time series of molar Zn/Fe ratios. While significant variability exists at any given time, the overall trend is a relatively static range in Zn/Fe over geological time, except for the most modern samples (see discussion). Figure 2-4A puts these ratios in perspective by presenting simple models for quantitative Zn removal at marine Fe concentrations of 179 μM (10 ppm) and near-modern Zn concentrations of 10 nM (0.65 ppb); nearly all data fall within the range predicted by our models and crucially, indicate paleomarine Zn concentrations within an order of magnitude of modern oceans. An iron concentration of 179 μM was applied as it represents the upper limit of conservative estimates based on the work of Holland (1984) and would subsequently correspond to the lowest estimate of paleomarine Zn (i.e., decreasing Fe from 179 to 17.9 μM results in increasing estimates for paleomarine Zn).

At assumed Fe concentrations of 179 μM, a minimum Zn concentration of 0.1 nM is indicated by Zn/Fe ratios preserved in ancient iron oxides, yet the majority of samples are well represented by a concentration within 10-fold of modern Zn values (Fig. 2-4A). Estimates are considered conservative as our models assume 100% adsorption of Zn onto the primary ferric oxyhydroxide; this quantitative scavenging relationship represents maximum possible partitioning efficiency and thereby returns a minimum possible concentration; partial Zn adsorption would lead to increased estimates for paleomarine Zn concentrations. Conversely, increased dissolved Fe concentrations would result in a decreased estimate of paleomarine Zn concentrations. However, even at a high-end estimate of 1790 μM Fe, realistic only for essentially undiluted hydrothermal fluids (Edmond et al., 1982) and ~30X higher than limits imposed by siderite solubility (Holland, 1984), near modern Zn levels are still indicated by the authigenic iron

mineral record (Fig. 2-4B). There exists a high level of agreement between the filtered and unfiltered records in this regard (Fig. 2-3; Appendix Fig. A1-1).

2.4 Discussion

Zn/Fe ratios in IF through time appear relatively constant (Fig. 2-3) despite dramatic changes in ocean chemistry from the Archean to today. The spread in Zn enrichments may be related to (1) vertical/lateral paleomarine spatial variability, (2) local or short-term fluctuations in the marine Zn reservoir, or (3) diagenetic effects. Firstly, it is anticipated that vertical/lateral spatial variability might be similar to that of modern oceans where Zn concentrations are heterogeneous between, and within, ocean basins. In terms of vertical distribution in the Precambrian, we expect that similar to today, enriched Zn fluids would resupply a depleted photic zone via diffusion and advection from deep waters. Future work examining Zn isotope compositions may reveal whether ancient upper water columns were depleted due to biological activity (c.f. Kunzmann et al., 2013). As the precipitation of metastable IF precursor minerals (e.g., ferrihydrite) likely occurred in the photic zone (e.g., Konhauser et al., 2002; Kappler et al., 2005), it is possible that the spread in IF values record dynamics in depletion of the upper water column. Secondly, it is a possibility that variation within a single basin (and thus IF deposit) may be driven by potential pulse-like influxes of Zn along with Fe resulting from episodic hydrothermal activity as well as a potential drawdown of Zn due to protracted IF deposition. Events such as these may account for the highest and lowest Zn/Fe ratios, respectively. Thirdly, little information is available regarding further Zn adsorption or release upon iron mineral diagenesis or metamorphism. Experimental data indicates that for Zn-ferrihydrite co-precipitates, aging and mineral transformation, with or without added organics, has little effect on equilibrium Zn solubility (Martinez and McBride, 1999). With regards to metamorphism, Bhattacharya et al. (2007) presented a suite of IF data from the Jharkhand-Orissa region, that showed similar Zn concentrations between hydrothermally metasomatized IF and ‘unaltered’ IF in the same region. In addition, samples used in our analyses were devoid of obvious supergene

alteration (i.e., severe chert re-crystallization, martite formation). These results, combined with the relatively coherent rock record dataset provided here, suggest minimal post-depositional Zn mobilization in IF. Given the comprehensive nature of our dataset, there are likely to be some samples that have been affected by secondary mineralization. Mineralization, however, is very unlikely to explain the overall trend of Zn abundances, a trend that differs from other elements that are commonly enriched during secondary mineralization (e.g., Cu, U) (Davidson and Large, 1994; Verma et al., 2003; Tallarico et al., 2005).

In addition to the three factors described above, variability in the IF record may reflect subtle changes in the reactivity of the solid-phase iron minerals for dissolved Zn. When considering only Precambrian data, linear regression between Zn and Fe is poorly supported (Appendix Figure A1-1B); this may reflect variable contribution of less reactive and Zn-poor reduced iron minerals such as siderite or greenalite, which would also introduce variability in Zn/Fe ratios for any given deposit. Regression between Zn and Fe for Phanerozoic samples is more robust, and along similar lines might reflect a fully oxidized and thus consistently zinc-reactive aspect of Phanerozoic hydrothermal iron precipitates. Indeed, a 10-100 fold increase in the Zn/Fe ratio of recent sediments may reflect the rapidity of Fe(III) precipitation under a fully oxygenated water column, resulting in increased contribution of Zn from enriched hydrothermal fluids proximal to modern vents. Under oxic conditions, iron mineral precipitation in closer proximity to hydrothermal sources, as well as a lack of co-precipitating reduced and thus Zn-poor iron mineral phases, could explain both the tighter relationship between Zn and Fe and the recent rise in Zn/Fe observed for the Phanerozoic.

In pyritic marine sediments, there is an apparent relationship between the degree to which a metal is preferentially hosted in pyrite (degree of trace metal pyritization, DTMP) and log $K_{metal\text{-}S}/K_{FeS}$ (see Morse and Luther, 1999; their Figure 2-3). This feature is akin to a linear free-energy relationship between the equilibrium partitioning of trace metals into pyrite and the equilibrium solubility of individual trace metal sulfide mineral phases, and is characteristic of trace metal substitution into pyrite (Morse and Luther, 1999). Zn, as well as Cd and Pb,

depart significantly from this trend in that they are anonymously low in concentration in the pyrite fraction of pyritic marine sediments, indicating that these elements are primarily sequestered as independent mineral phases rather than as a minor constituent of pyrite, likely as a natural consequence of the faster kinetics of their precipitation as metal sulfides (Morse and Luther, 1999). Accordingly, sphalerite (ZnS) solubility imposes an upper boundary on dissolved Zn in the presence of sulfide (e.g., Hsu-Kim et al., 2008). The formation of strong Zn-S complexes may further act to limit free Zn^{2+} under euxinic conditions (e.g., Landing and Lewis, 1992). Geochemical modeling (Fig. 2-1) demonstrates that under the ferruginous conditions necessary for the deposition of Precambrian IF, aqueous complexation and drawdown of bioavailable Zn^{2+} by sulfide may not be as important as previously thought. Saito et al. (2003) performed similar speciation calculations for Co, Fe, Mn, Zn, Ni, Cu, and Cd under hypothetical 'ferro-sulfidic' Archean ocean conditions, and indicated that the vast majority (>99%) of dissolved Zn should be complexed with sulfide as $ZnS_{(aq)}$. However, upon re-examination of Zn speciation for this study, it appears the conditional stability constant of the $ZnS_{(aq)}$ species was not parameterized correctly in Saito et al. (2003), leading to an overestimation of this species' abundance, while the other metal species were correctly parameterized. In our current modeling effort, such high degrees of aqueous Zn complexation by sulfide do not occur until well after supersaturation with respect to mackinawite (FeS) is reached (Fig. 2-1). Such high sulfide concentrations are effectively excluded by the fact that, with the exception of some highly reduced Algoma-type iron formations, iron sulfide minerals are typically absent. A lack of correlation between Zn and S in our dataset (see Appendix Fig. A1-2) further suggests a minimal role for S in Zn sequestration under Fe(III) oxyhydroxide depositional conditions. Several limitations also exist with respect to the thermodynamic modeling of ZnS complexes. For instance, modeling is dependent on the stoichiometry of modeled ZnS complexes and their respective stability constants; Rickard and Luther (2006) provide a short summary of ZnS complexation and list eleven possible ZnS complexes, several for which stability constants vary depending on the method used for determination.

In ancient oceans heterogeneous with respect to sulfide content (e.g., Poulton et al., 2010; Planavsky et al., 2011) and where sulfide effectively titrates iron such that the siderite-buffering effect inherent to our models no longer occurs, it is possible that bioavailable Zn would have been drawn down below biolimiting concentrations in sulfide-rich zones as per Saito et al. (2003). However, these zones were likely restricted to near shore and other high productivity regions of the oceans (e.g., Poulton et al., 2010). In such instances, Zn may have been buffered against sulfide by organic ligand complexation (Fig 2-1B and C), potentially becoming bioavailable again once reaching the overlying oxic or underlying ferruginous waters. It seems unlikely given the consistency of the shales and IF record (Scott et al., 2013; this work), that sulfide water masses controlled Zn bioavailability throughout much of the Precambrian. Accordingly, the Zn speciation models presented here for IF depositional conditions imply that bioavailable (non-complexed) Zn may well have been abundant and readily available to primitive eukaryotes.

An important alternative to the modeling described thus far is the possibility that strong and persistent organic complexes of zinc may have played an important role in controlling Zn solubility, speciation and possibly bioavailability. This scenario is modeled in Figures 2-1B and 2-1C, and demonstrates that organic complexation of Zn plays a crucial role in determining the speciation of the reservoir, such that whenever the concentrations of strong Zn-binding organic ligands approach that of total dissolved Zn, organic Zn complexes will dominate the dissolved pool. Considering that poorly-ventilated and reducing ocean conditions would have acted to stabilize strong organic ligands in seawater, such as those with reduced sulfur groups (e.g., thiols and cysteine-rich peptides), the possibility that organic complexation of Zn played a more important role in the Precambrian cannot be excluded. It, therefore, represents a strong caveat to the interpretations presented herein, potentially limiting the bioavailability of Zn. Interestingly in the modern ocean, strong Zn-complexing ligands appear only in the upper water column (Bruland, 1989; Jakuba et al., 2012) where they are likely continually produced by microbial

phytoplankton (Lohan et al., 2002). By contrast, in the deeper oxygenated water column, these ligands are subsequently oxidized, and the sorbed Zn is released back into solution. How this potential scenario would have influenced the evolution of nutritional requirements is not clear; there is recent data indicating that the complexation of Zn by organic ligands can actually enhance phytoplankton Zn uptake (Aristilde et al., 2012). Such high affinity systems may have come at a metabolic cost, but could also have allowed access to this useful structural metal cation. It should be emphasized that the bioavailability of Zn-organic ligand complexes has a strong bearing on the interpretation of the second scenario. If Zn bound by organic ligands was indeed bioavailable in the Precambrian, it would suggest that under any of the conditions postulated here, Zn would be bioavailable to early eukaryotes. This would effectively represent a case where the two proposed scenarios become complimentary.

The two chemical speciation scenarios presented here, both constrain the bioavailable Zn inventory and have significant implications for paleomarine Zn geochemistry. In the first scenario where Zn speciation was not dominated by organic complexes, periods of ocean euxinia would have caused significant depletion of the oceanic Zn inventory due to precipitation of sphalerite with increased oceanic sulfide abundances (Fig. 2-1A). Such events may not have been captured by the IF record presented here due to the chemical incompatibility of extensive euxinia and the deposition of IF, but should be observable in parallel shale records (Scott et al., 2013). Periods of expanded euxinia could have conceivably caused considerable oceanic Zn inventory instability, which itself could have been a temporal selection pressure against early adoption of Zn ions in metalloenzymes. However, relatively stable sedimentary concentrations indicated by both the IF (this work) and shale records (Scott et al., 2013) may be envisioned as a result of the second scenario, where oceanic Zn speciation is dominated by organic complexes such that the total Zn inventory would have remained stabilized despite large scale variations in the extent of euxinic marine conditions (Fig. 2-1C). Direct measurement of low-level Zn speciation conditions in analogous modern environments may contribute to our understanding of which of

these scenarios may have dominated. Moreover, future modeling work is planned to better understand the factors controlling the aqueous complexation of zinc by sulfide and organic ligands, and their sensitivity to model presuppositions under ferruginous and euxinic ancient ocean chemistry scenarios.

The persistence of a zinc inventory on the order of magnitude of modern oceans throughout history is particularly curious given the late expansion of Zn-binding domains in eukaryotes (Dupont et al., 2006; 2010). It is possible that the relatively late expansion of Zn-binding proteins over the course of eukaryotic metallome evolution reflected the regulatory needs inherent to increasingly complex genomes (see also Scott et al., 2013). Late-evolving Zn-binding domains in eukaryotic genomes are predominately structural and localized to the nucleus, specifically in DNA regulating elements (Dupont et al., 2010). Power-law scaling of Zn-binding domains as a function of total proteome size is >1 for *Eukarya* but <1 for *Archaea* and *Bacteria* (c.f. Fig S1 from Dupont et al., 2010). Essentially, eukaryotic genomes possess greater numbers of Zn-binding proteins with increasing genome size while prokaryotic genomes follow the opposite trend, suggesting that the difference in metallome composition may reflect the dramatic differences in eukaryotic and prokaryotic genome regulation. The proliferation of structural, nucleus-bound Zn-binding domains should be expected to accompany rapid evolutionary innovation during late Proterozoic eukaryote diversification in body plans. Future phylogenetic work examining the expansion of eukaryotic Zn-binding domains in light of their specific roles in eukaryotic homeostasis may be able to confirm or deny such a hypothesis. Despite uncertainties relating to organic complexation of Zn in ancient oceans, this work provides important constraints and insight into the evolution of the Zn metallome, and the possibilities regarding intrinsic and biological influences, versus extrinsic and geochemical, driving forces.

2.5 Conclusion

We conclude that the record of Zn enrichments in IF points toward a relatively constant marine Zn reservoir through geological time, with paleomarine

concentrations within an order of a magnitude of modern values throughout much of the Precambrian. Equilibrium speciation modeling reveals that under IF depositional conditions and modern organic ligand concentrations, the Zn reservoir should have been dominated by free and bioavailable Zn^{2+}, with aqueous Zn complexation by sulfide becoming important (>50% of the total dissolved reservoir) only at sulfide concentrations reaching FeS mineral saturation. Our finding of a near modern bioavailable Zn reservoir through time as recorded by the IF record, and supported by detailed geochemical models, is also in line with that of the other common sedimentary proxy for paleomarine conditions, the euxinic shale record (Scott et al., 2013). The agreement between these records testifies to the robustness of the model presented here. Furthermore, strong organic complexes of Zn, for example involving structures with reduced sulfur groups of high Zn affinity, may have been more important in ancient oceans for lack of an oxidative sink. This may have allowed stabilization of the Zn inventory through both ferruginous and euxinic ocean conditions, but potentially may have depressed Zn bioavailability, as the availability of Zn-organic complexation is not fully understood.

Together, this IF-based inventory and chemical speciation study places constraints on our understanding of the geochemical evolution of the Precambrian Zn reservoir and its potential coupling to eukaryotic metallome evolution. A novel possibility stemming from this work is that the late proliferation of Zn metalloenzymes in eukaryotes could have been a biologically intrinsic process related to the regulation of increasingly complex genomes, rather than solely dependent on the dramatic changes in the marine bioavailability of aqueous Zn species.

a)

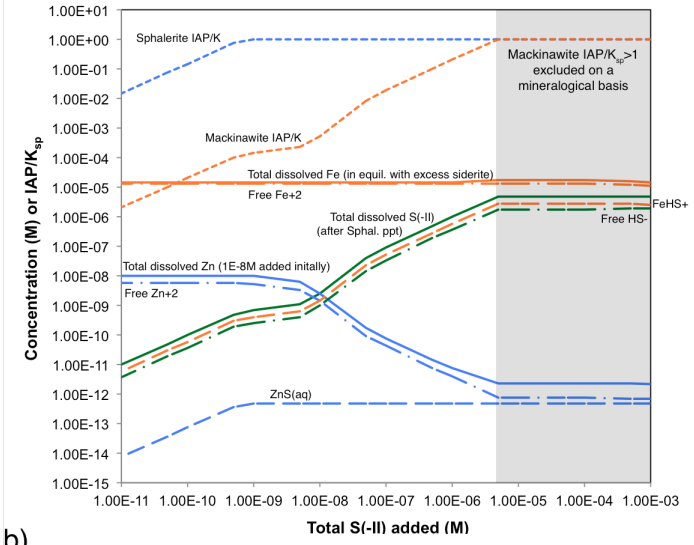
Concentration (M) or IAP/K$_{sp}$
Total S(-II) added (M)
Sphalerite IAP/K
Mackinawite IAP/K$_{sp}$>1 excluded on a mineralogical basis
Mackinawite IAP/K
Total dissolved Fe (in equil. with excess siderite)
Free Fe+2
Total dissolved S(-II) (after Sphal. ppt)
FeHS+
Free HS-
Total dissolved Zn (1E-8M added initally)
Free Zn+2
ZnS(aq)

b)

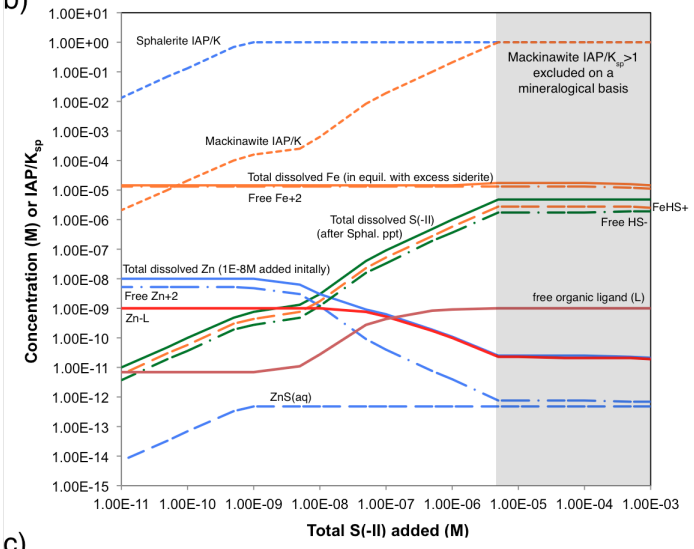
Concentration (M) or IAP/K$_{sp}$
Total S(-II) added (M)
Sphalerite IAP/K
Mackinawite IAP/K$_{sp}$>1 excluded on a mineralogical basis
Mackinawite IAP/K
Total dissolved Fe (in equil. with excess siderite)
Free Fe+2
Total dissolved S(-II) (after Sphal. ppt)
FeHS+
Free HS-
Total dissolved Zn (1E-8M added initally)
Free Zn+2
Zn-L
free organic ligand (L)
ZnS(aq)

c)

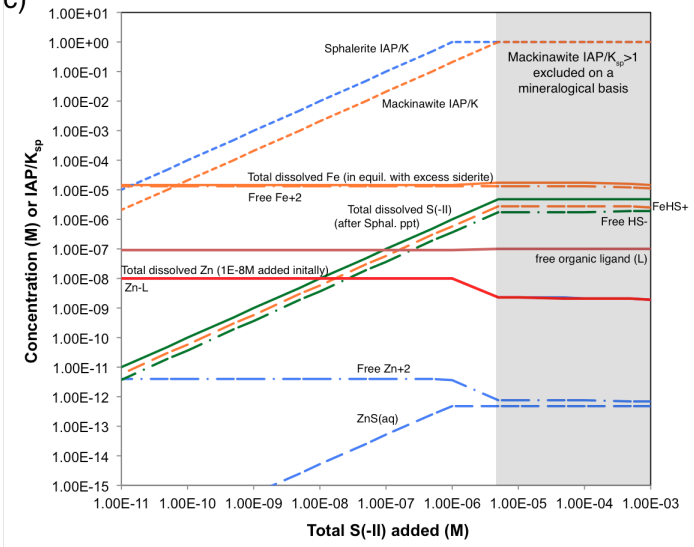
Concentration (M) or IAP/K$_{sp}$
Total S(-II) added (M)
Sphalerite IAP/K
Mackinawite IAP/K$_{sp}$>1 excluded on a mineralogical basis
Mackinawite IAP/K
Total dissolved Fe (in equil. with excess siderite)
Free Fe+2
Total dissolved S(-II) (after Sphal. ppt)
FeHS+
Free HS-
free organic ligand (L)
Total dissolved Zn (1E-8M added initally)
Zn-L
Free Zn+2
ZnS(aq)

Figure 2-1. Modeled chemical equilibrium concentrations for major Zn and Fe species and mineral saturation indices (IAP/K_{sp}) as a function of total sulfide (HS^-) added for simulated seawater with (A) no organic complexation, (B) organic complexation as described for central north Pacific seawater (Bruland, 1989), and (C) same as (B) but with 100X higher organic ligand concentration. Blue lines represent inorganic Zn species, orange lines represent inorganic Fe species, green lines represent sulfide species, and red/burgundy lines represent organic ligands. Modeling was performed with visual MINTEQ 3.0 (Gustafsson, 2011) under anoxic conditions, at 25°C, 0.56 M NaCl and a pCO_2 of 10 times present atmospheric levels. Zn and Fe hydroxide and chloride species were also considered but are not plotted. The default thermodynamic database was adapted to account for multiple ZnS complexes and organic complexation (Appendix Table A1-1). Saturation with respect to calcite and siderite was assumed in all models and ultimately determined Ca and Fe concentrations, as well as pH, the latter ranging from 7.70 – 7.74 over the S(-II) range considered. Zn-S complexes included in Appendix Table A1-1, but not present in Figure 2-1, are not indicated to exist at significant levels. Mineral saturation indices equal to one indicates saturation; in this model supersaturation was not permitted, such that changes in total dissolved Zn and Fe are directly linked to mineral precipitation or dissolution. The grey area represents saturation with respect to Mackinawite and is excluded by the sulfide-deplete mineralogy of IF.

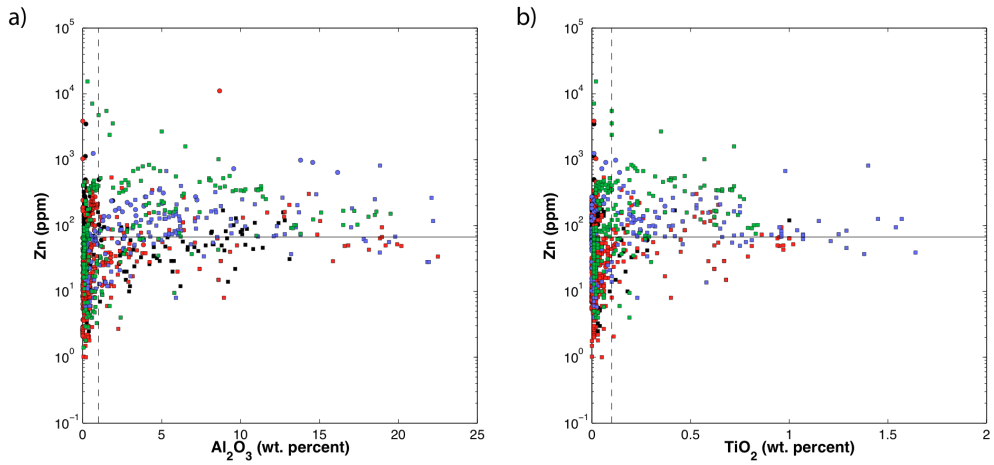

Figure 2-2. Cross-plots of Zn versus (A) Al_2O_3 and (B) TiO_2. Dashed lines represent detrital contamination cutoffs of 1 and 0.1 weight percent for Al_2O_3 and TiO_2, respectively. Black lines correspond to crustal values for Zn (67 ppm (Rudnick and Gao, 2003)) and indicate that above these cutoffs, Zn in IF approach crustal values. Colors correspond to varying IF types: Algoma (black), Superior (red), ironstone (blue) and Phanerozoic hydrothermal (green); c.f. methods. Additionally, circles represent laser ablation data and squares indicate analyses after bulk digestion.

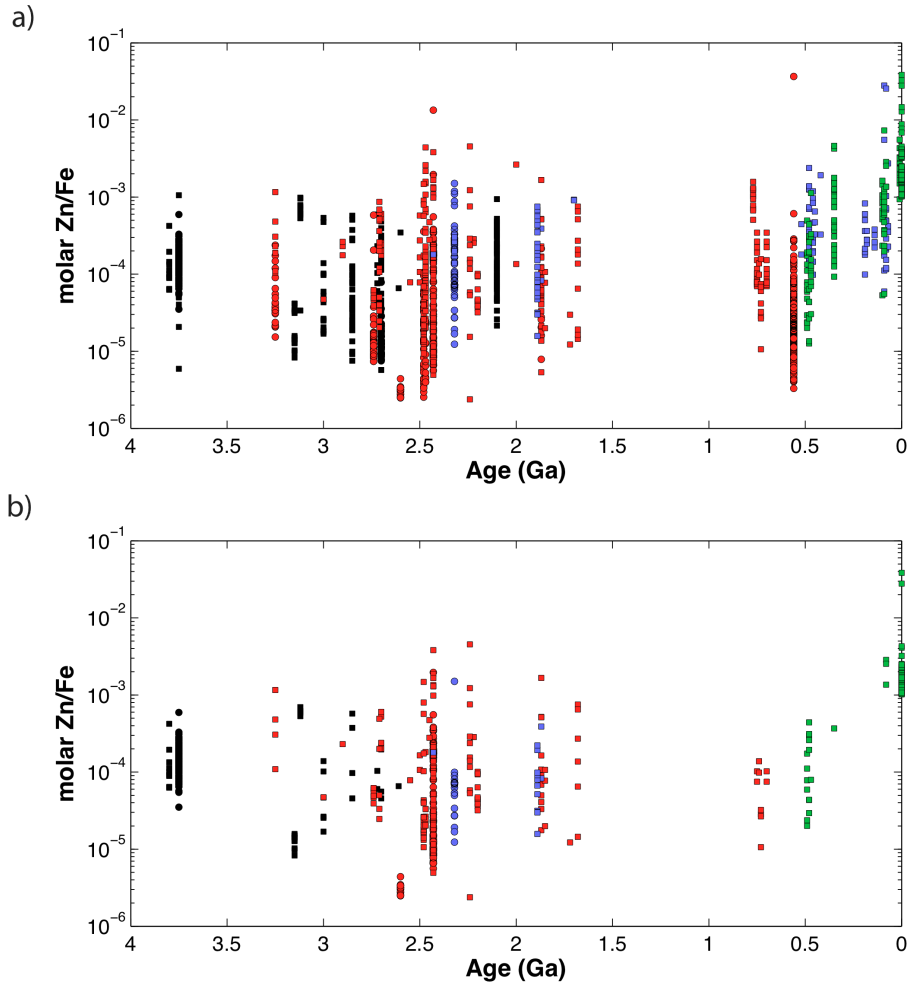

Figure 2-3. (A) Unfiltered record of available molar Zn/Fe data in authigenic iron oxides through time, comprising Precambrian iron formation, Phanerozoic ironstones, and exhalites. When samples with appreciable detrital or hydrothermal influence are included in the record, there is a greater degree of variation than in the filtered record (B) Molar Zn/Fe ratios in authigenic iron oxides, spanning Archean through Proterozoic IF, Phanerozoic ironstones and exhalites; filtered for detrital contamination as per Figure 2-2. Variability in Zn/Fe ratios at a given time may reflect heterogeneous marine Zn distributions, temporal variations (e.g., Zn drawdown during protracted deposition), or potential diagenetic modification. Importantly, no Zn/Fe data exists in our compilation that suggests the low, biolimiting dissolved Zn concentrations previously predicted by chemical equilibrium models for Precambrian oceans (Saito et al., 2003). Symbols as per Fig. 2-2.

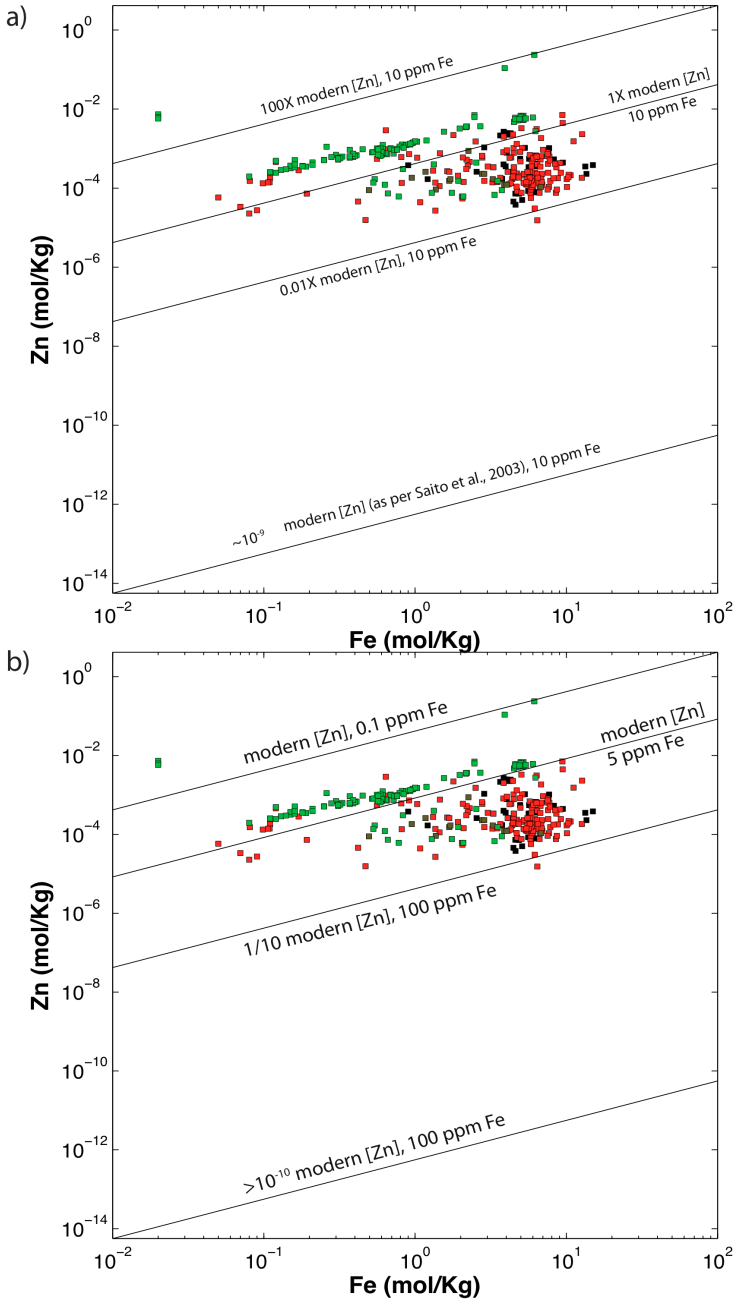

Figure 2-4. (A) Zn-Fe cross plot revealing paleomarine Zn partitioning recorded by the authigenic iron oxide record. Lines represent conservative models of Zn-Fe co-precipitation behavior for hypothetical paleomarine Zn and Fe reservoirs, including those previously predicted by chemical equilibrium modeling (Saito et al., 2003). Near-modern paleomarine Zn concentrations are clearly indicated

regardless of sample age. (B) Zn-Fe cross plot further restricting paleomarine Zn concentrations under expanded boundaries of hypothesized paleomarine Fe conditions. Even at elevated Fe concentrations of 1790 μM (100 ppm), a dissolved Zn concentration of ~1/10 of modern (1 nM) is indicated. At low total Fe concentrations (1.79 μM), a dissolved Zn concentration of ~10 nM, effectively that of modern oceans, is still indicated. Symbols as per previous figures.

2.6 References

Anbar AD, Knoll AH (2002) Proterozoic ocean chemistry and evolution: A bioinorganic bridge? *Science*, **297**, 1137-1142.

Aristilde L, Xu Y, Morel FMM (2012) Weak organic ligands enhance zinc uptake in marine phytoplankton. *Environmental Science and Technology*, **46**, 5438-5445.

Bhattacharya HN, Chakraborty I, Ghosh KK (2007) Geochemistry of some banded iron-formations of the archean supracrustals, Jharkhand-Orissa region, India. *Journal of Earth System Science*, **116**, 245-259.

Bekker A, Slack JF, Planavsky N, Krapež B, Hofmann A, Konhauser KO, Rouxel OJ (2010) Iron Formation: The sedimentary product of a complex interplay among mantle, tectonic, oceanic and biospheric processes. *Economic Geology*, **105**, 468-508.

Benjamin MM, Leckie JO (1981), Multiple-site adsorption of Cd, Cu, Zn, and Pb on amorphous iron oxyhydroxide. *Journal of Colloid and Interface Science*, **79**, 209-221.

Berg JM, Shi Y (1996) The galvanization of biology: a growing appreciation for the roles of zinc. *Science*, **271**, 1081-1085.

Brand LE, Sunda WG, Guillard RRL (1983) Limitation of marine phytoplankton reproductive rates by Zinc, Manganese, and Iron. *Limnology and Oceanography*, **28**, 1182-1198.

Bruland KW (1980) Oceanographic distributions of cadmium, zinc, nickel, and copper in the north pacific. *Earth and Planetary Science Letters*, **47**, 176-198.

Bruland KW (1989) Complexation of Zinc by natural organic ligands in the Central North Pacific. *Limnology and Oceanography*, **34**, 269-285.

Bruland KW, Orians KJ, Cowen JP (1994) Reactive trace metals in the stratified central North Pacific. *Geochimica et Cosmochimica Acta*, **58**, 3171-3182.

Crawford DW, Lipsen MS, Purdie DA, Lohan MC, Statham PJ, Whitney FA, Putland JN, Johnson WK, Sutherland N, Peterson TD, Harrison PJ, Wong CS (2003) Influence of zinc and iron enrichments on phytoplankton growth in the Northeastern Subarctic Pacific. *Limnology and Oceanography*, **48**, 1583-1600.

Coale KH, Michael Gordon R, Wang X (2005) The distribution and behavior of dissolved and particulate iron and zinc in the Ross Sea and Antarctic circumpolar current along 170ºW. *Deep Sea Research I*, **52**, 295-318.

Davidson GJ, Large RR (1994) Gold metallogeny and the copper-gold association of the Australian Proterozoic. *Mineralium Deposita*, **29**, 208-223.

Doe BR (1994) Zinc, copper, and lead in mid-ocean ridge basalts, and the source rock control on Zn/Pb in ocean-ridge hydrothermal deposits. *Geochimica et Cosmochimica Acta*, **58**, 2215-2223.

Duce RA, Liss PS, Merrill JT, Atlas, EL, Buat-Menard P, Hicks BB, Miller MJ, Prospero JM, Arimoto R, Church TM, Ellis W, Galloway JN, Hansen L, Jickells TD, Knap AH, Reinhardt KH, Schneider B, Soudine A, Tokos JJ, Tsunogai S, Wollast R, Zhou M (1991) The atmospheric input of trace species to the world ocean. *Global Biogeochemical Cycles*, **5**, 193-259.

Dupont CL, Yang S, Palenik B, Bourne PE (2006) Modern proteomes contain putative imprints of ancient shifts in trace metal geochemistry. *Proceeding of the National Academy of Sciences*, **103**, 17822-17827.

Dupont CL, Butcher A, Valas RE, Bourne PE, Caetano-Anollés G (2010) History of biological metal utilization inferred through phylogenetic analysis of protein structures. *Proceedings of the National Academy of Sciences*, **107**, 10567-10572, doi: 10.1073/pnas.0912491107.

Edgcomb VP, Molyneaux SJ, Saito MA, Lloyd K, Böer S, Wilson CO, Atkins MS, Teske A (2004) Amelioration of metal toxicity by sulphide for Archaea at deep-sea hydrothermal vents. *Applied Environmental Microbiology*, **70**, 2551-2555.

Edmond JM, Von Damm KL, McDuff RE, Measures CI, (1982) Chemistry of hot springs on the East Pacific Rise and their effluent dispersal. *Nature,* **297**, 187-191.

Franck VM, Bruland KW, Hutchins DA, Brzezinski MA (2003) Iron and zinc effects on silicic acid and nitrate uptake kinetics in three high-nutrient, low-chlorophyll (HNLC) regions. *Marine Ecology Progress Series*, **252**, 15-33.

Gardner LR (1974) Organic versus inorganic trace metal complexes in sulfidic marine waters – some speculative calculations based on available stability constants. *Geochimica et Cosmochimica Acta*, **38**, 1297-1302.

German CR, Campbell AC, Edmond JM (1991) Hydrothermal scavenging at the Mid-Atlantic Ridge: modification of trace element dissolved fluxes. *Earth and Planetary Science Letters*, **107**, 101-114.

Gustafsson JP (verified 10 October 2012). Visual Minteq 3.0: http://www2.lwr.kth.se/English/OurSoftware/vminteq.

Holland HD (1984) *The Chemical Evolution of the Atmosphere and Oceans*. Princeton University Press, New Jersey.

Hsu-Kim H, Mullaugh KM, Tsang JJ, Ucel M, Luther GW III (2008) Formation of Zn- and Fe-sulfides near hydrothermal vents at the Eastern Lau Spreading Center: implications for sulfide bioavailability to chemoautotrophs. *Geochemical Transactions*, **9**: 6.

Jakuba RW, Saito MA, Moffett JW, Bidigare B, Xu Y (2012) Dissolved zinc in the North Pacific: Distribution, speciation, and importance to primary producers. *Global Biogeochemical Cycles,* **26**, GB2015.

Jochum KP, Weis U, Stoll B, Kuzmin D, Yang Q, Raczek I, Jacob DE, Stracke A, Birbaum K, Frick DA, Günther D, Enzweiler J (2011) Determination of reference values for NIST SRM 610-617 glasses following ISO guidelines. *Geostandards and Geoanalytical Research*, **35**, 397-429.

John SG (2007) The marine biogeochemistry of zinc isotopes. PhD thesis, MIT/WHOI, Cambridge, Massachusetts, 2007-2008.

Klein C (2005) Some Precambrian banded iron-formations (BIFs) from around the world: Their age, geological setting, mineralogy, metamorphism, geochemistry and origin. *American Mineralogist*, **90**, 1473-1499.

Kappler A, Pasquero C, Konhauser KO, Newman DK (2005) Deposition of banded iron formations by anoxygenic phototrophic Fe(II)-oxidizing bacteria. *Geology*, **33**, 865-868.

Konhauser KO, Hamade T, Raiswell R, Morris RC, Ferris FG, Southam G, Canfield DE (2002) Could bacteria have formed the Precambrian banded iron formation? *Geology*, **30**, 1079-1082.

Konhauser KO, Pecoits E, Lalonde SV, Papineau D, Nisbet EG, Barley ME, Arndt NT, Zahnle K, Kamber BS (2009) Oceanic nickel depletion and a methanogen famine before the Great Oxidation Event. *Nature*, **458**, 750-753.

Konhauser, KO Lalonde SV, Planavsky NJ, Pecoits E, Lyons TW, Mojzsis SJ, Rouxel OJ, Barley ME, Rosìere C, Fralick PW, Kump LR, Bekker A (2011) Aerobic bacterial pyrite oxidation and acid rock drainage during the Great Oxidation Event. *Nature*, **478**, 369-373.

Kunzmann M, Halverson GP, Sossi PA, Raub TD, Payne JL, Kirby J (2013) Zn isotope evidence for immediate resumption of primary productivity after snowball Earth. *Geology*, **41**, 27-30.

Landing WM, Burnett WC, Lyons WB, Orem WH (1991) Nutrient Cycling and the Biogeochemistry of Manganese, Iron, and Zinc in Jellyfish Lake, Palau. *Limnology and Oceanography*, **36**, 515-525.

Landing WM, Lewis BL (1992) Thermodynamic modeling of trace element speciation in the Black Sea. In: *Black Sea Oceanography* (eds. Izdar E, Murray JW). NATO-ASI Series C, **351**, Kluwer Academic Publishers, Netherlands, pp. 125-160.

Lohan MC, Statham PJ, Crawford DJ (2002) Total dissolved zinc in the upper water column of the subarctic North East Pacific. *Deep-Sea Research II: Topical*

Studies in Oceanography, **49**, 5793-5808.

Luther GW, Rickard DT, Theberge S, Olroyd A (1996) Determination of metal (bi)sulfide stability constants of Mn^{2+}, Fe^{2+}, Co^{2+}, Ni^{2+}, Cu^{2+}, and Zn^{2+} by voltammetric methods. *Environmental Science & Technology*, **30**, 671-679.

Luther GW, Theberge SM, Rickard DT (1999) Evidence for aqueous clusters as intermediates during zinc sulfide formation. *Geochimica et Cosmochimica Acta*, **63**, 3159-3169.

Maret W (2001) Zinc biochemistry, physiology, and homeostasis- recent insights and current trends. *Biometals*, **14**, 187-190.

Martinez CE, McBride MB (1999) Dissolved and labile concentrations of Cd, Cu, Pb, and Zn in aged ferrihydrite-organic matter systems. *Environmental Science and Technology*, **33**, 745-750.

Morris RC (1993) Genetic modeling for banded iron-formation of the Hamersley Group, Pilbara Craton, Western Australia. *Precambrian Research*, **60**, 243-286.

Morse JW and Luther GW III (1999) Chemical influences of trace metal-sulfide interactions in anoxic sediments. *Geochimica et Cosmochimica Acta*, **63**, 3373-3378.

Nolting RF, de Baar HJW (1994) Behaviour of nickel, copper, zinc and cadmium in the upper 300 m of a transect in the Southern Ocean (57º-62ºS, 49ºW). *Marine Chemistry*, **45**, 225-242.

Ohmoto H, Watanabe Y, Kumazawa K (2004) Evidence from massive siderite beds for a CO_2-rich atmosphere before ~1.8 billion years ago. *Nature*, **429**, 395-399.

Planavsky NJ, Bekker A, Rouxel OJ, Kamber B, Hofmann A, Knudsen A, Lyons TW (2010) Rare Earth Element and yttrium compositions of Archean and Paleoproterozoic Fe formations revisited: New perspectives on the significance and mechanisms of deposition. *Geochimica et Cosmochimica Acta*, **74**, 6387-

6405.

Planavsky NJ, McGoldrick P, Scott CT, Li C, Reinhard CT, Kelly AE, Chu X, Bekker A, Love GD, Lyons TW (2011) Widespread iron-rich conditions in the mid-Proterozoic ocean. *Nature*, **477**, 448-451.

Poulton SW, Fralick PW, and Canfield DE (2010) Spatial variability in oceanic redox structure 1.8 billion years ago. *Nature Geoscience*, **3**, 486-490, doi: 10.1038/NGEO0889.

Rickard D, Luther III GW (2006) Metal sulfide complexes and clusters. *Reviews in Mineralogy & Geochemistry*, **61**, 421-504.

Robbins LJ, Lalonde SV, Saito MA, Planavsky NJ, Mloszewska AM, Pecoits E, Scott C, Dupont CL, Kappler A, Konhauser KO (2013) Authigenic iron oxide proxies for marine Zinc over geological time and implications for eukaryotic metallome evolution. *Geobiology*, in press.

Rudnick RL, Gao S (2003) Composition of the continental crust. In: Treatise on Geochemistry, Volume 3 (eds. Holland HD, Turekian KK). Elsevier Science, Amsterdam, The Netherlands, p. 1-64.

Saito MA, Moffett JW, Chisholm SW, Waterbury JB (2002) Cobalt limitation and uptake in *Prochlorococcus*. *Limnology and Oceanography*, **47**, 1629-1636.

Saito MA, Sigman DM, and Morel FMM (2003) The bioinorganic chemistry of the ancient ocean: the co-evolution of cyanobacterial metal requirements and biogeochemical cycles at the Archean-Proterozoic boundary? *Inorganica Chimica Acta*, **356**, 308-318.

Scott C, Planavsky NJ, Dupont CL, Kendall B, Gill B, Robbins LJ, Husband KF, Arnold GL, Wing B, Poulton SW, Bekker A, Anbar AD, Konhauser KO, Lyons TW (2013) Bioavailability of zinc in marine systems through time. *Nature Geoscience*, **6**, 125-128.

Shaked Y, Xu Y, Leblanc K, Morel FMM (2006) Zinc availability and alkaline phosphatase activity in *Emiliania huxleyi*: Implications for Zn-P co-limitation in the ocean. *Limnology and Oceanography*, **51**, 299-309.

Sleep NH, Windley BF (1982) Archean Plate Tectonics: Constraints and Interferences. *The Journal of Geology*, **90**, 363-379.

Sunda W, Huntsman SA (1995) Cobalt and zinc interreplacement in marine phytoplankton: Biological and geochemical implications. *Limnology and Oceanography*, **40**, 1404-1417.

Tallarico FHB, Figueiredo BR, Groves DI, Kositcin N, McNaughton NJ, Fletcher IR, Rego JL (2005) Geology and SHRIMP U-PB Geochronology of the Igarapé Bahia Deposit, Carajás Copper-Gold Belt, Brazil: An Archean (2.57 Ga) Example of Iron-Oxide Cu-Au-(U-REE) Mineralization. *Economic Geology*, **100**, 7-28.

Tortell PD, Price NM (1996), Cadmium toxicity and zinc limitation in centric diatoms of the genus *Thalassiosira*. *Marine Ecology Progress Series*, **138**, 245-254.

Trocine RP, Trefy JH (1988) Distribution and chemistry of suspended particles from an active hydrothermal vent site on the Mid-Atlantic Ridge at 26ºN. *Earth and Planetary Science Letters*, **88**, 1-15.

Verma, MB, Roy MK, Saxena VP (2003) Uranium and Polymetallic Sulphide Mineralisation in the Banded Iron Formation at Udaisagar, Udaipur District, Rajasthan. *Journal of the Geological Society of India*, **61**, 703-710.

Wheat GC, Mottl MJ, Rudnick M (2002) Trace element and REE composition of a low-temperature ridge-flank hydrothermal spring. *Geochimica et Cosmochimica Acta*, **66**, 3693-3705.

Williams RJP, da Silva JJRF (1996) The Natural Selection of the Chemical Elements. Bath Press Ltd., Great Britain.

Zirino A, Yamamoto S (1972) A pH-dependent model for the chemical speciation of copper, zinc, cadmium and lead in seawater. *Limnology and Oceanography*, **17**, 661-671.

CHAPTER 3

Experimental considerations on paleomarine Zn and Ni concentrations as recorded in iron formations[1]

3.1 Introduction

3.1.1 Iron formations as paleomarine proxies

Iron formations (IF) are chemical sediments that were deposited over large areas of anoxic seafloor during the Precambrian. By the trace element enrichments that they have inherited from seawater, IF have become critical proxies for estimating the inventories and potential bioavailability of trace metals in the early oceans, especially with regards to bioessential transition metals (e.g., Konhauser et al., 2002; 2009; Robbins et al., 2013). IF were deposited in the Precambrian ocean between ~3.8 and 1.8 Ga with a brief resurgence in the Neoproterozoic (e.g., Klein, 2005); the depositional gap is often attributed to expanded marine euxinia (e.g., Canfield, 1998), the extent of which remains an active debate (e.g., Planavsky et al., 2011; Reinhard et al., 2013). IF are predominantly comprised of oxidized, mixed valence and reduced iron (Fe) minerals, such as hematite, magnetite and siderite, in a cherty matrix (e.g., Klein et al., 2005). The current Fe mineralogy of IF is the result of post-depositional alteration of primary Fe and silica precipitates by burial diagenesis and low-grade metamorphism, likely from precursor sediments consisting of ferric oxyhydroxides (e.g., ferrihydrite), amorphous silica, and amorphous ferrous-ferric silicate phases (Bekker et al., 2010). The extensive depositional history of IF in the Precambrian, combined with the hydrogenous origin of their trace element enrichments, makes them important paleomarine proxies.

Numerous studies have utilized the reactivity of metal cations toward Fe(III) oxyhydroxides to infer paleomarine conditions at the time of deposition,

[1] This chapter is in preparation for submission as Robbins et al.

such as the abundance of trace elements in seawater, the magnitude of hydrothermal versus terrestrial fluxes or prevalent paleoredox conditions (e.g., Alexander et al., 2008; Bau and Möller, 1993; Bau and Dulski, 1996; Bjerrum and Canfield, 2002; Konhauser et al., 2007; 2009; Planavsky et al., 2009). Trace metal cations adsorb to the charged surface of Fe oxyhydroxides as a function of pH, with the degree of cation adsorption increasing with pH (Dzombak and Morel, 1990). Here our interest lies primarily in the adsorption of zinc (Zn) onto Fe oxyhydroxides, but nickel (Ni) is also relevant, as they are transition elements that have biological importance in both the early and modern oceans (Dupont et al., 2010; Konhauser et al., 2009; Saito et al., 2003, Robbins et al., 2013). From studies at pH values relevant to paleomarine conditions (~7-8, Grotzinger and Kasting (1993)), Dyer et al. (2004) showed that ferrihydrite adsorbs up to 0.46 mol of Zn per mol of Fe at pH 7.5; while Zn and Ni show similar adsorption behavior to goethite (Trivedi and Axe, 2001). At seawater pH, effectively 100% of Zn and Ni are adsorbed from dilute solution, depending on the Fe(III) oxyhydroxide mineralogy and ionic strength (e.g., Dyer et al., 2004; Trivedi and Axe, 2001; Trivedi et al., 2004).

Bjerrum and Canfield (2002) were first to utilize the partitioning coefficient behaviour of phosphate (PO_4^{3-}) to modern marine Fe oxyhydroxides to extrapolate paleomarine concentrations from the IF record. Subsequently, Konhauser et al. (2007) showed that for PO_4^{3-} this approach is sensitive to ambient dissolved Si, which both competes for adsorption site and effects Fe particle reactivity. This methodology can also be applied to transition metals, such as Ni, where the effect of silica is similarly important (Konhauser et al., 2009). Paleomarine silica conditions, represented here by corresponding silicon (Si) concentrations, likely approached saturation with respect to amorphous phases prior to the evolution of biological Si secretion (e.g., Siever, 1992; Maliva et al., 2005), so reconstructions of Precambrian seawater ion abundances from the IF record must take elevated paleomarine Si into account.

Such reconstructions from the IF record have been recently achieved for Zn and Ni (Robbins et al., 2013 and Konhauser et al., 2009, respectively).

Thermodynamic modeling (Saito et al., 2003), based on cyanobacterial trace metal requirements, further led to the suggestion that in a 'ferro-sulfidic' ocean, where both Fe and sulfide are relatively abundant, Zn concentrations would drop to below biolimiting levels of approximately 10^{-13} M (e.g., Brand et al., 1983), where the growth of eukaryotes becomes depressed. However, the recent evaluation of the IF record by Robbins et al. (2013) has shown that the marine Zn reservoir has remained relatively unchanged from the Precambrian to the modern. This evaluation involved the use of both hypothetical partitioning scenarios and a new thermodynamic modeling effort, and is in good agreement with the shale record (Scott et al., 2013). This finding has significant implications on the bioavailability of Zn to primitive eukaryotes, as they generally have higher Zn demands (Dupont et al., 2010) and suggests a likely decoupling of geochemical and biological evolution.

Unlike Zn, which has a relatively stable marine reservoir from the Archean throughout to the modern (Scott et al., 2013; Robbins et al. 2013), Ni has exhibited dramatic evolution in both the upper continental crust and seawater. Between about 2.7 and 2.5 Ga, and just prior to the onset of the Great Oxidation Event (GOE), the marine Ni reservoir experienced a rapid decline (Konhauser et al., 2009). This decline is recorded in the IF record by changes in the maximum value spread in Ni/Fe ratios. Based on experimentally derived partitioning coefficients for Ni under maximum hypothesized Si concentrations (2.20 mM), IF record an Archean Ni reservoir of ~400 nM Ni, collapsing to ~100 nM by 2.5 Ga, and to near modern levels of ~9 nM by 0.5 Ga (Konhauser et al., 2009). An important but poorly understood caveat to these partition coefficient-based estimates is that sedimentary and diagenetic processes could have altered the concentration and distribution of transition elements during early diagenesis and metamorphism.

3.1.2 Trace element mobility during iron formation diagenesis

Despite clear evidence for profound diagenetic and metamorphic evolution form original chemical sediment to the mineral assemblage currently comprising IF,

geochemical data to date argue against significant post-depositional trace element mobility. Preservation of marine-like rare earth element (REE) patterns is common (e.g., Derry and Jacobsen, 1990; Alexander et al., 2008, Planavsky et al., 2010); Bau (1993) concluded that REE in IF are not generally fractionated by diagenesis or metamorphism if low water-rock ratios and closed-system conditions exist, but REE may be affected by hydrothermal alteration or surface weathering. The preservation of short-term variations in the magnitude of Eu anomalies (e.g., in the Penge and Kuruman IF; Bau and Dulski, 1996), as well as intra-grain and intra-layer iron isotopic variability (e.g., Frost et al., 2007; Johnson et al., 2008) that may be preserved despite amphibolite grade metamorphism (e.g., Whitehouse and Fedo, 2007), further argue against significant diagenetic or metamorphic element remobilization. Experimental work has shown a low migration capacity for cations that decreases as either the charge or ionic radius increase (e.g., McConchie, 1984). McConchie (1984) further demonstrated that ion mobility rates are an order of magnitude lower in Fe-hydroxide gels than in silica gels, suggesting that during IF deposition, the precursor Fe-precipitates may act as a trap for ions adsorbed during precipitation. Therefore, the iron oxide minerals of IF should preferentially preserve primary signatures relative to the silicate phases of IF.

Recent experimental work by Frierdich and Catalano (2012) indicates that in Fe(II)-bearing solution, both Ni and Zn adsorbed to the Fe(III) oxyhydroxides goethite and hematite may be remobilized by electron transfer and atom exchange between the aqueous Fe(II) and oxide surface Fe(III) pools. Trace metal remobilization is promoted by periodic replacement of Fe(II) solution (15% of Zn from hematite and 28% of Ni from goethite), relative to a closed system at equilibrium (6% of Zn from hematite and 9% of Ni from goethite) (Frierdich and Catalano, 2012). Subsequently, the same authors showed that when hematite or goethite contained impurities, such as Al or Cr (conditions that are more relevant to nature Fe oxide minerals), the mobility of Zn and Ni during Fe(II)-driven recrystallization is decreased (Frierdich et al., 2012). This is a situation that may

be more realistic when considering naturally occurring Fe-oxyhydroxides, such as those that formed the precursor sediment to IF (e.g., Cismasu et al., 2011).

What remains unclear, however, is the effect that later IF diagenetic processes may have on trace metal mobility. This uncertainty represents a significant gap in our understanding of IF that is critical for framing paleomarine trace element reconstructions. Here we seek to further explore such uncertainties in light of recent paleomarine extrapolations of Zn (Robbins et al., 2013) and Ni (Konhauser et al., 2009) enabled by the IF record. These elements are of particular interest due to their crucial biological roles at the heart of eukaryotic (Zn) and methanogen (Ni) metalloenzymes (c.f. Konhauser et al., 2009; Dupont et al., 2010; Robbins et al., 2013). We first compare the results of previous hypothetical partitioning scenarios for Zn (Robbins et al., 2013) with results from experimentally derived partitioning isotherms developed here. We further investigate the mobility of Zn and Ni during simulated diagenesis to test the robustness of previous paleomarine estimates for trace metals (Konhauser et al., 2009; Robbins et al. 2013), and offer a preliminary assessment as to how diagenetic mobility related to process such as pressure and temperature affect these estimates.

3.2 Methods

3.2.1 Zn partitioning experiments

Samples and solutions were prepared with 18.2 MΩ ultrapure water (Barnstead Millipore water filtration system) and reagents low in background trace metals and contaminants. Experiments were conducted in 15 mL Teflon reaction vessels and samples stored in hydrochloric acid washed HDPE scintillation vials.

Isotherms for Zn and Fe co-precipitation experiments (Fig. 3-1) were generated by permitting Zn-doped Fe(II) solutions to react with atmospheric O_2 and oxidize at room temperature and at seawater ionic strength. The Fe(II) solution was prepared in concentrated form using ferrous ammonium sulfate hexahydrate ($FeSO_4(NH_4)_2SO_4 \bullet 6H_2O$), dissolved in 0.5 M $NaNO_3$ and 0.1 M H_3BO_3 electrolyte solutions and stabilized with several drops of trace metal grade

nitric acid (TM-HNO_3), for initial concentration of ~3 ppm. Silicon (Si) was previously added as sodium metasilicate nonahydrate ($Na_2SiO_3 \bullet 9H_2O$) to generate electrolyte solutions of varying silica concentrations, representing silica-deplete modern seawater (0 mM Si) and Precambrian seawater controlled by saturation with respect to silica minerals (cristobalite, 0.67 mM; and amorphous silica, 2.20 mM; c.f. Konhauser et al., 2007; 2009). Stock solutions were adjusted to pH 7.76 prior to iron addition and were strongly buffered about that pH by 0.1 M H_3BO_3; pH drift over the course of the experiments was less than ~0.2 units. Various amounts of dissolved Zn from a mono-elemental ICP-MS standard (SPEX CertiPrep, Metuchen, NJ, USA) were added to ~10 mL of the simulated seawater solution immediately prior to iron addition.

Co-precipitation samples were allowed to equilibrate for 48 hours and then passed through a 0.22μm nylon membrane filter to separate aqueous species from the Fe+Zn±Si precipitates. The filtrate was acidified with three drops of TM-HNO_3 and analyzed for Zn and Fe concentrations by Quadrupole Inductively Couple Plasma Mass Spectrometry (Q-ICP-MS) at the University of Alberta's Radiogenic Isotope Facility. Samples were corrected for background Zn contamination and potential removal of Zn by mechanisms other than co-precipitation with Fe-oxyhydroxides, such as adsorption to container walls or potential Zn-hydroxide precipitation, by an internal calibration (Appendix Fig. A2-1) using control samples with no added Fe; corrected values average 135.6% of raw measured values (see Appendix 2 for a discussion on data treatment for and limitations of isotherm generation).

3.2.2 Extrapolation of paleomarine Zn and Ni concentrations

A distribution coefficient (K_D) isotherm model for trace element (TE) co-precipitation with Fe oxyhydroxides was employed to enable extrapolation of paleomarine TE concentrations from the IF record as per Bjerrum and Canfield (2002) and Konhauser et al. (2007, 2009). This empirical partitioning approach defines the following relation:

$$K_D = \frac{Molar\ TE/FE_{IF}}{[TE]_{equilibrium}} \qquad \text{Eq. 1}$$

where the distribution coefficient K_D relates a solid-phase molar TE/Fe ratio to the equilibrium aqueous TE concentration at the time of co-precipitation. Paleomarine Zn concentrations may then extrapolated by combining molar TE/Fe ratios from the IF record with K_D values determined by isotherm experiments such as those reported by Konhauser et al. (2009) for Ni and as presented here for Zn (Figure 3-1; Table 3-1). Minimum, maximum and representative Zn/Fe values from the IF record (c.f. Fig. 3, Robbins et al., 2013) are $2x10^{-6}$, $4x10^{-3}$ and $1x10^{-4}$, respectively.

3.2.3 Diagenetic experimental design

Diagenetic capsule experiments on synthetic Fe oxyhydroxide precipitates (Posth et al., 2013) demonstrate that the Fe mineralogy observed in IF today can be reproduced after incubation of synthetic 2-line ferrihydrite (Fh) in the presence or absence of glucose (as a proxy for biomass) for a period of 14 days at 170ºC and 1.2 kbar. These conditions approximate the diagenetic pressure and temperature conditions of the Transvaal Supergroup BIF (Miyano and Klein, 1984; Miyano, 1987; Posth et al., 2013). The diagenetic experiments presented here were preformed at the University of Tübingen using similar procedures and apparatus as Posth et al. (2013). Our experiments consider diagenetic mobilization of Ni and Zn from typical Fh (as a proxy for primary Fe-oxyhydroxides formed from the chemical oxidation of Fe(II) with O_2) as well as mobilization from biogenic ferrihydrite (BF) harvested from Fe(II)-oxidizing phototrophic bacterial culture. Our experiment consisted of three general steps: (i) the synthesis of Fe-oxyhydroxides, either as abiotic Fh or BF cell-mineral aggregates, and the adsorption of trace elements to those phases, (ii) treatment of the minerals, with or without organic material, under conditions of simulated P/T conditions consistent with diagenesis, and (iii) determination and quantification of the concentration of trace elements re-mobilized during diagenesis.

Capsules were named according to a consistent scheme, i.e. ZnFh-1, where Ni and Zn refer to the trace element adsorbed, Fh indicating 2-line ferrihydrite and BF denoting the BF cell mineral aggregates. Finally, the prefix C- denotes a control capsule (e.g., C-ZnFh1; Table 3-3). Control capsules were set up to mirror experimental capsules but were stored in Eppendorf tubes at room temperature and pressure for the same period of time as experimental capsules. Abiotic Fh capsules with glucose added as an organic carbon source are experimental replicates 1 and 2, and replicates 3 and 4 lacked glucose. In experiments with biogenic ferrihydrite, no glucose was added because cell material served as a source of organic carbon, as such sample numbers serve only to identify the respective capsule among replicates. For example, NiFh-1 indicates a capsule containing Ni adsorbed to Fh with glucose, while ZnBF3 indicates Zn adsorbed to BF. Capsules ZnFh-1 and NiFh-3 and ZnBF1 were excluded from analysis as the integrity of the seals were compromised during diagenetic treatments.

3.2.3.1 Synthesis of biogenic and synthetic 2-line ferrihydrite

The two preferred explanations for the generation of ferric iron-containing precipitates under a generally anoxic Archean atmosphere involve oxidation of Fe^{2+} and precipitation of Fe oxyhydroxides at a marine redoxcline by (1) free oxygen produced by cyanobacteria (e.g., Cloud, 1968; 1973) or (2) direct microbial Fe^{2+} oxidation by anoxygenic Fe(II)-oxidizing bacteria (e.g., Konhauser et al., 2002; Kappler et al., 2005, Posth et al., 2008). If microorganisms were involved in the formation of IF, there would be organic matter (e.g., biomass) associated with the Fe minerals during deposition. Konhauser et al. (2005) suggested that this organic carbon, in the form of biomass, could serve as a reductant for Fe(III) oxides during microbial Fe(III) reduction or abiotic diagenetic reduction of Fe(III). This process not only explains the mixed valence Fe minerals, such as magnetite (Fe_3O_4), in IF, but it also accounts for the low organic carbon content of IF today (<0.5%, Gole and Klein (1981)). Additionally, aqueous Fe^{2+} can mobilize trace elements from Fe-oxyhydroxides (Frierdich et al.,

2011). Therefore, we consider the possibility that redox driven reactions between primary cell-mineral aggregates during diagenesis could affect metal mobility.

The marine photoferrotroph *Rhodovulum iodosum* was cultivated in artificial seawater medium as described by Straub et al. (1999), but 22 mM $NaHCO_3$ was used and the phosphate content was reduced to 1 mM, with additional NaCl added to maintain the same ionic strength. $FeCl_2$ was added to a concentration of 10 mM, but the medium was not filtered to remove initial iron carbonate and phosphate precipitates. The strain was then inoculated and grown at 12.82 μmol photons/m^2/s^2 until all Fe^{2+} was oxidized, as determined by the Ferrozine assay (Stookey, 1970). The cell-mineral aggregates were then collected by centrifugation and washed four times with the growth medium lacking bicarbonate buffer and harvested by centrifugation at 4000 rpm for 10 minutes before freeze-drying.

Synthetic Fh used in abiogenic experiments was prepared via methods previously described (c.f. Cornell and Schwertmann, 2003) and freeze-dried prior to adsorption of Ni or Zn.

3.2.3.2 Mobilization experiments

Adsorption of Zn and Ni to both Fh and BF was accomplished by introducing ~50 μM of Zn or Ni (from ICP-MS standards) in the presence of 1g/L ferrihydrite in solution prepared to seawater ionic strength with 0.5M $NaNO_3$ and buffered by 0.1 M H_3BO_3 to a pH value of 8. Adsorption occurred over a 24-hour period, before the solution was passed through a 0.2 μM Millipore filter, and the Fe particles were recovered. Filtrates were analyzed for Zn and Ni by Inductively Coupled Plasma Optical Emission Spectroscopy (ICP-OES), on a Perkin Elmer Optima 5300 at the University of Tübingen, to determine the amount of Zn or Ni lost due to adsorption. Calculations of the percentage of Zn or Ni adsorbed, as well as the amount normalized to the weight of Fe particles, are provided in Table 3-2. Ferrihydrite was then dried in air at room temperature prior to being loaded in experimental gold capsules.

Three experiments were conducted with Zn and Ni adsorbed independently to: (1) Fh mixed with glucose in the capsule, (2) Fh only, and (3) BF. Experimental gold capsules with synthetic ferrihydrite were set-up such that 100 mg of ferrihydrite with Zn or Ni adsorbed was loaded into the capsules. For capsules with ferrihydrite and glucose, 4 mg of glucose were added to achieve a ratio of electron reducing equivalents of 0.6 that could be transferred from glucose to ferrihydrite during diagenetic treatment. This approximates the low organic carbon content of IF, which would limit the number of electrons available for diagenetic Fe reduction (Konhauser et al., 2005). Capsules with BF contained approximately 35 mg of BF cell-mineral aggregate. Gold capsules were crimped closed and then sealed using an arc welder. During welding the capsule remained cool to the touch, precluding any temperature reaction prior to capsule incubation. The capsules were weighed before and after a sonication treatment in a water bath to ensure that the contents were sealed. Capsules were then incubated at 170ºC and 1.2 kbar for 14 days in a high-pressure autoclave (Sitec Sieber Engineering Ag, Zürich, Switzerland). In tandem with experimental capsules, control capsules were incubated at room temperature for 14 days to account for any reactions under ambient conditions.

Following the 14-day incubation period, capsules were opened using steel shears and pliers to maximize the diameter of the gold capsules, which had collapsed during incubation due to increased pressure. Pliers and shears were wrapped in parafilm prior to opening capsules in order to minimize contamination, but potentially may have contributed to contamination in either Fe or Ni. Capsule section exteriors were lightly cleaned with acetone and placed in Falcon tubes; particles from control capsules were transferred directly into Falcon tubes. To each Falcon tube 5 mL of pH-buffered seawater ionic strength solution (0.5 M $NaNO_3$ and 0.1 M H_3BO_3, pH 8) was added and then the capsules were sonicated for 30 minutes. After 30 minutes the solution was drained into a separate falcon tube and the particle sonication was repeated. After the second sonication the supernatants were combined and filtered through 0.22 μM Millipore filters. Samples were then acidified with HNO_3 to a final concentration

of 1-2%. For a schematic representation of the experimental protocol refer to Appendix Fig. A2-2.

To assess the effect of diagenesis on Zn and Ni mobility the filtrates were analyzed at the University of Tübingen by ICP-OES, using matrix matched standards. The concentration of Zn or Ni in each sample was used to determine the percent mobilized in each experimental capsule. Errors (in percent mobilized) were calculated at the two-sigma level based on the standard deviations of Zn and Ni as measured by ICP-OES analysis.

3.2.3.3 Calculation of C to Fe ratios

Ratios of the moles of carbon to mass of Fe particles were calculated for each sample containing organic matter. For capsules with Fh we utilized an ideal formula of $Fe(OH)_3$, molar mass = 106.87 g/mol and glucose (180.15 g/mol). This allowed for the determination of the moles of glucose based on the percentage of the molecular weight that carbon accounts for in glucose and the mass of glucose added (see equation 2). Where the ratio of 72.06 to 180.15, represents the molar mass of carbon in glucose to the molar mass of glucose. The calculated moles of carbon added as glucose were then normalized to the moles of Fe in the ferrihydrite added (equation 3).

$$mol\ C = \frac{(m_{glucose} * (72.06/180.15))}{12.01 g/mol} \quad \text{Eq. 2}$$

$$mol\ Fe = \frac{(g_{Fe-particles} * (55.85/106.87))}{55.85 g/mol} \quad \text{Eq. 3}$$

For experiments with BF the total carbon content was measured using an Elementar Vario EL at the University of Tübingen. Total inorganic carbon was not determined because the acid treatment required would have dissolved some of the BF as well. Inorganic carbon was present in the growth medium as $NaHCO_3$ buffer in equilibrium with N_2/CO_2 gas. However, the cell-mineral aggregates were washed four times in a basal medium without bicarbonate (see section 3.2.3.1 for

description) prior to freeze-drying and this should have removed any inorganic carbon in solution. The moles of carbon were calculated by equation 4 and normalized to the moles of Fe in the BF added to each capsule as calculated in equation 5. For the BF, the cell-mineral aggregates are a combination of $Fe(OH)_3$ and organic carbon (CH_2O) and these exist in a 4:1 ratio, resulting in a cell mineral aggregate molar mass of ~458 g/mol. A 5% variation in the molar mass of the cell-mineral aggregates would result in a corresponding ±5% change in the molar C to Fe ratios for the BF.

$$molC = \frac{((\%C_{organic}/100) * m_{biogenic\ particles})}{12.01 g/mol} \quad \text{Eq. 4}$$

$$mol\ Fe = \frac{(m_{biogenic\ particles} * ((4 * 55.85)/458))}{55.85 g/mol} \quad \text{Eq. 5}$$

3.3 Results

3.3.1 Zn partitioning isotherms

Isotherms and their respective K_D and R^2 values are presented in Fig. 3-1. Below an equilibrium Zn concentration of approximately 0.5 μM the K_D isotherms for each of the three Si conditions appear to converge as they approach the origin. The calculated K_D for the 2.20 mM Si condition is slightly higher than for the 0.67 mM or no added Si condition with values of 0.03940, 0.03337 and 0.03096 μM^{-1}, respectively. The K_D values for all three conditions are quite close and are discussed further below.

3.3.2 Paleomarine Zn concentrations

Paleomarine Zn concentrations were extrapolated for each Zn+Fe±Si isotherm using minimum, maximum and representative Zn/Fe values from the IF record (for a detailed discussion on the Zn in IF record refer to Robbins et al., 2013) are presented in Table 3-1. The representative value of 10^{-4} was taken as an

intermediate value in the range of molar Zn/Fe ratios observed in IF (between ~0.004 and $2x10^{-6}$), and a majority of samples display values that are comparable within an order of magnitude. In all cases, values extrapolated from the IF record are within one to two orders of magnitude of modern marine Zn concentrations of ~10 nM, and range from 0.05 nM (for the no added Si K_D and a minimum value from the IF record) to 129.20 nM (at the maximum Zn/Fe ratio in IF and the K_D for 2.20 mM Si), effectively spanning the maximum potential range record by the IF record. At the representative Zn/Fe ratio of 10^{-4}, the partitioning experiments at all three Si concentrations result in extrapolated paleomarine Zn concentrations between 2.54 to 3.23 nM.

3.3.3 Trace metal mobility during diagenesis

Trace metals adsorbed to the Fh at values of $4.86x10^{-3}$ mol Zn/mol Fe and $0.392x10^{-3}$ mol Ni/mol Fe. This corresponds to ~94% of initial Zn and approximately 66% of initial Ni being absorbed. For BF, Zn was absorbed at ~$5.41x10^{-3}$ mol Zn/mol Fe, approximately 97% of the initial Zn concentration. Similarly, about 94% of Ni was adsorbed to the BF ($6.04x10^{-3}$ mol Ni/mol Fe). For a summary refer to Table 3-2. Capsules with Fh and glucose have a molar ratio of C to Fe (mol:mol) of ~0.1446±0.0008 This is close to the molar ratio of C to Fe in BF experiment particles of ~0.1792.

The results for capsules investigating Zn mobility from (1) Fh with glucose added, (2) Fh without glucose, and (3) BF are presented in Fig. 3-2A-C respectively. Overall, mobilization of Zn appears to be quite low and in most cases the percentage of Zn released was <1%. When uncertainties are considered, it is apparent that the greatest amount of mobilization is in the BF capsules (Fig. 3-2C). Control capsules showed effectively no desorption or release of Zn and uncertainties were generally low at <4.4% for Fh capsules and <7.2% for BF capsules.

Results for capsules examining Ni mobility for (1) Ni on Fh with glucose, (2) Ni on Fh without glucose, and (3) Ni on BF are presented in Table 3-4 and Fig. 3-3A-C, Overall, Ni mobility was also quite low, <8.15%, however, standard

deviations of ICP-OES measurements for Ni were much greater than for Zn, up to 33.56%, but generally under ~14%. This increased uncertainty may be due to either slight background contamination of Ni by the salts used in the experiments (as reflected by the low levels of Ni in several Zn capsules (Table 3-3; see discussion); or a function of concentrations being close to the ICP-OES detection limit as samples were diluted prior to analysis to account for initial high salt concentrations on par with seawater ionic strength. The greatest amount of Ni mobilized was observed in capsules containing Ni adsorbed to Fh when glucose was added. Mobilization of 5.28% to 8.15% of initial Ni was observed for the capsules run under this condition. Ni mobility for BF was slightly less at 3.25% and 3.55%. When Ni was adsorbed to Fh in the absence of organic matter there was effectively zero mobilization, and final Ni concentrations were indistinguishable from controls. Control capsules for Ni showed very little mobilization, <0.3% for Fh capsules regardless of the presence of organics, and <1.2% for BF. Uncertainties in Fh control capsules for Ni were <2.1% in all cases and <6.8% for BF.

3.4 Discussion

3.4.1 Zn partitioning behavior

Constraints on the partitioning of Zn to Fe oxyhydroxides in the presence of Si, and at levels representative of the Precambrian ocean, are critical to our understanding of the IF record of evolving paleomarine Zn concentrations prior to the development of Si-precipitating organisms in the Phanerozoic (e.g., Siever, 1992; Grenne and Slack, 2003). Isotherms generated here were fit with a K_D model, which is a special form of the Freundlich isotherm where the exponent is equal to one (Langmuir, 1997; Konhauser, 2005). This model was selected because there was no strong curvature to the data points or a plateau at higher Zn concentrations, indicative of site-specific saturation during Zn adsorption.

Despite the absence of a plateau in the Zn isotherm data, a slight curvature is observed in the low Zn data points (Fig. 3-1), and a greater amount of Zn is removed high concentrations in the presence of Si. Previous work established that

Zn can co-precipitate directly with silica at levels as low as ~0.071 mM (or 2 ppm) in both fresh and marine waters Wiley (1978). However, the work of Wiley did not include consideration of Fe-oxyhydroxides. Nevertheless, this may potentially explain why we observe increased adsorption to co-precipitating Fe-oxyhydroxides at higher Zn concentrations, when Si is present (Fig. 3-1A). Anderson and Benjamin (1985) conducted a study that considered silica while investigating Zn adsorption onto Fe-oxyhydroxides, and they observed no noticeable effect of dissolved silica on the sorption of Zn to surface sites of preformed Fe particles. The finding of Anderson and Benjamin (1985) is in contrast to the relationship observed for other sorbents toward Fe-oxyhydroxides in the presence of Si, notably Ni and PO_4^{3-}. In both cases, less sorption took place the greater the silica content in the ferrihydrite particles (Konhauser et al., 2007; 2009).

Another key difference, compared to Ni or PO_4^{3-}, is that at low concentrations of Fe the isotherms become almost indistinguishable. Again, this may be envisioned to represent a scenario where at low concentrations of Zn, regardless of the presence of Si, Fe particles are reactive enough to adsorb essentially all the Zn. The most critical difference between the Zn isotherms presented here and those for PO_4^{3-} and Ni, in terms of their application to paleomarine conditions (Konhauser et al., 2007; 2009, respectively), is the range of K_D values vs. Si concentration. For PO_4^{3-} and Ni the K_D values for 0 mM Si versus 2.20 mM Si were ~37.5 and ~10.9 times higher, respectively. For Zn this factor is ~0.79, suggesting that despite the potential for Si-Zn co-precipitation, Si does not exert a strong control on the adsorption of Zn to co-precipitating Fe-oxyhydroxides, which is largely consistent with the lack of an effect seen by Anderson and Benjamin (1985).

The lowest Zn concentrations used here to develop the isotherms, are several orders of magnitude greater than the range of ~0.2 – 20 nM concentrations observed in modern oceans (e.g., Bruland et al., 1994; Nolting and de Baar, 1994); for the purpose of discussion we refer to a modern Zn concentration of approximately 10 nM. Because of the offset between experimental and natural

conditions, the isotherms and respective K_D values presented here must be interpreted as a first order estimate for paleomarine Zn concentrations (see Appendix 2 for a discussion on the limitations of generating partitioning isotherms for Zn). However, the linear fit of the K_D relationship allows for extrapolation to lower paleomarine concentrations, as the greatest differences in the three Si conditions are observed at high Zn concentrations.

3.4.2 Paleomarine Zn and Ni concentrations

Table 3-1 presents paleomarine concentrations of Zn extrapolated from three values from the IF record: the maximum, minimum and a representative value. Under any of the partitioning scenarios examined (i.e. 0, 0.67 and 2.20 mM Si), the range of Zn concentrations indicated by the IF record is about 0.05 to129.20 nM, which is universally within approximately two orders of magnitude of modern levels of ~10 nM.

Importantly, at the lowest levels of Zn predicted here, ~0.05-0.06 nM, concentrations are at least two orders of magnitude above the sub-picomolar concentrations at which Zn becomes biolimiting (e.g., Brand et al., 1983). Critically, this is also at least seven orders of magnitude above estimates for free Zn^{2+} based on thermodynamic models for 'ferro-sulfidic' paleomarine conditions (Saito et al., 2003) and those invoked to explain the delayed expansion of eukaryotic Zn-binding proteins and stagnant eukaryote evolution through the Precambrian (Dupont et al., 2006; 2010). The values derived from the representative IF Zn/Fe value suggest a paleomarine concentration of ~2.5-3.2 nM, which is on the order of modern concentrations and in excellent agreement with the consistent reservoir of ~10 nM Zn predicted by Robbins et al. (2013) based on Zn-Fe relationships displayed by the IF record dataset itself. The different approaches used by the two studies, hypothesized versus experimental partitioning behavior, provide an independent check and suggest that the finding of a consistent paleomarine Zn reservoir of near modern levels is robust. In addition, this result is also consistent with the recent examination of the shale Zn record (Scott et al., 2013). The emerging picture is that Zn was not likely

biolimiting to primitive eukaryotes in the Proterozoic (as per Scott et al., 2013) and Robbins et al. (2013)), differing from pervious estimates for paleomarine Zn concentrations derived from mineral saturation states (Saito et al., 2003) and eukaryotic metalloenzymes (Dupont et al., 2010).

The available data would thus suggest that the IF record reflects authigenic marine signatures, and thereby, records a fairly reasonable estimate for paleomarine Zn, as well those previously derived for Ni (Konhauser et al., 2009). However, the isotherms, hypothetical or experimental, do not account for any potential diagenetic mobility of transition elements. As such, we also consider Zn (and for comparison Ni) mobility during diagenetic pressure and temperature treatments and the resultant implications for paleomarine reconstructions.

3.4.3 Diagenetic mobility of Zn and Ni

3.4.3.1 Assessment of diagenetic transition metal mobility

Understanding the mobility of key transition metals during diagenesis is critical to our understanding of IF as paleomarine proxies. We use the work of Posth et al. (2013) as the basis for our diagenesis experiments, as their pressure and temperature experiments were capable of reproducing the current mineralogy of IF from precursor Fe oxyhydroxides, such as ferrihydrite. As such, this methodology presents an excellent platform for the investigation of trace element mobility. The capsule and control experiments for Zn were low in Ni, and vice versa (see Tables 3-3 and 3-4), suggesting minimal levels of contamination or background Zn or Ni. There was no indication of Zn release from Ni capsules. However, there was some release of Ni from Zn capsules. This was generally an order of magnitude below the levels released from Ni capsules, suggesting relatively minor contamination.

Based on the Zn experimental capsule data presented here, Zn is effectively immobile during Fe mineral diagenesis. Moreover, the lack of mobility in the control samples suggests that Zn is not easily desorbed from Fh, regardless of the presence of glucose, and may be only minimally desorbed from BF. The lack of mobility of Zn in BF capsules is fully consistent with the results from Fh

capsules with glucose, suggesting that for Zn, the presence of organic carbon does not appear to affect mobility (see below for a discussion on the role of organic carbon in mobility of Ni). These findings suggest that during pressure and temperature treatments, Zn is either retained on a surface site where it is not easily desorbed, or it may be moved to an interior structural site where it is held more strongly.

Posth et al. (2013) showed that for diagenetic capsule experiments undergoing pressure and temperature treatment, an initial mix of ferrihydrite and glucose results in a mineralogy dominated by hematite, magnetite and siderite, producing a similar mineralogy to what is observed in IF today. Zn is known to adsorb to hematite; 100% of Zn is adsorbed to hematite above a pH of ~8 (e.g., Rose and Bianchi-Mosquera, 1993). The affinity of Zn for hematite, and Fe-oxyhydroxides in general, may be a contributing factor to the lack of mobility observed here. The mechanism responsible for the observed lack of mobility during diagenetic capsule treatment is presently unclear, and will require further study of the bonding mechanisms via analyses such as X-ray absorption (XAS) in both pre- and post-diagenetic samples. This may be a powerful tool as Waychunas et al. (2002) have shown the ability for K-edge XAS and X-ray adsorption extended fine structure spectroscopy (EXAFS) to determine the adsorption mechanism for Zn to ferrihydrite for both surface adsorption and co-precipitation experiments. Waychunas et al. (2002) found that both the sorption of Zn to ferrihydrite and co-precipitation were generally well characterized by inner sphere complexes. However, for the purpose of this preliminary assessment the important observation is the lack of mobility of Zn following simulated IF diagenesis.

The lack of Zn mobility observed here is consistent with some previous work. For instance, Martinez and McBride (1999) demonstrated that Zn does not show increased solubility during aging and mineral transformations in the absence of organic matter. This is likely due to adsorption of Zn to hydrous ferrous oxides; however at high organic carbon to Fe ratios of 1:1 the formation of iron-organic carbon complexes may block some Zn reaction sites and potentially slightly increase the solubility of Zn (Martinez and McBride, 1999). Further, Bhattacharya

et al. (2007) showed that for the IF of the Jharkand-Orissa region that was in places intruded by granite, Zn concentrations in strongly metamorphosed granite-rafted IF and unintruded IF are quite similar. Both studies are broadly consistent with the results seen here.

More than 90% of Ni is immobilized during simulated diagenesis, with <8.2% being lost to the capsule solution phase under all the conditions examined here. Even when the maximum observed mobility of Ni is considered (8.15±33.56% for capsule NiFh-2), we can see that at the lower end of the confidence interval there is likely less than 10% mobilization of Ni. However, if maximum uncertainty reflects the true amount of Ni mobilized, at least 50% of the initially adsorbed Ni remains, with the remaining 50% of the initial Ni load being mobilized during IF diagenesis. This would result in paleomarine constructions based on the IF record being underestimated by a factor of about two. Despite the slightly increased mobility of Ni compared to Zn, in experimental capsules mobility is generally <5%. This is less than predicted by previous work investigating transition metal mobility during IF deposition and diagenesis (Frierdich et al., 2011, Frierdich and Catalano, 2012; see below for a discussion).

3.4.3.2 Presence of organic matter

The potential effect of organic matter availability during diagenesis was tested by examining mobility of Zn and Ni in the presence of glucose (a proxy for organic carbon), or when adsorbed to the BF cell-mineral aggregates. The presence of organic matter did not affect the mobility of Zn during diagenesis, as under all conditions studied Zn was effectively immobile. In both experiments involving Zn, there was no increase in Zn mobility when organic matter was present, either as glucose or cell-mineral aggregates. Additionally, Zn was not easily desorbed from control capsules when organic carbon was present (see Fig. 3-2 and Table 3-3).

By contrast, Ni mobilization did exhibit a slight increase in mobility when organic matter was present (Fig. 3-3A and C, Table 3-4). In the presence of

glucose, up to 8.15% of Ni was mobilized from Fh, and up to 3.55% from BF. Additionally, Ni was more readily desorbed from BF control capsules at ~1.11% lost, where as in Fh, both in the presence and absence of glucose, control desorption was <0.25%. This may be the result of Ni adsorbing to the organic component of the cell-mineral aggregate and subsequently being desorbed. These cell-mineral aggregates contain extracellular polymeric substances whose presence may account for the increased desorption and subsequently mobility observed in BF capsules. Increased mobility of Ni form Fh in the presence of glucose (Fig. 3-3A) may also be the result of reactions involving the oxidation of organic carbon provided by the glucose, such as via the reduction of solid-phase Fe(III) to soluble Fe(II). However, in any case the overall mobility of Ni, although greater than Zn, was still less than <8.15%.

Overall, these findings suggest that the presence of organic carbon in IF depositional settings may lead to only a slight increase in the mobility of Ni during diagenesis. However, it is unlikely to affect all trace elements equally, as demonstrated by the observed differences between Zn and Ni. As mobility of Zn and Ni is still low in the presence of organic matter, this would further suggest that the IF record is likely faithfully recording authigenic paleomarine signatures on the order of magnitude of initially adsorbed abundances.

3.4.4 Further considerations on iron formation diagenesis and trace metal mobility

This work represents an important step forward in our understanding of the potential effects that burial diagenesis plays on controlling transition metal mobility in IF. Paleomarine constructions for transition metals based on IF have relied on the preservation of marine-like REE patterns under closed system conditions as an indicator that the primary element signatures in seawater are retained through diagenesis. Under closed system conditions, there is no input or removal of trace elements from the system; essentially the system is in a static state. Evidence for closed system conditions is based on the preservation of variations in REE signatures across multiple Fe-rich bands (e.g., Bolhar et al.,

2004; Pecoits et al., 2009). For example, significant differences in REE patterns, including Eu/Eu* anomalies, are observed at cm-scales in the Kuruman IF, suggesting a lack of post-depositional alteration of REE abundances (Bau and Dulski, 1996). Conversely, open system conditions, where fluids and cations could exchange freely during diagenesis, would homogenize REE patterns (Bau, 1993). Zn and Ni concentrations should similarly be homogenized during diagenesis if open system conditions existed and these transition elements became mobile. However, it has been demonstrated that IF mesobands retain both inter- and intra-band variability with respect to Zn and Ni, among other trace and transition elements (e.g., Pecoits et al., 2009).

Additionally, there is the preservation of small-scale differences in Fe isotope composition in the inter- and intra-band of IF (e.g., Frost et al., 2007; Steinhoefel et al., 2010). For instance, Frost et al. (2007) showed that during diagenesis of the Biwabik IF, secondary fluid flow was generally in a plane parallel to the layers coincident with fluid flow. Such a scenario may lead to horizontal homoginization of trace elements but is unlikely to affect vertical distribution, thereby maintaining temporal variations in transition metal abundances. Further, in a closed system, a bulk analytical technique is likely to account for any local trace element mobilization within a given band, as the measurement of a bulk sample would act to normalize any small-scale variations due to localized fluid flow.

The lack of mobility seen here differs from the interpretation of Frierdich et al. (2011), who suggested that exchange with trace-metal-free solutions mobilized Ni and Zn to the point where IF can no longer be used as proxies for seawater composition. However, their work assumes open system conditions during diagenesis, as well as interaction with a trace-metal-free solution, conditions that are obviously not be realistic for many IF (e.g., Bau, 1993; Pecoits et al., 2009). Early diagenetic fluids would either be generated via dewatering of amorphous Fe oxyhydroxides (i.e. transformations to hematite, Posth et al., 2013) in which case the fluid may be free of trace elements, or with a pore water fluid that is unlikely to be trace–metal-free. However, to be conservative, the fluids

used to rinse the particles following the temperature and pressure treatment here were free of Zn or Ni, but were of the same ionic strength and composition as when Zn or Ni were originally adsorbed. Also, the high water-rock ratios characteristic of our post-diagenetic treatment rinse, approximately 50:1 by weight, were repeated twice and should favor mobilization or desorption of Zn or Ni. Furthermore, if mobilization were to occur in a closed system, where clear authigenic marine signatures are recorded, any Ni or Zn mobilized by dehydration reactions would likely remain in the IF and be incorporated into recrystallized minerals during ongoing diagenesis. Indeed, as shown by Konhauser et al. (2009), Ni concentrations were very similar in both hematite and magnetite grains. As such, the estimates for Ni and Zn mobility provided here represent first order estimates for early diagenetic mobility and suggests that IF are largely capable of maintaining the signatures of seawater contemporaneous to their deposition following diagenetic pressure and temperature reactions.

Another important issue is the potential for Ni and Zn mobilization during processes where unstable and largely amorphous ferric oxyhydroxides form early diagenetic and secondary, more crystalline mineral phases (e.g., Raiswell et al., 2011; Posth et al., 2013). These types of reactions are common when Fe-carbonate and Fe-oxides are pyritized; although, it is likely that these types of reactions are more characteristic of geological settings in which there is high organic matter loading relative to Fe supply (see Köhler et al., 2013). A caveat, is that ferrihydrite is not stable and will transform to hematite or may also be subject to microbial Fe(III) reduction. However, it is likely that oxide-facies IF, such as those approximated here by organic carbon-free experimental capsules, retain original seawater signatures. The caveat to this may be siderite-facies IF where trace metals can adsorb or co-precipitate with Fe-carbonates. Encouragingly, as we have shown here, even in capsules with organic carbon present and where siderite is likely to form during diagenesis in a closed system (c.f. Posth et al., 2013), no Zn and only little Ni is mobilized.

An additional mechanism is the mobilization of trace metals by Fe(III) reducing bacteria. Previous studies have shown that phosphate, for example, can

be liberated in modern hydrothermal sediments with burial – the amount was typically less than 50% (Poulton and Canfield, 2006). Moreover, it has been shown in modern lake settings that bacterial Fe(III) reduction of Fe oxyhydroxides has the potential to mobilize adsorbed arsenic (Cummings et al., 1999). Further, increased solubility of Ni and cobalt have been known to accompany manganese- and Fe-reduction by anaerobic bacteria in modern surface soil horizons (Quantin et al., 2001).

Predicting the magnitude of trace metal release during IF diagenesis, however, requires further investigation. To date, the only study that has attempted to model ancient Fe(III) recycling was by Konhauser et al. (2005) who modeled the Archean marine Fe cycle by making two assumptions. First, they assumed that the bulk of the Fe(II) component in Fe-rich BIF-type macrobands formed diagenetically through biological Fe(III) reduction, i.e., the magnetite is not primary. Based on a predicted rate of Fe(III) deposition annually (1 mm $year^{-1}$), they then quantified how many electrons were needed to generate that amount of magnetite reported in BIF (⅓ of the ferric oxides minerals; Morris, 1993). Second, they quantified the amount of photosynthetic Fe(II)-oxidizer biomass that may have been generated in the photic zone of the water column (based on Kappler et al., 2005) in order to estimate the amount of Fe recycled prior to burial. The results demonstrated that under ideal growth conditions, as much as 70% of the biologically formed Fe(III) could have been recycled back into the water column via fermentation and organic carbon oxidation coupled to microbial Fe(III) reduction.

In light of these considerations and the lack of mobility observed in this work, we can be fairly confident that IF indeed record authigenic marine signatures. This finding is highly favorable for the use of IF in paleomarine reconstructions and inferring transition element bioavailability from the IF record.

3.4.5 Implications for paleomarine reconstructions

The Zn partitioning isotherms and mobility trends presented here, suggest that the finding of a near modern reservoir for paleomarine Zn (as proposed by Scott et

al., 2013 and Robbins et al., 2013) is quite robust. Moreover, the low mobility of Ni observed here suggests that for a range of transition elements, the IF record likely records authigenic signatures with high fidelity, with little mobilization during reactions occurring at temperatures and pressures characteristic of IF diagenesis. Considering the slightly more mobile nature of Ni, we observe a maximum potential mobility of ~8.15%. This value represents an upper limit for Ni mobilized in the presence of organic matter, and is greater than in the absence of organics, possibly due to reactions involving electron transfer (c.f. Frierdich et al., 2011; Frierdich and Catalano, 2012; Posth et al., 2013). This would strongly suggest that paleomarine reconstructions of Ni based on IF (i.e. Konhauser et al., 2009) are at least on the correct order of magnitude.

Overall, we must consider the results here to represent a generalization as not all IF are exposed to the same post-depositional or diagenetic conditions and there is the potential for variability in the amount of transition metals released between different formations. Another caveat is that paleomarine reconstructions of Ni are based on the co-precipitation of Ni with varied amounts of Si, where as mobility experiments only considered Fe-oxyhydroxides with or without organic matter. It should be emphasized that in paleomarine reconstructions aimed at determining trace element concentrations in the Precambrian, it is the order of magnitude rather than the absolute value that is of the most importance. As such, small changes in trace metal concentrations during diagenetic reactions do not necessarily preclude the use of IF as a proxy for Precambrian marine conditions. The results presented herein support the notion that IF are likely faithful recorders of marine conditions contemporaneous with IF deposition and likely faithfully track dissolved Zn and Ni abundances in ancient seawater, and by extension their bioavailability, through geological time.

3.5 Conclusions

Experimentally derived partitioning behaviour was examined for Zn co-precipitating with Fe-oxyhydroxides under varied Si concentrations. By combining this behaviour with Zn/Fe ratios from the IF record, we extrapolate

paleomarine Zn concentrations between ~0.05-129.2 nM throughout the Precambrian, within a few orders of magnitude of a modern ~10 nM value. This is wholly consistent with recent estimates based on Zn systematics in the IF and shale sedimentary records (Robbins et al. 2013; Scott et al., 2013). Further, the magnitude of the partitioning between Zn and Fe-oxyhydroxides was similar to that for Ni reported by Konhauser et al. (2009), but differed in several key aspects; (i) at low concentrations of Zn (<0.5 μM), the isotherms converge, (ii) Zn seems to be less sensitive to the presence of Si during adsorption than Ni or PO_4^{3-} and, (iii) at high concentrations of Si, Zn is adsorbed in higher concentrations to Fe-oxyhydroxides, rather than attenuated as is the case with PO_4^{3-} and Ni.

It is clear that IF mineral diagenesis is a complex process and largely dependent on precursor materials, especially with regards to the presence of organic matter, and that understanding these diagenetic reactions is critical to our understanding of IF as proxies for the chemical composition of Precambrian oceans. Under pressure and temperature conditions realistic for IF diagenesis (170ºC and 1.2 kbar), the key biological transition elements Zn and Ni are relatively immobile. The limited mobility observed suggests that recent paleomarine estimates of Zn (Robbins et al. (2013) and values derived in this work) are likely robust, while paleomarine Ni estimates (Konhauser et al., 2009) are also likely to be on the correct order of magnitude. Unlike previous studies (Frierdich et al., 2011; Frierdich and Catalano 2012), the results here show lower mobility for Ni and Zn under conditions which are more representative of IF diagenesis. In order to better exploit the IF record, it will be necessary to more fully understand the implications of IF diagenesis for the mobility of trace elements such as Zn, Ni and other biologically relevant trace and transition elements. The approach and results from this study are valid in evaluating the effects of diagenesis, and suggest that the record of IF that experienced closed system behaviour can reflect authigenic paleomarine enrichments transition metal concentrations These results are consistent with indications from the REE record that trace elements were stable during IF diagenesis.

$[SiO_2]$ (mM)	Kd (μM^{-1})	Upper Estimate [Zn] (nM)	Representative [Zn] (nM)	Lower Estimate [Zn] (nM)
0	0.03096	129.20	3.23	0.06
0.67	0.03337	119.87	3.00	0.06
2.20	0.03940	101.52	2.54	0.05

Table 3-1. Paleomarine Zn concentrations extrapolated from partitioning isotherms in Fig. 3-1 and maximum (0.004), representative (0.0001) and minimum ($2x10^{-6}$) Zn/Fe values from the IF record (cf. Robbins et al., 2013).

TE + Mineral Combination	Mass of Fe particles (g)	Fe (mol)	Initial TE (ppm)	Final TE (ppm)	Volume of TE solution (L)	TE adsorbed (mol)	% TE adsorbed	TE/Fe-particles (mol/g)	mol Zn/ mol Fe	mol Ni/ mol Fe
Zn on 2-line synthetic ferrihydrite	1.0224	0.0096	3.238	0.195	0.99866	4.6460E-05	93.978	4.5442E-05	4.8564E-03	-
Ni on 2-line synthetic ferrihydrite	0.9965	0.0093	3.245	1.105	1.00188	3.6529E-05	65.948	3.6658E-05	-	3.9176E-03
Zn on biogenic ferrihydrite	0.5023	0.0044	3.231	0.096	0.49516	2.3733E-05	97.029	4.7248E-05	5.4099E-03	-
Ni on biogenic ferrihydrite	0.4769	0.0042	3.200	0.212	0.49638	2.5270E-05	93.375	5.2988E-05	-	6.0671E-03

Table 3-2. Adsorption of Zn and Ni to 2-line synthetic, and biogenic ferrihydrite.

Capsule	Mass Fe particles (g)	Mass Glucose (g)	Zn/Fe-particles (mol/g)	Zn/capsule (mol)	Zn released (mol)	Ni released (mol)	% Zn mobilized	Zn ICP-OES σ (ppm)	±2σ Zn (mol)	±2σ Zn (%)	Capsule Contents*
ZnFh-2	0.09998	0.00407	4.544E-05	4.543E-06	0.000	1.1498E-08	0.00	0.0031	9.48E-08	2.09	Zn+Fh+G
ZnFh-3	0.09997	-	4.544E-05	4.543E-06	0.000	3.2712E-10	0.00	0.0031	9.48E-08	2.09	Zn+Fh
ZnFh-4	0.10003	-	4.544E-05	4.546E-06	0.000	0	0.00	0.0024	7.34E-08	1.61	Zn+Fh
C-ZnFh1	0.09996	0.00406	4.544E-05	4.542E-06	0.000	0	0.00	0.0064	1.96E-07	4.31	Zn+Fh+G
C-ZnFh2	0.09997	0.00408	4.544E-05	4.543E-06	0.000	0	0.00	0.0030	9.17E-08	2.02	Zn+Fh+G
C-ZnFh3	0.09999	-	4.544E-05	4.544E-06	0.000	0	0.00	0.0033	1.01E-07	2.22	Zn+Fh
C-ZnFh4	0.10004	-	4.544E-05	4.546E-06	0.000	0	0.00	0.0029	8.87E-08	1.95	Zn+Fh
ZnBF2	0.03408	-	4.725E-05	1.610E-06	0.000	4.99E-10	0.00	0.0036	1.10E-07	6.84	Zn+BF
ZnBF3	0.03625	-	4.725E-05	1.713E-06	5.724E-09	1.64E-10	0.33	0.0020	6.12E-08	3.57	Zn+BF
C-ZnBF1	0.03527	-	4.725E-05	1.666E-06	1.486E-08	1.34E-09	0.89	0.0029	8.87E-08	5.32	Zn+BF
C-ZnBF2	0.03509	-	4.725E-05	1.658E-06	0.000	0.000	0.00	0.0039	1.19E-07	7.19	Zn+BF

Table 3-3. Percentage of Zn mobilized in experimental pressure and temperature treatments and control capsules; and associated error calculations. *Capsule contents include Zn adsorbed to 2-line synthetic ferrihydrite (Fh) in the presence of absence of glucose (G) or adsorbed to biogenic ferrihydrite cell-mineral aggregates (BF).

Capsule	Mass Fe particles (g)	Mass Glucose (g)	Ni/Fe-particles (mol/g)	Ni/capsule (mol)	Zn released (mol)	Ni released (mol)	% Ni mobilized	Ni ICP-OES σ (ppm)	±2σ Ni (mol)	±2σ Ni (%)	Capsule Contents
NiFh-1	0.10000	0.00409	3.666E-05	3.666E-06	0.000	1.936E-07	5.28	0.0229	7.80E-07	21.29	Ni+Fh+G
NiFh-2	0.09998	0.00406	3.666E-05	3.665E-06	0.000	2.987E-07	8.15	0.0361	1.23E-06	33.56	Ni +Fh+G
NiFh-4	0.10008	-	3.666E-05	3.669E-06	0.000	1.656E-10	0.00	0.0003	1.02E-08	0.28	Ni+Fh
C-NiFh1	0.10008	0.00405	3.666E-05	3.669E-06	0.000	6.847E-09	0.19	0.0022	7.50E-08	2.04	Ni+Fh+G
C-NiFh2	0.10009	0.00403	3.666E-05	3.669E-06	0.000	6.279E-09	0.17	0.0012	4.09E-08	1.11	Ni+Fh+G
C-NiFh3	0.10006	-	3.666E-05	3.668E-06	0.000	8.665E-09	0.24	0.0010	3.41E-08	0.93	Ni+Fh
C-NiFh4	0.10004	-	3.666E-05	3.667E-06	0.000	5.856E-09	0.16	0.0011	3.75E-08	1.02	Ni+Fh
NiBF1	0.03550	-	5.299E-05	1.881E-06	0.000	6.109E-08	3.25	0.0075	2.56E-07	13.59	Ni+BF
NiBF2	0.03542	-	5.299E-05	1.877E-06	0.000	6.666E-08	3.55	0.0072	2.45E-07	13.07	Ni+BF
C-NiBF1	0.03553	-	5.299E-05	1.883E-06	0.000	1.977E-08	1.05	0.0009	3.07E-08	1.63	Ni+BF
C-NiBF2	0.03522	-	5.299E-05	1.866E-06	0.000	2.070E-08	1.11	0.0037	1.26E-07	6.76	Ni+BF

Table 3-4. Percentage of Ni mobilized in experimental pressure and temperature treatments and control capsules; and associated error calculations. *Capsule contents include Ni adsorbed to 2-line synthetic ferrihydrite (Fh) in the presence of absence of glucose (G) or adsorbed to biogenic ferrihydrite cell-mineral aggregates (BF).

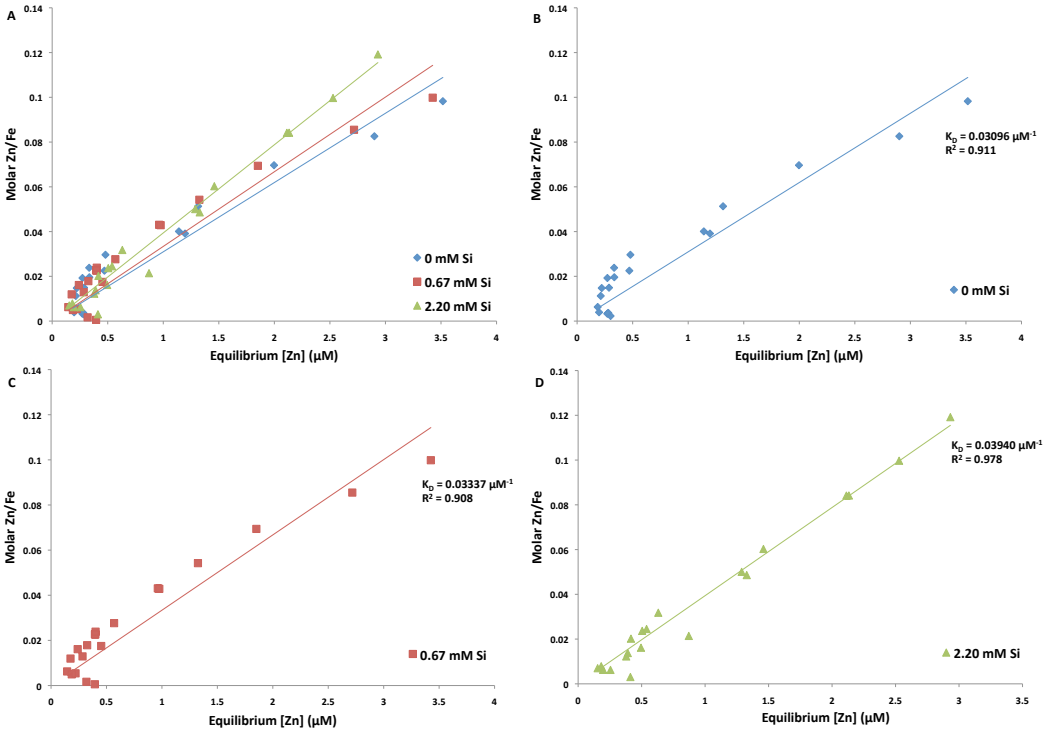

Figure 3-1. Experimentally derived partitioning coefficients for Zn-Fe co-precipitation experiments. (A) All three conditions presented together. Isotherms were developed under varied Si concentrations of (B) 0, (C) 0.67 and (D) 2.20 mM as per Konhauser et al. (2007; 2009). For the internal calibration and data used to generate the isotherms refer to Appendix 2.

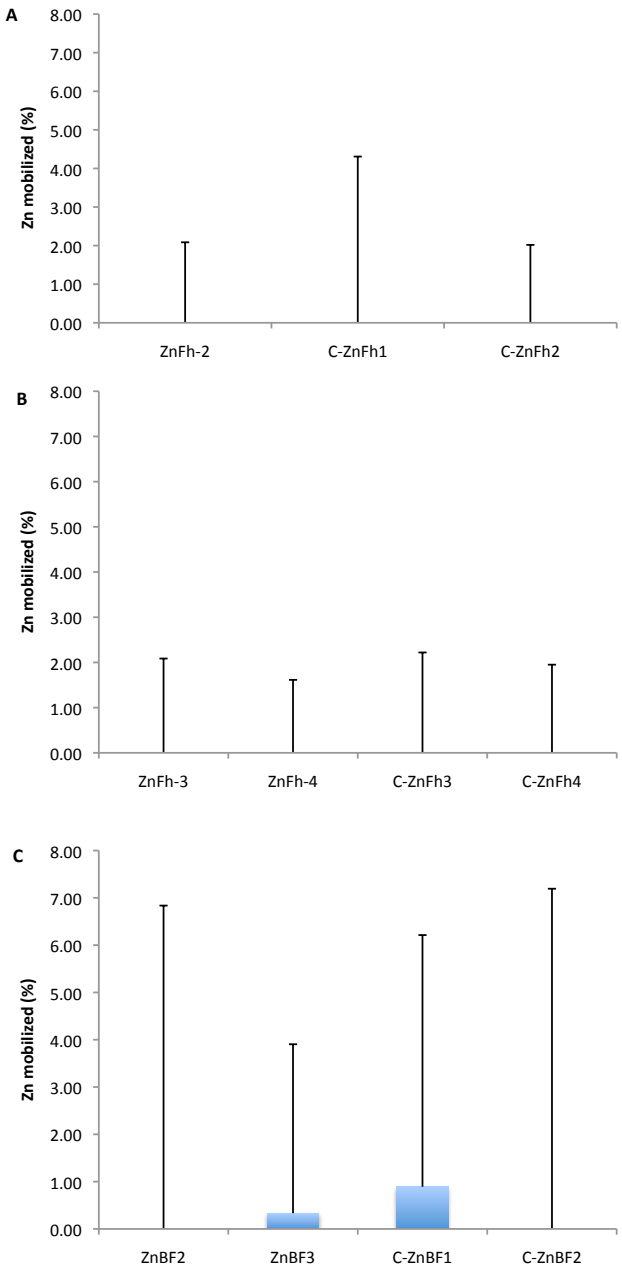

Figure 3-2. The percentage of initially adsorbed Zn mobilized from (A) synthetic 2-line ferrihydrite with glucose added, (B) synthetic 2-line ferrihydrite, and (C) biogenic ferrihydrite, following incubation for 14 days at 170ºC and 1.2 kbar. Each bar represents a single experimental capsule; a precursor C denotes an un-incubated control capsule. Error bars represent the upper level of uncertainty based on 2σ variation in ICP-OES measurements of released Zn (refer to methods).

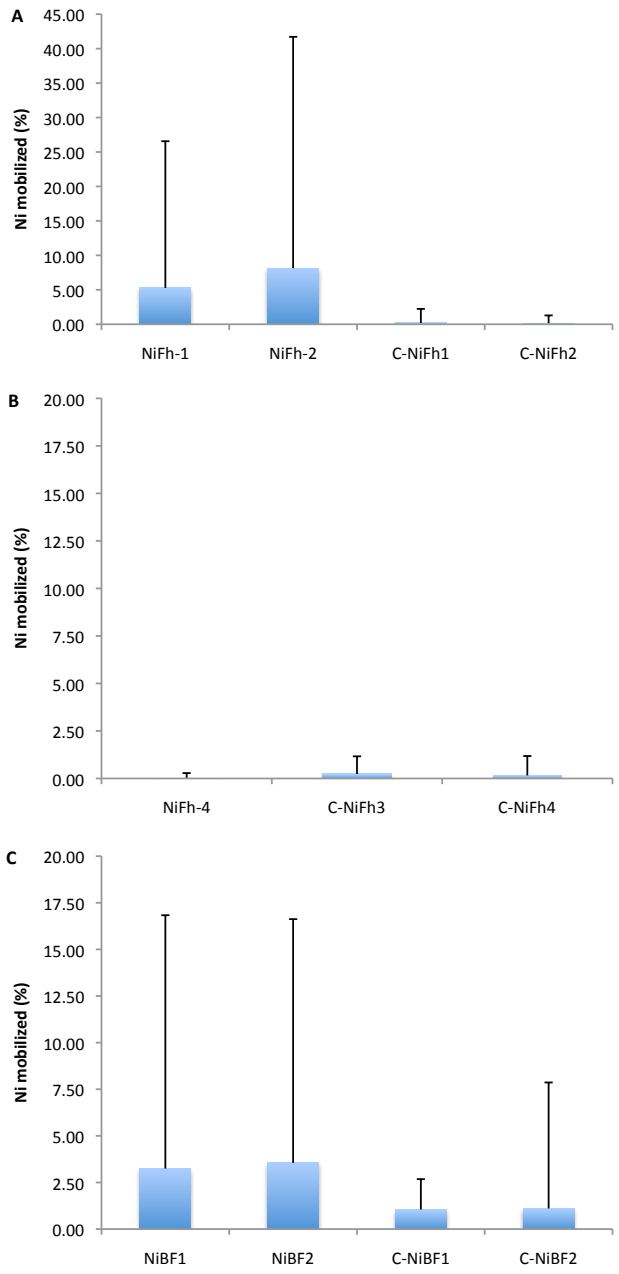

Figure 3-3. The percentage of initially adsorbed Ni mobilized from (A) synthetic 2-line ferrihydrite with glucose added, (B) synthetic 2-line ferrihydrite, and (C) biogenic ferrihydrite, following incubation for 14 days at 170ºC and 1.2 kbar. Each bar represents a single experimental capsule; a precursor C denotes an un-incubated control capsule. Error bars represent the upper level of uncertainty based on 2σ variation in ICP-OES measurements of released Ni (refer to methods).

3.6 References

Alexander BW, Bau M, Andersson P, Dulski P (2008) Continentally-derived solutes in shallow Archean seawater: Rare earth element and Nd isotope evidence in iron formations form the 2.9 Ga Pongola Supergroup, South Africa. *Geochimica et Cosmochimica Acta*, **72**, 378-394.

Anderson PR, Benjamin MM (1985) Effect of silicon on the crystallization and adsorption properties of ferric oxides. *Environmental Science and Technology*, **19**, 1048-1053.

Bau M (1993) Effects of syn- and post depositional processes on the rare-earth element distribution in Precambrian iron-formations. *European Journal of Mineralogy*, **5**, 257-267.

Bau M, Möller P (1993) Rare earth element systematics of the chemically precipitated component in Early Precambrian iron formations and the evolution of the terrestrial atmosphere-hydrosphere-lithosphere system. *Geochimica et Cosmochimica Acta*, **57**, 2239-2249.

Bau M, Dulski P (1996) Distribution of yttrium and rare-earth elements in the Penge and Kuruman iron-formations, Transvaal Supergroup, South Africa. *Precambrian Research*, **79**, 37-55.

Bekker A, Slack JF, Planavsky N, Krapež B, Hofmann A, Konhauser KO, Rouxel OJ (2010) Iron Formation: The sedimentary product of a complex interplay among mantle, tectonic, oceanic and biospheric processes. *Economic Geology*, **105**, 468-508.

Bhattacharya HN, Chakraborty I, Ghosh KK (2007) Geochemistry of some banded iron-formations of the archean supracrustals, Jharkand-Orissa region, *Indian Journal of Earth System Science*, **116**, 245-259.

Bolhar R, Kamber BS, Moorbath S, Fedo CM, Whitehouse MJ (2004) Characterisation of early Archaean chemical sediments by trace element signatures. *Earth and Planetary Science Letters*, **222**, 43-60.

Bjerrum CJ, Canfield DE (2002) Ocean productivity before about 1.9 Gyr ago limited by phosphorous onto iron oxides. *Nature*, **417**, 159-162.

Brand LE, Sunda WG, Guillard RRL (1983) Limitation of marine phytoplankton reproductive rates by Zinc, Manganese and Iron. *Limnology and Oceanography*, **28**, 1182-1198.

Bruland KW, Orians KJ, Cowen JP (1994) Reactive trace metals in the stratified central North Pacific. *Geochimica et Cosmochimica Acta*, **58**, 3171-3182.

Canfield DE (1998) A new model for Proterozoic ocean chemistry. *Nature*, **396**, 450-453.

Cismasu AC, Michel FM, Tcaciuc AP, Tyliszczak T, Brown Jr GE (2011) Composition and structural aspects of naturally occurring ferrihydrite. *Comptes Rendus Geoscience*, **343**, 210-218.

Cloud P (1968) Atmospheric and hydrospheric evolution on the primitive earth. *Science*, **160**, 729-736.

Cloud P (1973) Paleoecological significance of the banded iron-formation. *Economic Geology*, **68**, 1132-1143.

Cornell RM, Schwertmann U (2003) *The iron oxides: structures, properties, reactions, occurrences and uses*, second ed. Weinheim, Viley-VCH Verlag.

Cummings DE, Caccavo Jr. F, Fendorf S, Rosenzweig RF (1999) Arsenic Mobilization by the Dissimilatroy Fe(III)-Reducing Bacterium *Shewanella alga* BrY. *Environmental Science and Technology*, **33**, 723-729.

Derry LA, Jacobsen SB (1990) The chemical evolution of Precambrian seawater: evidence from REEs in banded iron formations. *Geochimica et Cosmochimica Acta*, **54**, 2965-2977.

Dupont CL, Yang S, Palenik B, Bourne PE (2006) Modern proteomes contain putative imprints of ancient shifts in trace metal geochemistry. *Proceedings of the National Academy of Sciences*, **103**, 17822-17827.

Dupont CL, Butcher A, Valas RE, Bourne PE, Caetano-Anollés G (2010) History of biological metal utilization inferred through phylogenomic analysis of protein structures. *Proceedings of the National Academy of Science*, **107**, 10567-10572.

Dyer JA, Trivedi P, Scrivner NC, Sparks DL (2004) Surface complexation modeling of zinc sorption onto ferrihydrite. *Journal of Colloid and Interface Science*, **270**, 56-65.

Dzombak DA, Morel FMM (1990) *Surface complexation modeling: hydrous ferric oxide*. Wiley-Interscience, New York.

Frierdich AJ, Luo Y, Catalano JG (2011) Trace element cycling through iron oxide minerals during redox driven dynamic recrystallization. *Geology*, **39**, 1083-1086.

Frierdich AJ, Catalano JG (2012) Controls on Fe(II)-activated trace element release from Goethite and Hematite. *Environmental Science and Technology*, **46**, 1519-1526.

Frierdich AJ, Scherer MM, Bachman JE, Engelhard MH, Rapponotti BW, Catalano JG (2012) Inhibition of trace element release during Fe(II)-activated recrystallization of Al-, Cr-, and Sn-substituted goethite and hematite. *Environmental Science and Technology*, **46**, 10031-10039.

Frost CD, von Blanckenburg F, Schoenberg R, Frost BR, Swapp SM (2007) Preservation of Fe isotope heterogeneities during diagenesis and metamorphism of banded iron formation. *Contributions to Mineralogy and Petrology*, **153**, 211-235.

Gole MJ, Klein C (1981) Banded Iron-Formations through Much of Precambrian Time. *The Journal of Geology*, **89**, 169-183.

Grenne T, Slack JF (2003) Paleozoic and Mesozoic silica-rich seawater: Evidence from hematitic chert (jasper) deposits. *Geology*, **31**, 319-322.

Grotzinger JP, Kasting JF (1993) New Constraints on Precambrian Ocean Composition. *The Journal of Geology*, **101**, 235-243.

Johnson CM, Beard BL, Klein C, Beukes NJ, Roden EE (2008) Iron isotopes constrain biologic and abiologic processes in banded iron formation genesis. *Geochimica et Cosmochimica Acta*, **72**, 151-169.

Kappler A, Pasquero C, Konhauser KO, Newman DK (2005) Deposition of banded iron formations by anoxygenic phototrophic Fe(II)-oxidizing bacteria. *Geology*, **33**, 865-868.

Klein C (2005) Some Precambrian banded iron-formations (BIFs) from around the world: Their age, geologic setting, mineralogy, metamorphism, geochemistry, and origin. *American Mineralogist*, **90**, 1473-1499.

Köhler I, Konhauser KO, Papineau D, Bekker A, Kappler A (2013) Biological carbon precursor to diagenetic siderite with spherical structures in iron formations. *Nature Communications*, doi: 10.1038/ncomms2770.

Konhauser KO, Hamade T, Raiswell R, Morris RC, Ferris FG, Southam G, Canfield DE (2002) Could bacteria have formed the Precambrian banded iron formations? *Geology*, **30**, 1079-1082.

Konhauser KO (2005) *Introduction to Geomicrobiology*. Wiley-Blackwell, Oxford, United Kingdom.

Konhauser KO, Newman DK, Kappler A (2005) The potential significance of microbial Fe (III) reduction during deposition of Precambrian banded iron formations. *Geobiology*, **3**, 167-177.

Konhauser KO, Lalonde SV, Amskold L, Holland HD (2007) Was there really an Archean phosphate crisis? *Science*, **315**, 1234.

Konhauser KO, Pecoits E, Lalonde SV, Papineau D, Nisbet EG, Barley ME, Arndt NT, Zahnle K, Kamber BZ (2009) Oceanic nickel depletion and a methanogen famine before the Great Oxidation Event. *Nature*, **458**, 750-753.

Langmuir D (1997) *Aqueous Environmental Geochemistry*. Prentice Hall, Upper Saddle River, New Jersey.

Maliva RG, Knoll AH, Simonson BM (2005) Secular change in the Precambrian silica cycle: Insights form chert petrology. *Geological Society of America Bulletin*, **117**, 835-845.

Martinez CE, McBride MB (1999) Dissolved and labile concentrations of Cd, Cu, Pb, and Zn in aged ferrihydrite–organic matter systems. *Environmental Science and Technology*, **33**, 745-750.

McConchie D (1984) The geology and geochemistry of the Joffre and Whaleback Shale members of the Brockman Iron Formation, Western Australia. PhD Thesis, University of Western Australia.

Miyano T (1987) Diagenetic to low-grade metamorphic conditions of Precambrian iron-formations in Appel PWU and LaBerge GL, eds., *Precambrian Iron Formations*: Athens, Theophrastus Publications, 155-186.

Miyano T, Klein C (1984) Evaluation of the stability relations of amphibole asbestos in metamorphosed iron formations. *Mining Geology*, **33**, 213-222.

Morris RC (1993) Genetic modeling for banded iron-formation of the Hamersley Group, Pilbara Craton, Western Australia. *Precambrian Research*, **60**, 243-286.

Nolting RF, de Baar HJW (1994) Behaviour of nickel, copper, zinc and cadmium in the upper 300 m of a transect in the Southern Ocean (57º-62ºS, 49ºW). *Marine Chemistry*, **45**, 225-242.

Pecoits E, Gingras MK, Barley ME, Kappler A, Posth NR, Konhauser KO (2009) Petrography and geochemistry of the Dales Gorge banded iron formation: Paragenetic sequence, source and implication for palaeo-ocean chemistry. *Precambrian Research*, **172**: 163-187.

Planavsky N, Rouxel O, Bekker A, Shapiro R, Fralick P, Knudsen A (2009) Iron-oxidizing microbial ecosystems thrived in late Paleoproterozoic redox-stratified oceans. *Earth Planetary Science Letters*, **286**, 230-242.

Planavsky N, Bekker A, Rouxel OJ, Kamber B, Hofmann A, Knudsen A, Lyons TW (2010) Rare earth element and yttrium compositions of Archean and Paleoproterozoic Fe formations revisited: New perspectives on the significance and mechanisms of deposition. *Geochimica et Cosmochimica Acta*, **74**, 6387-6405.

Planavsky NJ, McGoldrick P, Scott CT, Li C, Reinhard CT, Kelly AE, Chu X, Bekker A, Love GD, Lyons TW (2011) Widespread iron-rich conditions in the mid-Proterozoic ocean. *Nature*, **477**, 448-451.

Posth NR, Hegler F, Konhauser KO, Kappler A (2008) Alternating Si and Fe deposition caused by temperature fluctuations in Precambrian oceans. *Nature Geoscience*, **1**, 703-708.

Posth NR, Köhler I, Swanner E, Schröder C, Wellmann E, Binder B, Konhauser KO, Neumann U, Berthold C, Nowak M, Kappler A (2013) Simulating Precambrian banded iron formation diagenesis. *Chemical Geology*, in press.

Poulton SW, Canfield DE (2006) Co-diagenesis of iron and phosphorus in hydrothermal sediments from the southern East Pacific Rise: Implications for the evaluation of paleoseawater phosphate concentrations. *Geochimica et Cosmochimica Acta*, **70**, 5883-5898.

Quantin C, Becquer T, Rouillier JH, Berthelin J (2001) Oxide weathering and trace metal release by bacterial reduction in a New Caledonia Ferralsol. *Biogeochemistry*, **53**, 323-340.

Raiswell R, Reinhard CT, Derkowski A, Owens J, Bottrell SH, Anbar AD, Lyons TW (2011) Formation of syngenetic and early diagenetic iron mineral in the late Archean Mt. McRae Shale, Hamersley Basin, Australia: New insights on the patterns, controls, and paleoenviromental implications of authigenic mineral formation. *Geochimica et Cosmochimica Acta*, **75**, 1072-1087.

Reinhard CT, Planavsky NJ, Robbins LJ, Partin CA, Gill BC, Lalonde SV, Bekker A, Konhauser KO, Lyons TW (2013) Proterozoic ocean redox and biogeochemical stasis. *Proceedings of the National Academy of Sciences*, **110**, 5357-5362.

Robbins LJ, Lalonde SV, Planavsky NJ, Mloszewska AM, Pecoits E, Dupont CL, Saito M, Kappler A, Konhauser KO (2013) Authigenic iron oxide proxies for marine Zinc over geological time and implications for eukaryotic metallome evolution. *Geobiology*, doi: 10.1111/gbi.12036.

Rose AW, Bianchi-Mosquera GC (1993) Adsorption of Cu, Pb, Zn, Co, Ni and Ag on Goethite and Hematite: A control on metal mobilization from red beds into stratiform copper deposits. *Economic Geology* **88**, 1226-1236.

Saito MA, Sigman DM, Morel FMM (2003) The bioinorganic chemistry of the ancient ocean: the co-evolution of cyanobacterial metal requirements and biogeochemical cycles at the Archean-Proterozoic boundary? *Inorganica Chimica Acta*, **356**, 308-318.

Scott C, Planavsky NJ, Dupont CL, Kendall B, Gill B, Robbins LJ, Husband KF, Arnold GL, Wing B, Poulton SW, Bekker A, Anbar AD, Konhauser KO, Lyons TW (2013) Bioavailability of zinc in marine systems through time. *Nature Geoscience*, **6**, 125-128.

Siever R (1992) The silica cycle in the Precambrian. *Geochimica et Cosmochimica Acta* **56**, 3265-3272.

Steinhoefel G, von Blanckenburg F, Horn I, Konhauser KO, Beukes NJ, Gutzmer J (2010) Deciphering formation processes of banded iron formations from the Transvaal and the Hamersley successions by combined Si and Fe isotope analysis using UV femtosecond laser ablation. *Geochimica et Cosmochimica Acta*, **74**, 2677-2696.

Stookey LL (1970) Ferrozine – a new spectrophotometric reagent for iron. *Analytical Chemistry*, **42**, 779-781.

Straub KL, Rainey FA, Widdel F (1999) *Rhodovulum iodosum* sp. nov. and *Rhodovulum robiginosum* sp. nov., two new marine phototrophic ferrous-iron-

oxidizing purple bacteria. *International Journal of Systematic Bacteriology*, **49**, 729-735.

Trivedi P, Axe L (2001) Ni and Zn sorption to amorphous versus crystalline iron oxides: macroscopic studies. *Journal of Colloid and Interface Science*, **244**, 221-229.

Trivedi P, Dyer JA, Sparks DL, Pandya K (2004) Mechanistic and thermodynamic interpretations of zinc sorption onto ferrihydrite. *Journal of Colloid and Interface Science*, **270**, 77-85.

Waychunas GA, Fuller CC, Davis JA (2002) Surface complexation and precipitate geometry for aqueous Zn(II) sorption on ferrihydrite I: X-ray absorption extended fine structure spectroscopy analysis. *Geochimica et Cosmochimica Acta*, **66**, 1119-1137.

Whitehouse MJ, Fedo CM (2007) Microscale heterogeneity of Fe isotopes in >3.71 Ga banded iron formation from Isua Greenstone Belt, southwestern Greenland. *Geology*, **35**, 719-722.

Wiley JD (1977) Coprecipitation of zinc with silica in seawater and in distilled water. *Marine Chemistry*, **5**, 267-290.

CHAPTER 4

Summary and Conclusions: Implications for Zn bioavailability and diagenetic mobility

4.1 Summary

The paleomarine behavior of Zn, as recorded in the IF sedimentary record, has been explored to test the hypothesis that Zn was biolimiting in the Precambrian ocean and a contributing factor to the delay in eukaryotic diversification (cf. Saito et al., 2003 and Dupont et al., 2010). This was accomplished in three broad steps: (1) updating thermodynamic geochemical models in order to reconcile the IF record with previous modeling, (2) by examining temporal trends in Zn/Fe through time, and (3) utilizing the relationship between Zn and Fe, which is a function of particle formation. Under the thermodynamic models presented herein, the maintenance of a uniform Zn reservoir through time is largely attributed to buffering of Zn loss by sphalerite precipitation under marine conditions when organic ligands are low, or potentially by organic ligand complexation in the event that organic ligands were abundant relative to modern oceans. Taken in light of the IF record, and given the constrained relationship between Zn and Fe, a near modern concentration of Zn is indicated from the Precambrian through to the modern. Furthermore, the interpretation of the IF record is considered from an experimental view, addressing the partitioning of Zn under high silica conditions and potential for Zn mobilization during diagenesis. The mobility of Ni was also investigated to offer a comparison against another trace element of biological importance.

In Chapter 2 the IF record was investigated for temporal trends in Zn abundances in the form of Zn/Fe ratios. It is clear that although there is a spread of over four orders of magnitude, there is no drastic change in Zn abundances relative to Fe between the Precambrian and modern, or coincident to the Great Oxidation Event, as observed with other trace elements such as Ni or Cr (e.g.,

Konhauser et al., 2009; 2011, respectively). The paleomarine Zn reservoir is estimated to be on the same order of magnitude as modern, about 10 nM, based on the consistency of the record and hypothetical partitioning scenarios between Zn and precipitating Fe oxyhydroxides. This would suggest that Zn in the Precambrian ocean was several orders of magnitude greater than previous estimates (e.g., Saito et al., 2003), and critically, at least three orders of magnitude above the 10^{-13} M concentration range at which Zn becomes biolimiting to eukaryotes.

In Chapter 3 the IF record of Zn is examined from an experimental approach, investigating the partitioning of Zn under high silica conditions as well as the mobility of Zn during IF diagenesis. It is highly encouraging that estimates for paleomarine Zn derived from combining experimentally determined partitioning coefficients and the IF record are on the same order of magnitude, and quite close in actual value to those derived from hypothetical partitioning scenarios used in Chapter 2. Both findings indicate a near modern level within an order of magnitude of ~10 nM Zn for the Precambrian oceans. Additionally, diagenetic pressure and temperature experiments, also presented in Chapter 3, show very little Zn mobilization under any of the experimental conditions considered including: (1) Zn adsorbed to 2-line ferrihydrite, (2) Zn adsorbed to 2-line ferrihydrite with glucose added, and (3) Zn adsorbed to biogenic ferrihydrite. Moreover, Zn mobility is consistent with that of Ni, which also shows very little mobilization (<10% under all conditions considered here). Taken together, these finding suggest that the IF record for Zn through time is not only capable of recording authigenic marine signatures, but is also a very robust proxy for paleomarine Zn and other trace metals such as Ni.

4.2 Conclusion: Implications for Zn bioavailabity and eukaryotic diversification

The finding of a consistent ~10 nM paleomarine Zn reservoir as recorded in IF has significant implications for how we view the rapid diversification of eukaryotes following Neoproterozoic ocean oxygenation. Previous models have

attributed, at least in part, the rapid diversification of eukaryotes following Neoproterozoic ocean oxygenation to increasing amount of bioavailable Zn (cf. Dupont et al., 2010). In this regard, the rapid diversification is viewed as the result of the proliferation of Zn enzymes coincident to increasing bioavailability of Zn and ocean oxygenation. However, a constant paleomarine Zn reservoir would suggest that the rapid proliferation of nucleus-bound Zn enzymes in eukaryotes is the result of eukaryotic diversification rather than a contributing factor.

This finding is highly robust due to the high levels of agreement with the shale record, which also records a constant, near modern Zn abundance from the Precambrian through to modern (Scott et al., 2013). When the collective view of the IF and shale record is taken, it is clear that Zn was likely not limiting to primitive eukaryotes and provides an example of where the 'bio-inorganic bridge' of Anbar and Knoll (2002), which links paleomarine geochemical and biological evolution, becomes decoupled.

4.3 References

Anbar AD, Knoll AH (2002) Proterozoic ocean chemistry and evolution: A bioinorganic bridge? *Science*, **297,** 1137-1142.

Dupont CL, Butcher A, Valas RE, Bourne PE, Caetano-Anollés G (2010). History of biological metal utilization inferred through phylogenomic analysis of protein structures. *Proceedings of the National Academy of Sciences*, **107,** 10567-10572.

Konhauser KO, Pecoits E, Lalonde SV, Papineau D, Nisbet EG, Barley ME, Arndt NT, Zahnle K, Kamber BS (2009) Oceanic nickel depletion and a methanogen famine before the Great Oxidation Event. *Nature*, **458,** 750-753.

Konhauser KO, Lalonde SV, Planavsky NJ, Pecoits E, Lyons TW, Mojzsis SJ, Rouxel OJ, Barley ME, Rosìere C, Fralick PW, Kump LR, Bekker A (2011) Aerobic bacterial pyrite oxidation and acid rock drainage during the Great Oxidation Event. *Nature*, **478**, 369-373.

Saito MA, Sigman DM, Morel FMM (2003) The bioinorganic chemistry of the ancient ocean: the co-evolution of cyanobacterial metal requirements and biogeochemical cycles at the Archean-Proterozoic boundary? *Inorganica Chimica Acta*, **356**, 308-318.

Scott C, Planavsky NJ, Dupont CL, Kendall B, Gill BC, Robbins LJ, Husband KF, Arnold GL, Wing BA, Poulton SW, Bekker A, Anbar AD, Konhauser KO, Lyons TW (2012) Bioavailability of zinc in marine systems through time. *Nature Geoscience*, **6**, 125-128.

Appendix 1: Supporting information for Chapter 2

A1.1: Supporting figures

a)

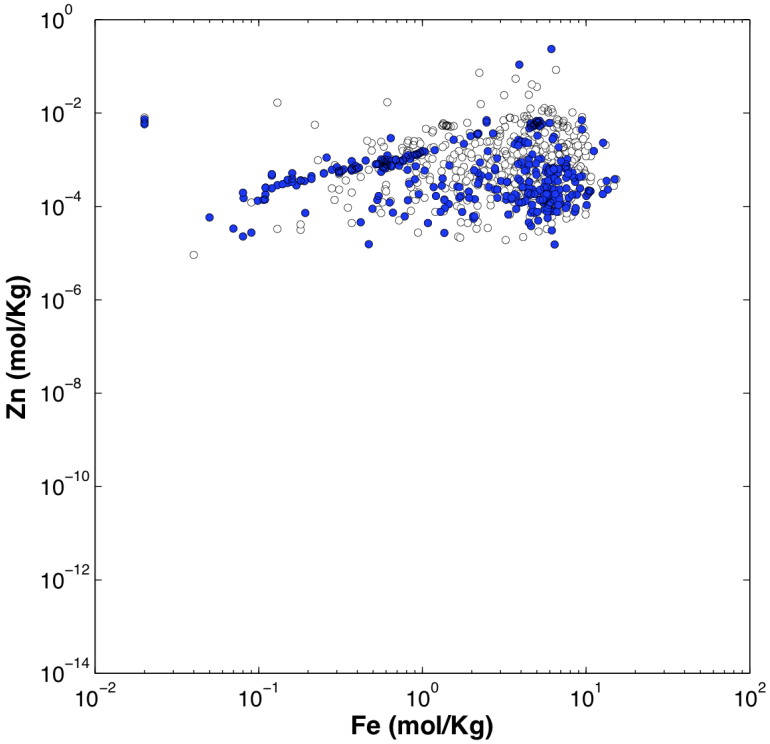

b)

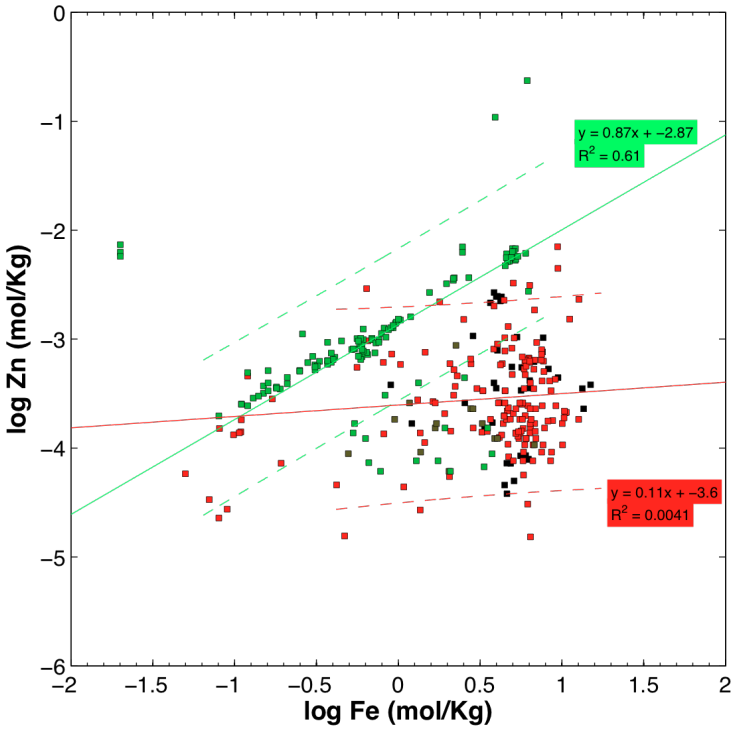

Appendix Figure A1-1. Molar Zn versus Fe cross plots. (A) Open circles represent all available Zn and Fe data, while blue points indicate samples passing filters for detrital contamination and hydrothermal influence (as per Fig. 2 and 3, main text). A high level of agreement exists between the unfiltered and filtered data; scale is the same as in previous Zn-Fe cross plots (Fig. 4A and B). (B) Linear regression lines, equations, and R^2 values for Zn/Fe scaling relationships. Points with an overly high influence on the fits were removed from consideration in the regression using a Cook's distance criteria of $D>n/4$ (Bollen and Jackman, 1990), but not from the figure itself. Solid lines indicate regressions while dashed lines indicate 95% confidence intervals about the regressions. Phanerozoic points (green symbols, green lines) and Precambrian points (red and black symbols, red lines) are considered and plotted separately. While both regressions are positive, the regression through Precambrian data points suffers from poor statistical support.

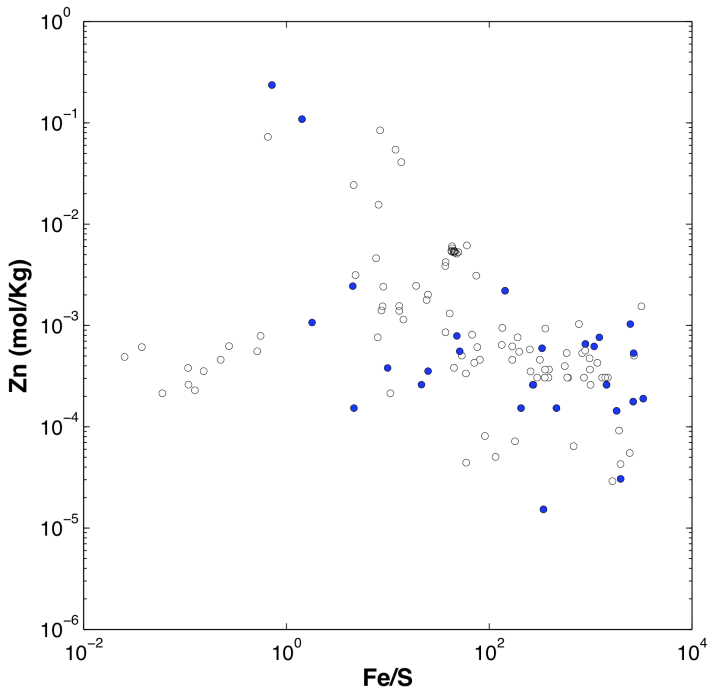

Appendix Figure A1-2. Zn abundances plotted against molar Fe/S ratio. At high Fe/S, there exists no positive relationship between Zn and Fe/S, indicating that sulfide did not likely play a role in Zn enrichment. Points represented by open circles indicate all available data and points with a blue center are samples which pass filters for detrital contamination.

A1.1.1: Reference for supporting figures

Bollen KA, Jackman RW (1990) *Regression diagnostics: An expository treatment of outliers and influential cases*. In *Modern Methods of Data Analysis* (eds Fox J, Long JS) Sage, Newbury Park, CA (pp. 257-291).

A1.2 Supporting tables

Reaction	Log K	Source
$Fe^{2+} + HS^- <--> FeHS^+$	5.62	2
$Zn^{2+} + HS^- + OH^- <--> ZnS + H_2O$	11.74	2
$Zn^{2+} + HS^- <--> ZnHS^+$	6.1	4
$2Zn^{2+} + 3HS^- <--> Zn_2S_3^{2-} + 3H^+$	41.09	2
$4Zn^{2+} + 6HS^- <--> Zn_4S_6^{4-} + 6H^+$	84.41	3
$Zn^{2+} + HS^- + OH^- <--> ZnS(s)$ (Sphalerite) $+ H_2O$	-10.82	5
$Fe^{2+} + HS^- + OH^- <--> FeS(s)$ (Mackinawite) $+ H_2O$	-8.6	5
$Zn^{2+} + L^{-1} <--> Zn\text{-}L^{+1}$	11	6

Appendix Table A1-1. Equilibrium constants in the Zn-Fe-S-organic ligand system used for geochemical modeling in MINTEQ[1].

A1.2.1 References for Appendix Table A1-1:

1. Gustafsson JP (verified 10 October 2012). Visual Minteq 3.0: http://www2.lwr.kth.se/English/OurSoftware/vminteq

2. Luther GW, Rickard DT, Theberge S, Olroyd A (1996) Determination of metal (bi)sulfide stability constants of Mn^{2+}, Fe^{2+}, Co^{2+}, Ni^{2+}, Cu^{2+}, and Zn^{2+} by voltammetric methods. *Environmental Science & Technology*, **30**, 671-679.

3. Luther GW, Theberge SM, Rickard DT (1999) Evidence for aqueous clusters as intermediates during zinc sulfide formation. *Geochimica et Cosmochimica Acta*, **63**, 3159-3169.

4. Rickard D, Luther GW (2006) Metal sulfide complexes and clusters. *Reviews in Mineralogy & Geochemistry*, **61**, 421-504.

5. Smith RM, Martell AE, Motekaitis RJ (2003) NIST critically selected stability constants of metal complexes database. NIST Standard Reference Database 46, Version 7. NIST, Gaithersburg MD, USA.

6. Bruland KW (1989) Complexation of zinc by natural organic ligands in the Central North Pacific. *Limnology and Oceanography*, **34**, 269-285.

Appendix Table A1-2. TiO_2, Al_2O_3, S, Zn, and Fe concentrations in ancient and modern authigenic iron oxides.

Refer to Appendix Table A1-2 on associated CD.

A1.2.2 References for Appendix Table A1-2:

1. This study; laser ablation analysis of hematite and magnetite grains at U of A.
2. This study; analysis of bulk sample digests at U of A.
3. Samples analyzed by Noah Planavsky at Woods Hole Oceanographic Institute.
4. Cates NL, Mojzsis SJ (2007) Pre-3750 supracrustal rocks from the Nuvvuagittuq supracrustal belt, northern Québec. *Earth and Planetary Science Letters*, **225**, 9-21.
5. Mloszewska AM, Pecoits E, Cates NL, Mojzsis SJ, O'Neil J, Robbins LJ, Konhauser KO (2012) The composition of Earth's oldest iron formations: The Nuvvuagittuq Supracrustal Belt (Québec, Canada). *Earth and Planetary Science Letters*, **317-318**, 331-342.
6. Bohlar R, Van Kranendonk MJ, Kamber BS (2005) A trace element study of siderite-jasper banded iron formation in the 3.45 Ga Warrawoona Group, Pilbara Craton – Formation from hydrothermal fluids and shallow seawater. *Precambrian Research*, **137**, 93-114.
7. Hofmann A (2005) The geochemistry of sedimentary rocks from the Fig Tree Group, Barberton greenstone belt: Implications for tectonic, hydrothermal and surface processes during mid-Archaean times. *Precambrian Research*, **143**, 23-49.
8. Bhattacharya HN, Chakraborty I, Ghosh KK (2007) Geochemistry of some banded iron-formations of the Archean supracrustals, Jharkhand-Orissa region, India. *Journal of Earth System Science*, **116**, 245-259.
9. Fralick P (personal communication) Localities described in Fralick P, Pufahl PK (2006) Iron formation in Neoarchean deltaic successions and the microbially mediated deposition of transgressive system tracks. *Journal of Sedimentary Research*, **76**, 1057-1066.

10. Breitkopf JH (1988) Iron formations related to mafic volcanism and ensialic rifting in the southern margin zone of the Damara Orogen, Namibia. *Precambrian Research*, **38**, 111-130.
11. Gole MJ (1981) Archean banded iron-formations, Yilgarn block, Western Australia. *Economic Geology*, **76**, 1954-1974.
12. Lascelles DF (2006) The Mount Gibson banded iron formation-hosted magnetite deposit: two distinct processes for the origin of high-grade iron ore. *Economic Geology*, **101**, 651-666.
13. Klein C, Ladeira AE (2002) Petrography and geochemistry of the least altered banded iron-formation of the Archean Carajás Formation, northern Brazil. *Economic Geology*, **97**, 643-651.
14. Alibert C, McCulloch MT (1993) Rare earth element and neodymium isotopic compositions of the banded iron formations and associated shales from Hamersley, western Australia. *Geochimica et Cosmochimica Acta*, **57**, 187-204.
15. Beukes NJ, Klein C (1990) Geochemistry and sedimentology of a facies transition from microbanded to granular iron-formation in the early Proterozoic Transvaal Supergroup, South Africa. *Precambrian Research*, **47**, 99-139.
16. Horstmann UE, Häblich IW (1995) Chemical composition of banded iron-formation of the Griqualand west sequence, Northern Cape Province, South Africa, in comparison with other Precambrian iron formations. *Precambrian Research*, **72**, 109-145.
17. Klein C, Beukes NJ (1989) Geochemistry and sedimentology of a facies transition from limestone to iron-formation deposition in the Early Proterozoic Transvaal Supergroup, South Africa. *Economic Geology*, **84**, 1733-1774.
18. Schröder S, Lacassie JP, Beukes NJ (2006) Stratigraphic and geochemical framework of the Agouron drill cores, Transvaal Supergroup (Neoarchean-Paleoproterozoic, South Africa). *South African Journal of Geology*, **109**, 23-54.

19. Klein C, Ladeira EA (2000) Geochemistry and petrology of some Proterozoic banded iron-formations of the Quadrilátero Ferrífero, Minas Gerais, Brazil. *Economic Geology*, **95**, 405-428.
20. Spier CA, de Oliveira SMB, Sial AN, Rios FJ (2007) Geochemistry and genesis of the banded iron formations of the Cauê Formation, Quadrilátero Ferrífero, Minas Gerais, Brazil. *Precambrian Research*, **152**, 170-206.
21. Dorland HC (1999) Paleoproterozoic laterites, red beds and ironstones of the Pretoria group with reference to the history of atmospheric oxygen: MSc Thesis, Rand Afrikaans University.
22. Schneiderhan EA, Gutzmer J, Strauss H, Mezger K, Beukes NJ (2006) The chemostratigraphy of a Paleoproterozoic MnF-BIF succession—The Voelwater Subgroup of the Transvaal Supergroup in Griqualand West, South Africa. *South African Journal of Geology*, **109**, 63-80.
23. Tsikos H, Moore JM (1997) Petrography and geochemistry of the Paleoproterozoic Hotazel iron-formation, Kalahari Manganese field, South Africa: Implications for Precambrian manganese metallogenesis. *Economic Geology*, **92**, 87-97.
24. Adekoya JA (1998) The geology and geochemistry of the Maru Banded Iron-Formation, northwestern Nigeria. *Journal of African Earth Sciences*, **27**, 241-257.
25. Mücke A (2005) The Nigerian manganese-rich iron-formations and their host rocks – from sedimentation to metamorphism. *Journal of African Earth Sciences*, **41**, 407-436.
26. Roscoe SM, Gandhi SS, Charbonneau BW, Maurice YT, Gibb RA (1987) Mineral resource assessment of the area in the East Arm (Great Slave Lake) and Artillery Lake Region, N,W,T, Proposed as a National Park: Geological Survey of Canada Open File 1434.
27. Slack JF, Grenne T, Bekker A (2009) Seafloor-hydrothermal Si-Fe-Mn exhalites in the Pecos greenstone belt, New Mexico, and the redox state of ca. 1720 Ma deep seawater. *Geosphere*, **5**, 302-314.

28. Hatton OJ, Davidson GJ (2004) Soldiers Cap Group iron-formations, MT Isa Inlier, Australia, as windows into the hydrothermal evolution of a base-metal-bearing Proterozoic rift basin. *Australian Journal of Earth Sciences*, **51**, 85-106.
29. Young GM (2002) Geochemical investigation of a Neoproterozoic glacial unit: The Mineral Fork Formation in the Wasatch Range, Utah. *Geological Society of America Bulletin*, **114**, 387-399.
30. Klein C, Beukes NJ (1993) Sedimentology and geochemistry of the glaciogenic late Proterozoic Rapitan iron-formation in Canada. *Economic Geology*, **88**, 542-565.
31. Klein C, Ladeira EA (2004) Geochemistry and mineralogy of Neoproterozoic banded iron-formations and some selected, siliceous manganese formations from the Urucum district, Mato Grosso do Sul, Brazil. *Economic Geology*, **99**, 1233-1244.
32. Lottermoser BG, Ashley PM (2000) Geochemistry, petrology and origin of Neoproterozoic ironstones in the eastern part of the Adelaide Geosyncline, South Australia. *Precambrian Research*, **101**, 49-67U.
33. Sturesson U (2003) Lower Paleozoic iron oolites and volcanism from a Baltoscandian perspective. *Sedimentary Geology*, **159**, 241-256.
34. Davidson GJ, Stolz AJ, Eggins SM (2001) Geochemical anatomy of silica iron exhalites: evidence for hydrothermal oxyanions cycling in response to vent fluid redox and thermal evolution (Mt. Windsor Subprovince, Australia). *Economic Geology*, **96**, 1201-1226.
35. Duhig NC, Stolz J, Davidson GJ, Large RR (1992) Cambrian microbial and silica gel textures in silica iron exhalites from the Mount Windsor Volcanic Belt, Australia: Their petrography, chemistry, and origin. *Economic Geology*, **87**, 764-784.
36. Sturesson U, Dronov A, Saadre T (1999) Lower Ordovician iron ooids and associated oolitic clays in Russia and Estonia: a clue to the origin of iron oolites? *Sedimentary Geology*, **123**, 63-80.

37. Mücke A, Farshad A (2005) Whole-rock and mineralogical composition of Phanerozoic ooidal ironstones: Comparison and differentiation of types and subtypes. *Ore Geology Reviews*, **26**, 227-262.
38. Grenne T, Slack JF (2005) Geochemistry of jasper beds from the Ordovician Løkken Ophiolite, Norway: Origin of proximal and distal siliceous exhalites. *Economic Geology*, **100**, 1511-1527.
39. Leistel JM, Marcoux E, Deschamps Y (1998) Chert in the Iberian Pyrite Belt. *Mineralium Deposita*, **33**, 59-81.
40. Karpoff AM, Walter AV, Pflumio C (1988) Metalliferous sediments within lava sequences of the Sumail ophiolite (Oman): Mineralogical and geochemical characterization, origin and evolution. *Tectonophysics*, **151**, 223-245.
41. Ravizza G, Sherrell RM, Field MP, Pickett EA (1999) Geochemistry of the Margi umbers, Cyprus, and the Os isotope composition of Cretaceous seawater. *Geology*, **27,** 971-974.
42. Mücke A, Badejoko TA, Akande SO (1999) Petrographic-microchemical studies and origin of the Agbaja Phanerozoic Ironstone Formation, Nupe Basin, Nigeria: A product of a ferruginized ooidal kaolin precursor not identical to the Minette-type. *Mineralium Deposita*, **34**, 284-296.
43. Hein JR, Yeh H-W, Gunn SH, Gibbs AE, Wang C-H (1994) Composition and origin of hydrothermal ironstones from central Pacific seamounts. *Geochimica et Cosmochimica Acta*, **58**, 179-189.
44. Kato Y, Fujinaga K, Suzuki K (2005) Major and trace element geochemistry and Os isotopic composition of metalliferous umbers from the Late Cretaceous Japanese accretionary complex. *Geochemistry Geophysics Geosystems*, **6**, Q07004.
45. Dunk RM, Mills RA (2006) The impact of oxic alteration on plume-derived transition metals in ridge flank sediments from the East Pacific Rise. *Marine Geology*, **229**, 133-157.

46. Marchig V, Gundlach H (1982) Iron-rich metalliferous sediments on the East Pacific Rise: Prototype of undifferentiated metalliferous sediments on divergent plate boundaries. *Earth and Planetary Science Letters*, **58,** 361-382.
47. Hrischeva E, Scott SD (2007) Geochemistry and morphology of metalliferous sediments and oxyhydroxides from the Endeavour segment, Juan de Fuca Ridge. *Geochimica et Cosmochimica Acta*, **71**, 3476-3497.

Appendix 2: Supplementary information for Chapter 3

A2.1 Internal isotherm calibration

An internal calibration to control for any Zn-hydroxide precipitation and/or adsorption to reaction vessels or sample holders was used to correct Zn values. After this correction isotherms should only account for Zn removed by co-precipitation and adsorption to Fe-oxyhydroxide particles. To minimize the effect of contamination the background Zn concentration for ultrapure 18.2 MΩ water in our laboratory, 0.0250 ppm (0.382 μM), was added to the initial concentration of each prepared sample. Standard methods for determining concentrations in diluted solutions were used to determine initial Fe and Zn concentrations. Analysis of control samples, spiked with Zn but not Fe, allowed for the development of a linear relationship (y = mx) relationship between sample Zn concentrations added (x) and Zn measured by Q-ICP-MS (y), (Appendix Figure A2-1 and Table A2-1). Experimental samples (Appendix Table A2-2, Figure 3-1) were then corrected using this relationship by equation (Eq. 1) to determine a final corrected Zn values.

$$Zn_{final-corrected} = \frac{[^{66}Zn]}{m} \qquad \text{Eq. 1}$$

Once $Zn_{final\text{-}corrected}$ values were calculated they were subsequently converted from ppm to μM. $Zn_{particle}$, $Fe_{particle}$ and Molar $Zn/Fe_{particle}$ were calculated by equations 2-4, respectively; data used in the generation of the isotherms is summarized in Appendix Table A2-2.

$$Zn_{particle} = Zn_{initial} - Zn_{final-corrected} \qquad \text{Eq. 2}$$

$$Fe_{particle} = Fe_{initial} - Fe_{Q-ICP-MS} \qquad \text{Eq. 3}$$

$$Molar\ Zn/Fe_{particle} = Zn_{particle}/Fe_{particle} \qquad \text{Eq. 4}$$

Data was corrected and isotherms were based off of ^{66}Zn. The advantage of this approach to calculating isotherms is that it corrects for any non-Fe related adsorption processes and accounts for the background contamination of Zn in the laboratory.

A2.2 Limitations on the generation of Zn isotherms

Although the methodology for establishing isotherms that can be used to extrapolate paleomarine concentrations is highly useful (e.g., Bjerrum and Canfield, 2002; Konhauser et al., 2007; Konhauser et al., 2009), it is not without its limitations. One issue with the isotherms presented here is that the initial Zn concentrations used are outside the range of modern and estimates for paleomarine Zn, which are generally on the order of ~ 10 nM (e.g., Bruland, 1989, Robbins et al., 2013; Scott et al., 2013). Initial concentrations used here range from 0.0373 – 0.5333 ppm equivalent to ~570 – 8153 nM. This is a necessity for these experiments based on both the sensitivity of the Perkin Elmer Elan6000 Q-ICP-MS as well as the ease with which Zn is contaminated in the laboratory. As the levels of Zn estimated for the paleomarine ocean is close to the detection limit on the Q-ICP-MS (~0.00008 ppm = 1 nM). Additionally, background Zn approaches the ppb range (25 ppb = 382 nM), again at least an order of magnitude above the nM range for paleomarine conditions. Contamination was minimized by acid washing all glassware used to store stock solutions aggressively with TM-HNO_3 prior to use, as well as minimizing sample contact time with air. Caps were kept on all samples and filtrate holders except when additions were being made; during sample preparation, Parafilm was used to cover the aperture of the stock solution containers and pipettes used in transferring solutions.

Date/Sample	[Si] (mM)	$[Zn]_{stock}$ (ppm)	$Zn_{initial}$ (mL)	V_{Stock} (mL)	$V_{Fe\text{-}stock}$ (mL)	V_{Final} (mL)	$[Zn]_{initial}$ (ppm)	$[Zn]_{initial\text{-}corrected}$ (ppm)	$[Fe]_{initial}$ (ppm)	$[^{54}Fe]$ (ppm)	$[^{66}Zn]_{measured}$ (ppm)
Jan 17, 2012											
0B1	0.00	9.6407	0.0289	9.9928	0.0000	9.9928	0.0279	0.0529	0.000	0.0921	0.02562
0B2	0.00	97.1368	0.0306	9.8514	0.0000	9.8514	0.3017	0.3267	0.000	0.1002	0.32128
0B3	0.00	97.1368	0.0595	9.8882	0.0000	9.8882	0.5845	0.6095	0.000	0.0990	0.44096
40B1	0.67	9.6407	0.0297	9.9828	0.0000	9.9828	0.0287	0.0537	0.000	0.1174	0.02729
40B2	0.67	97.1368	0.0319	9.9578	0.0000	9.9578	0.3112	0.3362	0.000	0.1164	0.24009
40B3	0.67	97.1368	0.0585	10.0659	0.0000	10.0659	0.5645	0.5895	0.000	0.1062	0.43321
130B1	2.20	9.6407	0.0285	9.9644	0.0000	9.9644	0.0276	0.0526	0.000	0.1105	0.02658
130B2	2.20	97.1368	0.0321	9.8812	0.0000	9.8812	0.3156	0.3406	0.000	0.1094	0.23195
130B3	2.20	97.1368	0.0596	10.0623	0.0000	10.0623	0.5754	0.6004	0.000	0.1113	0.42665
May 25, 2011											
C29	0.00	0.9550	0.0075	10.0772	0.0000	10.0772	0.0007	0.0257	0.0000	0.0873	0.0126
C30	0.00	9.7470	0.2981	10.3728	0.0000	10.3728	0.2801	0.3051	0.0000	0.0786	0.229
C31	0.67	0.9550	0.0147	10.0053	0.0000	10.0053	0.0014	0.0264	0.0000	0.0751	0.0131
C32	0.67	9.7470	0.2959	9.4484	0.0000	9.4484	0.3053	0.3303	0.0000	0.0856	0.244
C33	2.20	0.9550	0.0137	10.0504	0.0000	10.0504	0.0013	0.0263	0.0000	0.0985	0.0141
C34	2.20	9.7470	0.2945	10.0519	0.0000	10.0519	0.2856	0.3106	0.0000	0.0896	0.228

Appendix Table A2-1. Data used for the internal calibration for generation of Zn partitioning isotherms.

Batch	Sample	[Si] (mM)	$[Zn]_{stock}$ (ppm)	$Zn_{initial}$ (mL)	V_{stock} (mL)	$V_{Fe\text{-}stock}$ (mL)	V_{final} (mL)	$[Zn]_{initial}$ (ppm)	$[Zn]_{initial\text{-}corrected}$ (ppm)	$[Fe]_{initial}$ (ppm)	$[^{54}Fe]$ (ppm)	$[^{66}Zn]$ (ppm)	$[Zn]_{final\text{-}corrected}$ (ppm)	$[Zn]_{final}$ (µM)	$Zn_{particle}$ (M)	$Fe_{particle}$ (M)	Molar Zn/Fe
1	0-43	0.00	0.9550	0.0200	10.0808	0.1703	10.2511	0.0019	0.0269	3.0757	0.0551	0.0097	0.0129	0.1976	2.1312E-07	5.4085E-05	0.0039
1	0-44	0.00	0.9550	0.0295	10.0973	0.1703	10.2676	0.0027	0.0277	3.0708	0.0672	0.0148	0.0197	0.3014	1.2280E-07	5.3780E-05	0.0023
1	0-45	0.00	0.9550	0.0483	10.1040	0.1703	10.2743	0.0045	0.0295	3.0688	0.0499	0.0133	0.0178	0.2717	1.7914E-07	5.4053E-05	0.0033
1	0-46	0.00	0.9550	0.0679	10.0512	0.1706	10.2218	0.0063	0.0313	3.0900	0.0544	0.0138	0.0183	0.2805	1.9868E-07	5.4352E-05	0.0037
1	0-47	0.00	0.9550	0.0995	10.1433	0.1704	10.3137	0.0092	0.0342	3.0589	0.0678	0.0091	0.0121	0.1853	3.3775E-07	5.3556E-05	0.0063
1	0-48	0.00	9.7470	0.0303	10.1435	0.1707	10.3142	0.0286	0.0536	3.0641	0.0504	0.0104	0.0139	0.2128	6.0718E-07	5.3961E-05	0.0113
1	0-49	0.00	9.7470	0.0482	10.1523	0.1701	10.3224	0.0455	0.0705	3.0509	0.0890	0.0141	0.0188	0.2871	7.9093E-07	5.3033E-05	0.0149
1	0-50	0.00	9.7470	0.0695	10.1795	0.1706	10.3501	0.0655	0.0905	3.0517	0.0641	0.0164	0.0219	0.3346	1.0482E-06	5.3493E-05	0.0196
1	0-51	0.00	9.7470	0.0892	10.1520	0.1701	10.3221	0.0842	0.1092	3.0510	0.0757	0.0231	0.0308	0.4702	1.1998E-06	5.3273E-05	0.0225
1	0-52	0.00	9.7470	0.2003	10.0607	0.1705	10.2312	0.1908	0.2158	3.0853	0.0776	0.0560	0.0746	1.1407	2.1588E-06	5.3854E-05	0.0401
1	0-52*	0.00	9.7470	0.2003	10.0607	0.1705	10.2312	0.1908	0.2158	3.0853	0.0821	0.0587	0.0782	1.1958	2.1037E-06	5.3773E-05	0.0391
2	0-53	0.00	9.6407	0.0401	9.9605	0.1698	10.1303	0.0382	0.0632	2.8864	0.0709	0.0113	0.0145	0.2215	7.4413E-07	5.0412E-05	0.0148
2	0-54	0.00	9.6407	0.0594	10.0706	0.1708	10.2414	0.0559	0.0809	2.8719	0.0740	0.0139	0.0178	0.2725	9.6458E-07	5.0097E-05	0.0193
2	0-55	0.00	9.6407	0.0795	10.001	0.1707	10.1717	0.0753	0.1003	2.8899	0.0745	0.0170	0.0218	0.3330	1.2012E-06	5.0410E-05	0.0238
2	0-56	0.00	9.6407	0.1104	10.023	0.1715	10.1945	0.1044	0.1294	2.8970	0.0732	0.0245	0.0314	0.4797	1.4987E-06	5.0560E-05	0.0296
2	0-57	0.00	97.1368	0.024	9.9121	0.1702	10.0823	0.2312	0.2562	2.9070	0.0729	0.0670	0.0859	1.3138	2.6035E-06	5.0745E-05	0.0513
2	0-58	0.00	97.1368	0.0351	9.9224	0.1711	10.0935	0.3378	0.3628	2.9191	0.0730	0.1019	0.1306	1.9969	3.5496E-06	5.0960E-05	0.0697
2	0-59	0.00	97.1368	0.0455	9.9127	0.1702	10.0829	0.4383	0.4633	2.9068	0.0782	0.1479	0.1897	2.9003	4.1834E-06	5.0647E-05	0.0826
2	0-60	0.00	97.1368	0.0553	9.9909	0.1701	10.1610	0.5287	0.5537	2.8828	0.0705	0.1794	0.2300	3.5167	4.9478E-06	5.0354E-05	0.0983

Appendix Table A2-2.

Data used for the generation of Zn partitioning isotherms, Zn data is corrected using an internal calibration, see section A2.1 and figure A2-1. A (*) indicates a sample analyzed twice for quality control. Batch 1 was run on May 25, 2011 and batch 2 on January 17, 2012. Acidified Fe-stock solutions for batch 1 and 2 had initial Fe(II) concentrations of 185.1418 ppm and 172.2049 ppm, respectively.

Batch	Sample	[Si] (mM)	$[Zn]_{stock}$ (ppm)	$Zn_{initial}$ (mL)	V_{stock} (mL)	$V_{Fe\text{-}stock}$ (mL)	V_{final} (mL)	$[Zn]_{initial}$ (ppm)	$[Zn]_{initial\text{-}corrected}$ (ppm)	$[Fe]_{initial}$ (ppm)	$[^{54}Fe]$ (ppm)	$[^{66}Zn]$ (ppm)	$[Zn]_{final\text{-}corrected}$ (ppm)	$[Zn]_{final}$ (μM)	$Zn_{particle}$ (M)	$Fe_{particle}$ (M)	Molar Zn/Fe
1	40-43	0.67	0.9550	0.0184	10.0540	0.1707	10.2247	0.0017	0.0267	3.0909	0.0849	0.0154	0.0209	0.3189	8.9564E-08	5.3823E-05	0.0017
1	40-44	0.67	0.9550	0.03	10.0324	0.1706	10.2030	0.0028	0.0278	3.0957	0.0706	0.0191	0.0259	0.3953	2.9867E-08	5.4165E-05	0.0006
1	40-45	0.67	0.9550	0.05	10.0026	0.1706	10.1732	0.0047	0.0297	3.1047	0.0845	0.0090	0.0122	0.1866	2.6741E-07	5.4078E-05	0.0049
1	40-46	0.67	0.9550	0.0697	10.0339	0.1705	10.2044	0.0065	0.0315	3.0934	0.0783	0.0070	0.0095	0.1451	3.3687E-07	5.3986E-05	0.0062
1	40-47	0.67	0.9550	0.0898	10.1304	0.1704	10.3008	0.0083	0.0333	3.0627	0.0788	0.0106	0.0144	0.2209	2.8859E-07	5.3427E-05	0.0054
1	40-48	0.67	9.7470	0.03	10.0320	0.171	10.2030	0.0287	0.0537	3.1029	0.0872	0.0085	0.0115	0.1754	6.4494E-07	5.3996E-05	0.0119
1	40-49	0.67	9.7470	0.0496	10.1010	0.1705	10.2715	0.0471	0.0721	3.0732	0.0869	0.0116	0.0157	0.2401	8.6167E-07	5.3471E-05	0.0161
1	40-50	0.67	9.7470	0.0696	10.1192	0.1709	10.2901	0.0659	0.0909	3.0749	0.0833	0.0218	0.0296	0.4523	9.3784E-07	5.3565E-05	0.0175
1	40-51	0.67	9.7470	0.0894	10.0647	0.1707	10.2354	0.0851	0.1101	3.0877	0.0871	0.0193	0.0263	0.4014	1.2824E-06	5.3727E-05	0.0239
1	40-52	0.67	9.7470	0.1999	10.2271	0.1706	10.3977	0.1874	0.2124	3.0377	0.0735	0.0464	0.0630	0.9627	2.2845E-06	5.3074E-05	0.0430
1	40-52*	0.67	9.7470	0.1999	10.2271	0.1706	10.3977	0.1874	0.2124	3.0377	0.0785	0.0471	0.0639	0.9763	2.2708E-06	5.2984E-05	0.0429
2	40-53	0.67	9.6407	0.0385	9.2601	0.1701	9.4302	0.0394	0.0644	3.1062	0.0752	0.0135	0.0186	0.2838	7.0015E-07	5.4270E-05	0.0129
2	40-54	0.67	9.6407	0.0588	9.5437	0.1714	9.7151	0.0583	0.0833	3.0381	0.0713	0.0155	0.0213	0.3255	9.4875E-07	5.3121E-05	0.0179
2	40-55	0.67	9.6407	0.0797	10.0255	0.1700	10.1955	0.0754	0.1004	2.8713	0.0711	0.0190	0.0261	0.3995	1.1349E-06	5.0138E-05	0.0226
2	40-55*	0.67	9.6407	0.0797	10.0255	0.1700	10.1955	0.0754	0.1004	2.8713	0.0694	0.0188	0.0259	0.3956	1.1388E-06	5.0168E-05	0.0227
2	40-56	0.67	9.6407	0.1088	9.9647	0.1699	10.1346	0.1035	0.1285	2.8869	0.0661	0.0271	0.0372	0.5685	1.3960E-06	5.0507E-05	0.0276
2	40-57	0.67	97.1368	0.0252	10.0578	0.1704	10.2282	0.2393	0.2643	2.8689	0.0713	0.0631	0.0867	1.3248	2.7163E-06	5.0091E-05	0.0542
2	40-58	0.67	97.1368	0.034	10.0091	0.1712	10.1803	0.3244	0.3494	2.8959	0.0869	0.0882	0.1211	1.8516	3.4904E-06	5.0295E-05	0.0694
2	40-59	0.67	97.1368	0.0454	9.9934	0.1697	10.1631	0.4339	0.4589	2.8754	0.0673	0.1294	0.1777	2.7170	4.2993E-06	5.0280E-05	0.0855
2	40-60	0.67	97.1368	0.0553	10.0478	0.1700	10.2178	0.5257	0.5507	2.8651	0.0711	0.1632	0.2240	3.4252	4.9944E-06	5.0027E-05	0.0998

Appendix Table A2-2 Continued.

Batch	Sample	[Si] (mM)	$[Zn]_{stock}$ (ppm)	$Zn_{initial}$ (mL)	V_{stock} (mL)	$V_{Fe\text{-}stock}$ (mL)	V_{final} (mL)	$[Zn]_{initial}$ (ppm)	$[Zn]_{initial\text{-}corrected}$ (ppm)	$[Fe]_{initial}$ (ppm)	$[^{54}Fe]$ (ppm)	$[^{66}Zn]$ (ppm)	$[Zn]_{final\text{-}corrected}$ (ppm)	$[Zn]_{final}$ (μM)	$Zn_{particle}$ (M)	$Fe_{particle}$ (M)	Molar Zn/Fe
1	130-51	2.20	0.9550	0.0203	9.9395	0.1708	10.1103	0.0019	0.0269	3.1277	1.06	0.0074	0.0100	0.1536	2.5792E-07	3.6967E-05	0.0070
1	130-52	2.20	0.9550	0.0297	9.9813	0.1701	10.1514	0.0028	0.0278	3.1023	1.06	0.0094	0.0129	0.1972	2.2776E-07	3.6501E-05	0.0062
1	130-53	2.20	0.9550	0.0497	10.4071	0.1704	10.5775	0.0045	0.0295	2.9826	1.07	0.0087	0.0119	0.1817	2.6911E-07	3.4204E-05	0.0079
1	130-54	2.20	0.9550	0.0689	10.0742	0.1706	10.2448	0.0064	0.0314	3.0830	1.06	0.0122	0.0167	0.2548	2.2558E-07	3.6253E-05	0.0062
1	130-55	2.20	0.9550	0.0993	10.1553	0.1709	10.3262	0.0092	0.0342	3.0641	1.03	0.0197	0.0269	0.4117	1.1090E-07	3.6422E-05	0.0030
1	130-56	2.20	9.7470	0.0298	10.0877	0.1696	10.2573	0.0283	0.0533	3.0612	1.07	0.0181	0.0248	0.3787	4.3640E-07	3.5655E-05	0.0122
1	130-57	2.20	9.7470	0.0486	10.0539	0.1706	10.2245	0.0463	0.0713	3.0892	1.03	0.0237	0.0324	0.4952	5.9537E-07	3.6889E-05	0.0161
1	130-58	2.20	9.7470	0.0689	10.1651	0.1709	10.3360	0.0650	0.0900	3.0612	1.00	0.0242	0.0330	0.5044	8.7113E-07	3.6824E-05	0.0237
1	130-59	2.20	9.7470	0.0894	10.0559	0.1711	10.2270	0.0852	0.1102	3.0975	0.976	0.0418	0.0570	0.8715	8.1331E-07	3.7990E-05	0.0214
1	130-60	2.20	9.7470	0.1989	10.1923	0.1704	10.3627	0.1871	0.2121	3.0444	0.844	0.0636	0.0869	1.3280	1.9144E-06	3.9397E-05	0.0486
1	130-60*	2.20	9.7470	0.1989	10.1923	0.1704	10.3627	0.1871	0.2121	3.0444	0.863	0.0617	0.0842	1.2879	1.9545E-06	3.9051E-05	0.0500
2	130-61	2.20	9.6407	0.0395	10.0493	0.1703	10.2196	0.0373	0.0623	2.8696	0.5934	0.0180	0.0256	0.3909	5.6103E-07	4.0756E-05	0.0138
2	130-62	2.20	9.6407	0.0602	9.9914	0.1705	10.1619	0.0571	0.0821	2.8893	0.5678	0.0191	0.0272	0.4161	8.3925E-07	4.1567E-05	0.0202
2	130-63	2.20	9.6407	0.0798	10.0574	0.1700	10.2274	0.0752	0.1002	2.8624	0.5979	0.0248	0.0353	0.5390	9.9325E-07	4.0546E-05	0.0245
2	130-64	2.20	9.6407	0.1094	10.0589	0.1697	10.2286	0.1031	0.1281	2.8570	0.5241	0.0290	0.0413	0.6312	1.3274E-06	4.1771E-05	0.0318
2	130-65	2.20	97.1368	0.0255	10.0458	0.1704	10.2162	0.2425	0.2675	2.8723	0.4356	0.0670	0.0955	1.4595	2.6295E-06	4.3628E-05	0.0603
2	130-66	2.20	97.1368	0.0335	10.0943	0.1501	10.2444	0.3176	0.3426	2.5231	0.4623	0.0980	0.1395	2.1325	3.1060E-06	3.6899E-05	0.0842
2	130-66*	2.20	97.1368	0.0335	10.0943	0.1501	10.2444	0.3176	0.3426	2.5231	0.4479	0.0970	0.1382	2.1126	3.1259E-06	3.7158E-05	0.0841
2	130-67	2.20	97.1368	0.0454	9.9443	0.1703	10.1146	0.4360	0.4610	2.8994	0.3675	0.1161	0.1653	2.5279	4.5201E-06	4.5334E-05	0.0997
2	130-68	2.20	97.1368	0.055	9.8466	0.1712	10.0178	0.5333	0.5583	2.9429	0.3168	0.1347	0.1918	2.9318	5.6038E-06	4.7021E-05	0.1192

Appendix Table A2-2 Continued.

A

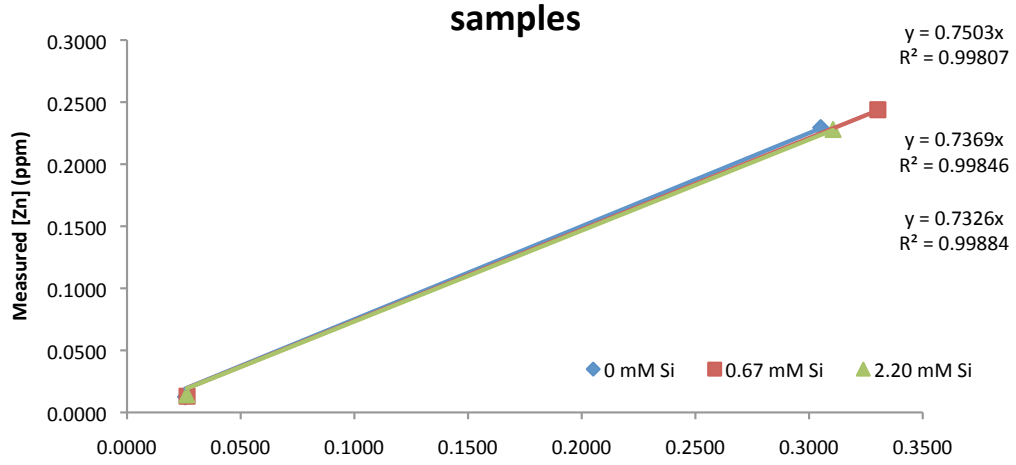

B

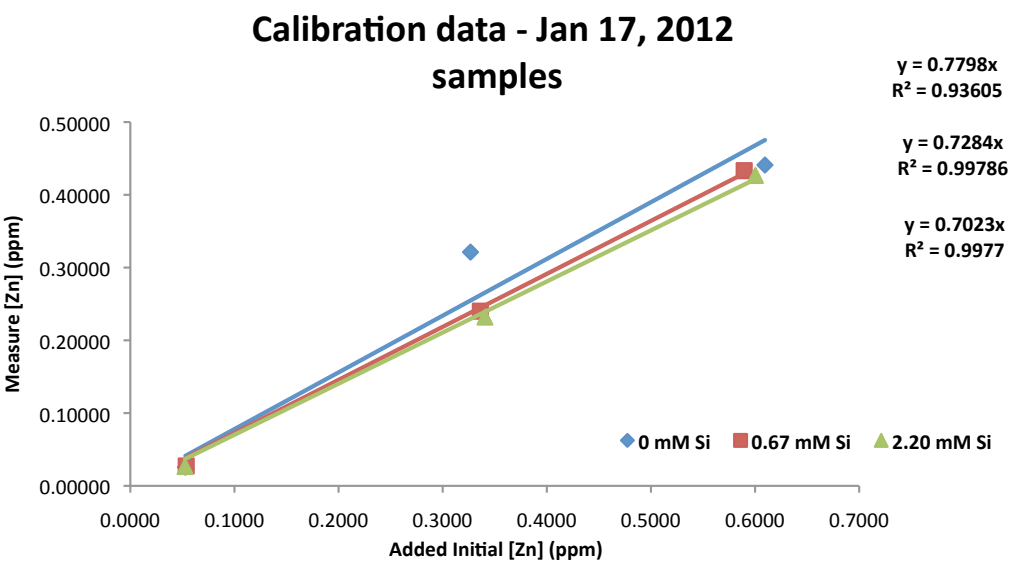

Appendix Figure A2-1. Internal isotherm calibration data for the 0, 0.67 and 2.20 mM Si conditions for (A) May 25, 2011 samples and (B) Jan 17th 2012 samples. The calibration equations are for the 0, 0.67 and 2.20 mM Si conditions from upper to lower, respectively.

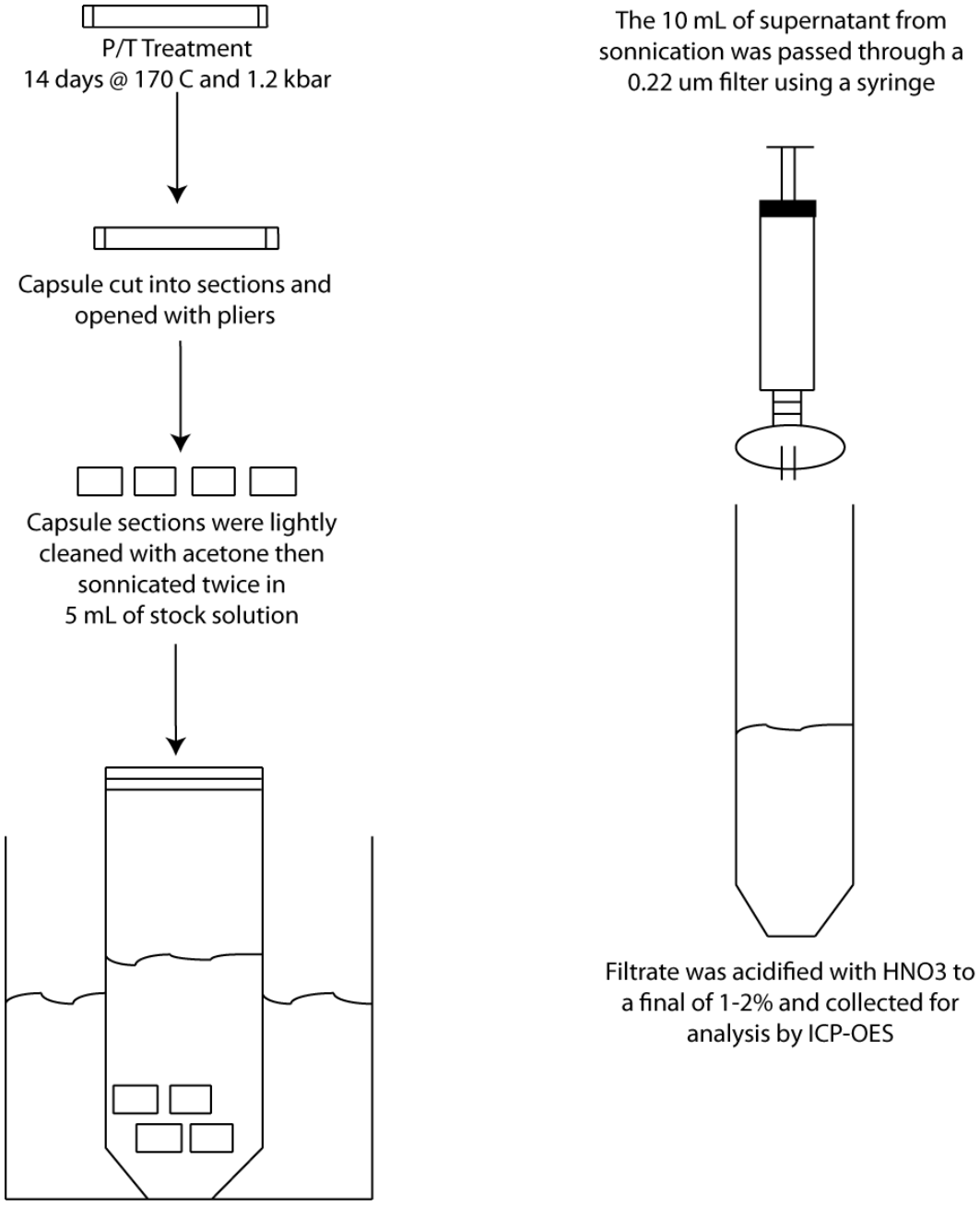

Appendix Figure A2-2. Schematic representation of the steps for experimental capsule treatment following the pressure and temperature treatment at 170ºC and 1.2 kbar. Capsules were then cut into small sections and lightly cleaned prior to being twice sonicated in 5 mL of 0.5 M $NaNO_3$ and 0.1 m H_3BO_3 stock solution. The supernatant from the sonications were then combined and passed through a 0.22 μM filter, prior to acidification and analysis by ICP-OES. Note: Figure not to scale.

A2.3 References

Bjerrum CJ, Canfield DE (2002) Ocean productivity before about 1.9 Gyr ago limited by phosphorus adsorption onto iron oxides. *Nature*, **417**, 159-162.

Bruland KW (1989) Complexation of zinc by natural organic ligands in the central North Pacific. *Limnology and Oceanography*, **34**, 269-285.

Konhauser KO, Lalonde SV, Amskold LA, Holland HD (2007) Was there really an Archean phosphate crisis? *Science*, **315**, 1234.

Konhauser KO, Pecoits E, Lalonde SV, Papineau D, Nisbet EG, Barley ME, Arndt NT, Zahnle K, Kamber BS (2009) Oceanic nickel depletion and a methanogen famine before the Great Oxidation Event. *Nature*, **458**, 750-753.

Robbins LJ, Lalonde SV, Saito MA, Planavsky NJ, Mloszewska AM, Pecoits E, Scott C, Dupont CL, Kappler A, Konhauser KO (2013) Authigenic iron oxide proxies for marine zinc over geological time and implications for eukaryotic metallome evolution. *Geobiology*, doi:10.111/gbi.12036.

Scott C, Planavsky NJ, Dupont CL, Kendall B, Gill BC, Robbins LJ, Husband KF, Arnold GL, Wing BA, Poulton SW, Bekker A, Anbar AD, Konhauser KO, Lyons TW (2013) Bioavailability of zinc in marine systems through time. *Nature Geoscience*, **6**, 125-128.